

**Analysis of Potential Nucleocytoplasmic Shuttling Mechanisms
of the Machado-Joseph Disease Protein, Ataxin-3**

Analysis of Potential Nucleocytoplasmic Shuttling Mechanisms
of the Machado-Joseph Disease Protein, Ataxin-3

By

Deborah Pinchev, B.Sc.

A Thesis
Submitted to the School of Graduate Studies
In Partial Fulfillment of the Requirements
For the Degree
Master of Science

McMaster University
©Copyright by Deborah Pinchev, November, 2006

Master of Science (2006)

McMaster University

(Biochemistry and Biomedical Sciences)

Hamilton, Ontario

Title: Analysis of Potential Nucleocytoplasmic Shuttling Mechanisms of
the Machado-Joseph Disease Protein, Ataxin-3

Author: Deborah Pinchev

Supervisor: Dr. Ray Truant

Number of Pages: x, 86

Abstract:

Machado-Joseph disease (MJD), also known as Spinocerebellar ataxia type 3 (SCA3) is one of nine polyglutamine neurodegenerative diseases caused by an expansion of CAG DNA triplets in the genes resulting in an expanded polyglutamine tract in the expressed proteins. These proteins are unrelated in function yet all manifest as specific neurological diseases. The Truant lab and others have previously shown that six of the nine polyglutamine proteins display nucleocytoplasmic shuttling capabilities and that this shuttling is affected by polyglutamine expansion. It is believed that deciphering the mechanism of nucleocytoplasmic transport may be important in understanding the normal function of these proteins, which in turn may lead to a better understanding of the pathogenesis of disease. Studies that looked at the subcellular localization of the MJD/SCA3 protein, ataxin-3, have shown that the normal protein is variably distributed between the nucleus and the cytoplasm, whereas mutant ataxin-3 is localized primarily in the nucleus. Using fluorescent protein technology and fluorescence microscopy, this thesis project attempts to analyze the nucleocytoplasmic shuttling capabilities of ataxin-3 and to evaluate the potential mechanisms that govern its translocation into and out of the nucleus.

It was revealed that ataxin-3 is able to shuttle into and out of the nucleus and that the shuttling dynamics are dependent on the length of the polyglutamine tract. As well, two putative, CRM1 dependent nuclear export signals and a putative, importin- α/β 1 dependent, classical, nuclear localization signal were tested and shown to be non-functional as transport signals. It was then discovered that ataxin-3 is marginally leptomycin B (an inhibitor of CRM1 dependent nuclear export) sensitive in NIH3T3 and MCF7 cells, more sensitive to the drug in *STHdh*^{Q7/Q7} cells and even more so in HEK 293 cells. This suggests that an exogenous factor mediates the nuclear import of ataxin-3 through the CRM1 pathway. Subsequently, four known binding partners, hHDAC1, hHDAC2, hHDAC6 and hHRAD23b, were tested for their potential ability to shuttle ataxin-3. It was concluded that although hHDAC6 had the greatest effect on ataxin-3 subcellular localization, we believe that it does not mediate its nuclear import or export. Future studies would involve an investigation as to how and why different polyglutamine lengths affect the nucleocytoplasmic shuttling of ataxin-3 and to identify the factor(s) that cause ataxin-3 to be more sensitive to LMB treatments in HEK 293 cells.

Acknowledgements:

First and foremost I would like to thank Ray Truant for the opportunity to learn and grow in his lab. As well, I would like to thank my committee members, David Andrews and Karen Mossman, for their brutal honesty and excellent advice. I would also like to thank the wonderful people that I worked with. To Sue MacMillan who brought a lot of laughter and common sense to the lab, to Jianrun Xia who is probably the nicest and most patient person I will ever have a chance to work with, to Randy Atwal for the great discussions we had about everything from science to Seinfeld while enjoying the endless cups of coffee and the infamous banana nut muffin, to Meghan Holmes for her excellent ability to clone and for all of her help with this project, to Carly Desmond for her positive attitude and happy demeanor and lastly, to Anjee Burtnik for her incredible and tireless work effort.

I would also like to thank the many people in the department who have also assisted with my learning and this project. To the Andrews lab and the Capone lab for providing important reagents, to the Trigatti lab for being excellent neighbours, to Cecile Fradin who gave me the knowledge to fully appreciate my FRAP data and to Tony Collins for answering my questions on the intricacies of fluorescent microscopy. Next, I would like to thank everyone in the department who made the last two and half years a lot of fun.

I would then like to thank my family for their support both financially and emotionally, even though they still have no idea what I do. I'll never forget the fear and horror in my parent's eyes when I showed them a plate of bacterial colonies. Lastly, I would like to thank my fiancé, Andy. He gave me his ear for listening, his shoulder to cry on and his hand to hold. Thank you for being there for me day in and day out no matter what.

Table of Contents:

	PAGE
ABSTRACT.....	ii
ACKNOWLEDGEMENTS.....	iii
TABLE OF CONTENTS.....	iv
LIST OF FIGURES.....	vi
LIST OF TABLES.....	vii
LIST OF SUPPLEMENTAL VIDEO AND FIGURES.....	viii
LIST OF ABBREVIATIONS.....	ix
INTRODUCTION.....	1
1.1 Trinucleotide Repeat Expansion Diseases.....	1
1.2 Polyglutamine Expansion Diseases.....	1
1.3 Machado Joseph Disease/Spinocerebellar Ataxia Type 3.....	4
1.4 Ataxin-3.....	5
1.5 Normal Function of Ataxin-3.....	5
1.6 Polyglutamine Expanded Ataxin-3.....	7
1.7 The Nuclear Pore Complex and Nucleocytoplasmic Transport.....	9
1.8 Fluorescent Protein Technology.....	11
1.9 Project Overview.....	12
MATERIALS AND METHOD.....	15
2.1 Plasmids.....	15
2.2 Tissue Culture.....	16
2.3 Transfections.....	17
2.4 Leptomycin B Assay.....	17
2.5 Epifluorescence Microscopy.....	17
2.6 Laser Confocal Microscopy.....	18
2.7 Inverse Fluorescence Recovery After Photobleaching.....	18
2.8 Image Analysis.....	18

2.9 Statistical Analysis.....	19
RESULTS AND DISCUSSION.....	20
3.1 Ataxin-3 is able to shuttle in and out of the nucleus	20
3.2 The two putative NES motifs and the NLS found in ataxin-3 do not function as nucleocytoplasmic transport signals.....	23
3.3 Ataxin-3 is more leptomycin B sensitive in HEK 293 and <i>STHdh^{Q7/Q7}</i> cells than in NIH3T3 and MCF7 cells.....	25
3.4 HDAC6 does not shuttle ataxin-3 but it does alter the subcellular localization.....	27
FUTURE DIRECTIONS.....	31
CONCLUDING REMARKS.....	33
FIGURES AND TABLES.....	35
SUPPLEMENTAL VIDEO AND FIGURES.....	64
REFERENCES.....	70

List of Figures:

	PAGE
Figure 1: The amino acid sequence of wild-type ataxin-3, isoform MJD1a with highlighted regions of interest.....	36
Figure 2: The subcellular localization of ataxin-3 [Q20] and [Q71] in mouse midline deep cerebellar nuclei.....	38
Figure 3: The equations used to quantify images for percent nuclear fluorescence intensity and for iFRAP analysis.....	40
Figure 4: Ataxin-3 is able to translocate to and from the nucleus and recovery into the nucleus is dependent on the length of the polyglutamine tract.....	42
Figure 5: The two putative NES motifs and the NLS found in ataxin-3 do not function as nucleocytoplasmic transport signals when analyzed by mutational studies.....	44
Figure 6: A structural comparison of the putative NESI in ataxin-3 to other known NES motifs in APC, p53 and STAT-1.....	46
Figure 7: Ataxin-3 is leptomycin B sensitive in HEK 293 cells.....	50
Figure 8: Ataxin-3 is slightly sensitive to leptomycin B in <i>SThdh</i> ^{Q71Q7} cells.....	52
Figure 9: Ataxin-3 is marginally leptomycin B sensitive in NIH3T3 cells.....	54
Figure 10: Ataxin-3 is marginally leptomycin B sensitive in MCF7 cells.....	56
Figure 11: hHDAC6 contains a functional NES.....	58
Figure 12: Representative images of co-expressed eYFP-ataxin-3 [Q28] and mCer-hHDAC6 variants and in NIH3T3 cells.....	62

List of Tables:

	PAGE
Table 1: Proteins in the karyopherin- β family.....	48
Table 2: hHDAC6 does not shuttle ataxin-3 but does alter its subcellular localization.....	60

List of Supplemental Video and Figures

	PAGE
Supplemental Video 1: A time lapsed video showing the formation of nuclear and cytoplasmic inclusions in a <i>STHdh</i> ^{Q7/Q7} cell, over-expressing ataxin-3 [Q166]-eGFP.....	65
Supplemental Figure 1: LMB assay of ataxin-3 in NIH3T3 cells co-expressed with hHRad23b, hHDAC1 and hHDAC2.....	66
Supplemental Figure 2: The formation of cytoplasmic inclusions occurs after 48 hours of mRFP or mCherry over-expression alone or as a fusion protein.....	68

List of Abbreviations:

%NFI	Percent Nuclear Fluorescence Intensity
A	Adenosine
Arg	Arginine
ATCC	American Type Culture Collection
ATP	Adenosine 5' Triphosphate
Atx3	Ataxin-3
C	Cytosine
CBP	CREB Binding Protein
CREB	cAMP Response Element
CRM1	Chromosome Region Maintenance-1 Protein
DMEM	Dulbecco's Modified Eagle Medium
DNA	Deoxyribonucleic Acid
DRPLA	Dentatorubralpallidoluysian Atrophy
DsRed	Discosoma Red Fluorescent Protein
eCFP	Enhanced cyan fluorescent protein
eGFP	Enhanced green fluorescent protein
ERAD	Endoplasmic reticulum associated degradation
eYFP	Enhanced yellow fluorescent protein
FRAP	Fluorescence Recovery After Photobleaching
G	Guanosine
G418	Geneticin
GDP	Guanosine Diphosphate
GTP	Guanosine Triphosphate
HD	Huntington's Disease
HDAC	Histone Deacetylase
HEK 293	Human Embryonic Kidney cells
HIV-1 Rev	Human Immunodeficiency Virus Type-1 Rev Protein
iFRAP	inverse FRAP
I κ B	inhibitor kappa B
Ile	isoleucine
JD	Josephin Domain
kDa	KiloDalton
Leu	Leucine
LMB	Leptomycin B
LSM	Laser Scanning Microscope
Lys	Lysine
mCher	Monomeric Cherry Fluorescent Protein
mCer	Monomeric Cerulean Fluorescent Protein
mL	Milliliter
mRFP	Monomeric Red Fluorescent Protein
MTOC	Microtubule Organizing Center
MCF7	Human Breast Cancer Epithelial Cells

NES	Nuclear Export Signal
NESm	NES mutant
NIH3T3	Cell line of highly contact-inhibited cells established from the NIH Swiss mouse embryo cultures.
NLS	Nuclear Localization Signal
NLSm	NLS mutant
ng	Nanogram
NPC	Nuclear Pore Complex
[Qn]	Polyglutamine tract with n glutamine residues
PBS	Phosphate Buffered Saline
RNA	Ribonucleic Acid
ROI	Region of Interest
SBMA	Spinobulbar and Muscular Atrophy
<i>STHdh</i> ^{Q7/Q7}	Clonal striatal cell line isolated from the striatum of a transgenic mouse expressing wild-type huntingtin with a polyglutamine stretch of 7 residues
UIM	Ubiquitin Interacting Motif
UPP	Ubiquitin Proteasome Pathway
Val	Valine
VCP/p97	Valosin Containing Protein
ZnF-UBP	Zinc-finger Ubiquitin Interaction Domain

Introduction:

1.1 Trinucleotide Repeat Expansion Diseases

Machado-Joseph Disease (MJD) also known as Spinocerebellar ataxia type 3 (SCA3) is one of the growing list of at least 20 trinucleotide repeat expansion diseases that are all caused by a similar genetic mutation where an unstable trinucleotide repeat is expanded. The diseases result in neurodegeneration, neuromuscular disease and/or mental retardation. There are two distinct classes based on the genetic mutation. Firstly, there are the non-coding triplet repeat diseases, where the expansion lies in the non-coding region of a gene (Brown and Brown, 2004; Cummings and Zoghbi, 2000). Fragile X syndrome (CGG repeats) and Friedreich ataxia (GAA repeats) are examples of such diseases where the trinucleotide expansion causes the associated gene to be improperly translated. Secondly, there are the coding triplet repeat diseases, which include the polyglutamine (CAG) and the polyalanine (GCG) repeat diseases. Blepharophimosis-ptosis-epicanthus inversus syndactyly and synpolydactyly disorder are examples of polyalanine diseases (Albrecht and Mundlos, 2005). There are nine known polyglutamine diseases, which include, Huntington's disease (HD), Spinocerebellar ataxias (SCA 1, 2, 3, 6, 7, 17 and DRPLA) and Kennedy's disease or spinal and bulbar muscular atrophy (SBMA).

The exact mechanism of trinucleotide repeat expansions is not entirely understood. The association of repeat length with mutation is known as 'dynamic mutation' and occurs in CG rich trinucleotides such as CAG/CTG and CCG/CGG repeats (Richards and Sutherland, 1992). The most widely accepted model of expansion is the DNA slippage hypothesis. Here, slipped-strand hairpin or triplex structures form within the long repeat tracts during lagging strand DNA synthesis, which causes the DNA polymerase to slip and synthesize the trinucleotide region (Pearson et al., 2002). It is believed that both cis-acting elements, such as tract length, sequence purity and orientation relative to replication origins and trans-acting elements, such as DNA repair and replication proteins contribute to repeat instability and expansion (Gorbunova et al., 2004; Cleary et al., 2002; Gomes-Pereira et al., 2001).

1.2 Polyglutamine Expansion Diseases

Polyglutamine expansion disorders share the same genetic mutation of a CAG expansion in the coding region of a gene, which results in an expansion in the polyglutamine tract of the translated protein. For most of the nine diseases that make up this family of neurodegenerative disorders the threshold before symptoms appear is 36 glutamine repeats. All nine of the diseases affect different genes that are unrelated by sequence similarity. Although the affected protein in each case differs in function, the group of polyglutamine disorders share several genetic features. They are all progressive, dominantly inherited (except for Kennedy's disease), typically begin in mid-life and result in severe neuronal dysfunction and cell death (Cummings and Zoghbi, 2000). As well, genetic anticipation is often seen in these diseases where subsequent generations of

patients will exhibit symptoms at an earlier age due to trinucleotide repeat instability in the affected genes (Carpenter, 1994). Moreover, parental origin also influences anticipation of the diseases with paternal transmission often carrying a greater risk of expansions (Pearson, 2003).

Despite the ubiquitous expression of all of the disease associated proteins only a certain subset of neurons are affected in each disease. For example, the Spinocerebellar ataxias (SCAs) tend to affect the cerebellum and brain stem while Huntington's Disease (HD) targets neurons in the striatum and cortex (Gilman, 2000; Joel, 2001; Lawrence et al., 1998). It is not precisely known why this is the case. It is hypothesized that the special characteristics of neurons such as their inability to divide, their unique morphology and distinct protein-protein interactions may lead to the specific neurodegeneration. Currently, there are many factors believed to be involved in mediating the pathogenesis of the disease. The factors that cover the spectrum of all nine polyglutamine disorders include: protein misfolding and aggregation; formation of nuclear inclusions; altered protein quality control; proteolytic processing; transcriptional dysfunction; and subcellular localization.

Early animal studies and tissue culture models have demonstrated that the diseases display a 'gain-of-function' phenotype and that the apparent cause of the disease lies in the polyglutamine tract (Houseman, 1995; Lin et al., 1999). This led to efforts directly targeting the polyglutamine tract within the affected proteins. Two early models proposed that self-association took place within this region by cross-linking the isopeptide bonds or by the tract organizing into polar zippers via hydrogen bonding (Green et al., 1993; Perutz et al., 1994). Both of these models have suggested that aggregation and protein misfolding, which potentially result from self-association, play key roles in polyglutamine disorders. In neurons, aggregates found in the nucleus are sometimes referred to as neuronal intranuclear inclusions (NII). Although NIIs may also be highly mobile and consist of high concentrations of localized protein. Eight of the nine proteins have been shown to form nuclear inclusions (NI) that are ubiquitin positive, whereas SCA6 appears as ubiquitin-free cytoplasmic aggregates (Zoghbi and Orr, 1999).

In vitro studies looking at aggregation in solution have shown that the ability of polyglutamine containing proteins to form insoluble aggregates increases as the number of repeats increase, with normal repeat lengths displaying little or no aggregation (Scherzinger et al., 1997; Chen et al., 2001; Bevivino and Loll, 2001). However, an ataxin-3 *in vitro* study suggested that polyglutamine repeats do not affect the folding and stability of the protein (Chow et al., 2004a). When studying SCA1, SCA3, SCA17, HD, and DRPLA in mice and human tissue samples, NIIs have been found in neurons specifically affected by disease (Vig et al., 2000; Nakamura et al., 2001; Paulson et al., 1997a; Schilling et al., 2001). Conversely, studies have also demonstrated that non-pathogenic cells display an abundance of NIIs made up of expanded polyglutamine protein or fragments of protein, whereas pathogenic neurons were only expressing soluble versions of the expanded protein (Becher et al., 1998; Klement et al., 1998; Yvert et al., 2001). In SCA7 knock-in mice, neuronal degeneration was apparent weeks before there were signs of aggregation or NIIs (Yoo et al., 2003). In studies using cell culture models a correlation between aggregation and toxicity has been shown (Ikeda et al.,

1996; Lunkes et al., 1999) while others demonstrated a lack of association or discovered a neuroprotective effect (Saudou et al., 1998; Taylor et al., 2006).

A potential cause of aggregation and neuronal toxicity is protein misfolding. Studies have shown that chaperones promote some form of neuroprotection against polyglutamine diseases even though it may not necessarily be through the removal of aggregates. A decrease in neuronal toxicity and a reduction in the presence of NI and aggregates have been demonstrated in SBMA cell models (Kobayashi and Sobue, 2001) and HD transgenic mouse models (Vacher et al., 2005). Alternatively, others have shown that in disease models neurodegeneration was reduced without having any effects on aggregation. This has been seen in both a SCA3 *Drosophila* model and a SCA1 mouse model when over-expressing Hsp70 (Warrick et al., 1999; Cummings et al., 2001). The formation of aggregates and NII do not necessarily result in cell death or disease but it is clear that knowing why and how aggregates form may further the overall understanding of polyglutamine diseases.

Proteolytic processing of the disease associated proteins has also been linked to progressive neuronal degeneration as well as a potential cause of aggregation. Amino-terminal fragments of huntingtin and the androgen receptor as well as carboxyl-terminal fragments of ataxin-3 have been detected in pathogenic tissue using antibodies specific to those regions of the protein (Lunkes et al., 2002, Li et al., 1998a; Goti et al., 2004). Moreover, there is evidence of mutant polyglutamine protein fragments of huntingtin, atrophin-1, and ataxin-7, for example, accumulating in the nucleus and exerting their toxic effects (DiFiglia et al., 1997, Tanaka et al., 2006; Nucifora et al., 2003; Yvert et al., 2001). Blocking cleavage of these proteins by either inhibiting the protease involved or by mutating the cleavage site has led to a decrease in cellular toxicity (Ellerby et al., 1999; Wellington et al., 2000; Graham et al., 2006). This evidence suggests that proteolytic processing of polyglutamine expanded proteins and the location of the cleavage products may be very important to the disease.

The subcellular localization of this group of proteins is related to proteolytic processing and aggregate formation. When examining normal versus expanded protein the shift in localization, whether to the nucleus (as seen in most cases) or the cytoplasm (as seen in SCA2) suggests that this change in distribution is relevant to disease pathogenesis. In the cytoplasm mutant proteins have been known to affect processes such as axonal transport and mitochondrial function (Gatchel and Zoghbi, 2005). In the nucleus mutant proteins may be involved in transcriptional dysregulation where changes in gene expression precede neuronal degeneration in some disease models (Yoo et al., 2003; Lin et al; 2000). Understanding the mechanism of translocation into and out of the nucleus may provide a way to alter the shift in subcellular localization in order to reduce the toxic effects of the mutant protein.

The best example of the importance of understanding the mechanism of nuclear localization of a polyglutamine protein is in spinal and bulbar muscular atrophy (SBMA). Here the protein of interest is the androgen receptor, a member of the hormone receptor family. In the absence of ligand, testosterone or dihydrotestosterone, the androgen receptor shuttles in and out of the nucleus and the rate of export is higher than the rate of import. When the androgen receptor is bound to its ligand, the nuclear export signal in

the protein is inhibited and the androgen receptor remains in the nucleus, activating transcription (Saporita et al., 2003). The polyglutamine expanded version of the androgen receptor becomes toxic in the nucleus of affected neurons and has been shown to form nuclear inclusions only in the presence of ligand (Piccioni et al., 2001; Walcott and Merry, 2002). In mouse models of SBMA, a depletion of androgens by castration or by treatment with leuprorelin, a gonadotropin-hormone releasing agonist, prevents motor neuron toxicity (Chevalier-Larsen et al., 2004, Katsuno et al., 2002). This has been an exciting discovery and currently clinical trials are being conducted in Japan (Banno et al., 2006). This finding demonstrates that by understanding the normal function of the androgen receptor and by knowing its transport mechanisms, researchers were able to manipulate its function in order to abrogate disease in animal models. The normal function of six other polyglutamine proteins is not fully understood and the mechanisms of subcellular localization are just beginning to be elucidated. Moreover, a further understanding of normal function will allow for the study of how events like aggregation, misfolding and protein cleavage affect the specific processes of polyglutamine proteins.

1.3 Machado-Joseph Disease/Spinocerebellar Ataxia Type 3

This neurodegenerative disorder was initially described based on symptoms found in families originating from the portugese Azorean islands and was named Machado-Joseph Disease (MJD). A similar dominantly inherited cerebellar ataxia, known as Spinocerebellar ataxia type 3 (SCA3), was first described in other parts of Europe and was being mapped to the same chromosome as MJD. With the discovery of the CAG expansion as the cause of the disease it soon became clear that the two disorders were one and the same (Schols et al., 1995; Matilla et al., 1995).

MJD/SCA3 is the most common dominantly inherited ataxia (Silveira et al., 1996; Kraft et al., 2005). The gene has been mapped to chromosome 14q32.1 (Kawaguchi et al., 1994). Normal individuals contain 12 to 43 CAG repeats with more than 90% of the population containing less than 31 repeats (Gaspar et al., 2001; Rubinsztein et al., 1995). Affected individuals generally contain 53 to 86 repeats and an inverse relationship exists between the age of onset and the number of repeats in the abnormal allele (Maciel et al., 1995; Matilla et al., 1995). Intermediate lengths of 48 to 51 repeats are not associated with a disease phenotype but can exhibit meiotic instability, resulting in a pathological expansion in subsequent generations (Maciel et al., 2001). The age of onset is also related to sex, where males exhibit an earlier onset of symptoms and gene dosage, with allelic homozygosity having an additive effect (Kawakami et al., 1995; Sobue et al., 1996).

The central clinical feature of MJD/SCA3 is progressive ataxia due to cerebellar and brainstem dysfunction. Ataxia refers to the unsteady and clumsy motion of the limbs due to a lack of muscle coordination. This coincides with the fact that the cerebellum is the region of the brain that coordinates sensory perception with motor output and the brainstem is the major route of communication between the forebrain, the spinal chord and the peripheral nerves. The range of secondary symptoms is highly variable but there are some symptom regularities seen in the majority of patients. Initially, gait imbalance,

accompanied by vestibular disturbance and speech difficulties are seen (Coutinho and Andrade, 1978; Sudarsky and Coutinho, 1995). This is followed by a wider range of manifestations that appear to involve visual and oculomotor problems and may include nystagmus, jerky ocular pursuits, slowing of saccades and bulging of the eyes (Maciel et al., 1995; Durr et al., 1996; Isashiki et al., 2000). In late stages of the disease patients have severe dysarthria and dysphagia and are often wheelchair-bound. Other signs that may occur at any stage include facial and temporal atrophy, dystonia, spasticity, parkinsonism, various sleeping disorders and restless leg syndrome (Sudarsky and Coutinho, 1995; Munchau et al., 1999; Tuite et al., 1995; Schols et al., 1998).

Similar to clinical features of MJD/SCA3, pathological features are widespread and highly variable. The most common pathology includes severe neuronal loss in the basal ganglia, numerous brainstem nuclei and the cerebellum (Sudarsky and Coutinho, 1995; Durr et al., 1996). Others signs of neurodegeneration have been described in various parts of the brain but regions generally spared of disease include the cerebral cortex, the olivary nuclei and the corticospinal tracts (Yamada et al., 2001). The expression levels of both normal and mutated forms of ataxin-3 were shown to be similar in various regions of the human brain despite the fact that only a subset of neurons are affected in MJD/SCA3 patients (Nishiyama et al., 1996).

1.4 Ataxin-3

The gene that harbours the mutation which causes MJD/SCA3 contains 11 exons with the CAG repeats residing in the 10th exon. The gene product, ataxin-3, in its normal form is a 42 kDa protein (Figure 1). There are four isoforms of ataxin-3 that contain regions of sequence variation downstream of the polyglutamine tract. Two of the major splice forms, MJD1a and MJD3c, have been specifically implicated with neurodegeneration (Kawaguchi et al., 1994; Schmidt et al., 1998). The first 176 residues are highly conserved across many species and is known as the Josephin domain (JD) (Albrecht et al., 2003). This domain is monomeric and globular and folds to a structure that has been recently solved by two separate groups using nuclear magnetic resonance (Mao et al., 2005; Nicastro et al., 2005). Conversely, the region downstream of the JD, which contains the polyglutamine tract, is highly unstructured (Masino et al., 2003). In addition, ataxin-3 also contains two ubiquitin interacting motifs (UIMs) upstream of the polyglutamine tract and in the MJD3c splice variant a third UIM downstream of the polyglutamine tract (Burnett et al., 2003).

1.5 Normal Function of Ataxin-3

The precise function of ataxin-3 is not known. However, studies intent on defining its domains and motifs, as well as elucidating binding partners have provided much information. Research into the role of ataxin-3 in the ubiquitin proteasome pathway (UPP) has been the most comprehensive due to several interesting studies involving the

JD and the UIMs. The UPP plays an essential role in controlling the degradation of important regulators of stress response, cell growth, and differentiation (Nandi et al., 2006). Proteins associated with the UPP include the 26S proteasome, the enzymes involved in targeting substrates to the proteasome by polyubiquitination and several other regulatory proteins, which include shuttling factors, deubiquitinating enzymes and other regulators (Schmidt et al., 2005).

Initially, through the use of bioinformatics, ataxin-3 was found to contain a catalytic site within the JD, similar to that found in ubiquitin proteases (Scheel et al., 2003). This deubiquitinating (DUB) activity was later confirmed in studies using test substrates such as polyubiquitinated lysozyme and GST (Burnett et al., 2003). Furthermore, the solution structure of ataxin-3 was solved by nuclear magnetic resonance, establishing the JD as a DUB enzyme and classifying it within the papain-like cysteine protease family (Mao et al., 2005; Nicastro et al., 2005). The first two UIM have been studied extensively and it is now known that ataxin-3 preferentially binds the ubiquitin of test substrates that have been polyubiquitinated by four or more ubiquitins in chains linked at K48 (Chai et al., 2004). Moreover, it has been proposed by Mao et al. that the UIMs act along with the Josephin domain to bind and stabilize ubiquitinated substrates during catalysis (Mao et al., 2005). This is also supported by the observation that when the DUB activity is inhibited there is enhanced stability in the binding of ataxin-3 with polyubiquitinated substrates indicating that such binding is required for proteolysis (Chai et al., 2004).

Through the use of a yeast two-hybrid system two human homologs of the yeast UV-damaged DNA repair protein Rad23, hHRad23a and hHRad23b were identified as ataxin-3 binding partners (Wang et al., 2000). In mammalian systems hHRad23 is proposed to be part of the UPP by acting as a "shuttling factor" for translocating proteins to the proteasome for degradation (Schauber et al., 1998). Its interaction with ataxin-3 was precisely defined using nuclear magnetic resonance and it involves the Ubl of hHRad23b and the exposed, complementary hydrophobic surfaces of ataxin-3 (Nicastro et al., 2005). Both normal and expanded ataxin-3 show no difference in the ability to interact with hHRad23b.

Another protein linking ataxin-3 to the proteasome is the valosin containing protein (VCP/p97), a molecular chaperone that is part of the AAA family of ATPases. Originally, it was identified as a binding partner of ataxin-3 through a pull down assay and mass spectrometry (Hirabayashi et al., 2002, Doss-Pepe et al., 2003). Its interaction was subsequently found to be modulated by an arginine/lysine motif in ataxin-3, which serves as a recognition site for VCP/p97 (Boeddrich et al., 2006). One of VCP/p97 proposed functions is to extract proteins from the endoplasmic reticulum (ER) for eventual degradation in the cytosol, as part of the ER associated degradation (ERAD) (Jarosch et al., 2002). A study examining ataxin-3 and its role in ERAD, presented the idea that ataxin-3 decreases the interaction of VCP/p97 with certain ERAD substrates in order to regulate their degradation (Zhong and Pittman, 2006). This study also stated that the UIM and DUB activities of ataxin-3 have a very small effect in modulating the degradation of ERAD substrates. Thus, it is still uncertain how its role in ERAD is related to its DUB activity and other potential functions of ataxin-3.

An alternative function for ataxin-3 links it to the formation of aggresomes, which are misfolded proteins that have accumulated at the microtubule-organizing center (MTOC). The MTOC is occupied by the centrosome and it specifically refers to the site where microtubule polymerization is nucleated. Aggresome formation requires active, retrograde transport of small aggregates or misfolded protein via microtubules (Kopito, 2000). Many proteins involved in protein folding and degradation processes are found at the aggresome, including the proteasome (Johnston et al., 1998). Burnett and Pittman, demonstrated that ataxin-3 is directly involved in the formation of aggresomes and that dynein and histone deacetylase 6 (HDAC6) are binding partners of ataxin-3 (Burnett and Pittman, 2005). Previous studies have established that the microtubule motor proteins dynein/dynactin and the microtubule-associated HDAC6 are important in transporting misfolding protein to the MTOC (Garcia-Mata et al., 1999). It was found that both the UIM and the deubiquitinating activity of ataxin-3 are both important to the formation of aggresomes (Burnett and Pittman, 2005).

Transcriptional repression has also been linked to ataxin-3 through the discovery of additional ataxin-3 binding partners. Studies have shown that both normal and polyglutamine expanded ataxin-3 interact with CREB binding protein (CBP) and p300 and that ataxin-3 is able to inhibit transcription that is mediated by these co-activators (Chai et al., 2001; Li et al., 2002). CBP and p300, both serve as co-activators for many diverse transcription factors (Janknecht, 2002). One study suggests that the mechanism of transcriptional inhibition requires ataxin-3 to bind to histones and restrict access of co-activators to acetylation sites on such histones (Li et al., 2002). A very recent study also suggests that ataxin-3 recruits histone deacetylase 3 and the nuclear receptor corepressor in order to promote the deacetylation of histones (Evert et al., 2006). The same study also showed that ataxin-3 binds histones for the purpose of repressing transcription. A more thorough understanding of the role of ataxin-3 in transcriptional repression could provide information on how the polyglutamine expanded protein could potentially cause transcriptional dysregulation.

1.6 Polyglutamine Expanded Ataxin-3

When the polyglutamine tract in ataxin-3 becomes expanded past 43 repeats a number of changes occur. At the protein level, altered protein interactions, conformational changes and increased proteolysis have all been observed. At the cellular level, the subcellular localization is altered and an increase in inclusion and aggregate formation is often seen.

In animal models, the mutant protein displays many of the phenotypes and features found in humans and is therefore extremely useful in studying MJD/SCA3 pathogenesis. When full length or carboxyl-terminal fragments of mutant ataxin-3 were expressed in *Drosophila*, late-onset neurodegeneration was observed (Warrick et al., 1998; Kim et al., 2004). This model has since been used to investigate toxicity of the truncated form, misfolding and inclusions and suppression of neurodegeneration by normal ataxin-3 (Warrick et al., 1998; Warrick et al., 2005). Mouse models have also

been effective in recapitulating disease. Both successfully produced MJD/SCA3 transgenic mouse models have demonstrated late-onset cerebellar dysfunction along with other disease phenotypes and have also exhibited selective neuronal atrophy, features that are found in MJD/SCA3 patients (Cemal et al., 2002).

Altered protein-protein interactions with nuclear ataxin-3 binding partners such as CBP, p300 and histone deacetylase 3 may potentially cause transcriptional dysregulation in MJD/SCA3. The sequestration model suggests that mutant ataxin-3 recruits the transcriptional co-activators to NIIS where they become immobilized and non-functional (Chai et al., 2002). Alternatively, mutant ataxin-3 displays altered binding to histones and reduced ability to recruit deacetylating proteins to chromatin (Evert et al., 2006). Both potential models of transcriptional dysfunction need to be further investigated to incorporate the tissue specificity and progressive nature of MJD/SCA3.

One of the most thoroughly investigated modes of pathology for polyglutamine expanded diseases is the misfolding and aggregation of the mutant protein and this is also true for MJD/SCA3. *In vitro* analysis of recombinant ataxin-3 has shown that the mutant form has an increased ability to form SDS insoluble aggregates and to adopt a misfolded β -fibril conformation (Bevivino and Loll, 2001; Chow et al., 2004; Eddisdon et al., 2006). When studying NII in the brains of MJD/SCA3 patients and in cellular models, several groups found that molecular chaperones and other components of the UPP occupied inclusions, providing further evidence for misfolding and aggregation (Chai et al., 1999; Donaldson et al., 2003; Jana et al., 2005). Moreover, in a *Drosophila* model of MJD/SCA3, neurodegeneration was suppressed by over-expressing the heat shock protein, HSP70, implying that a reduction in misfolded protein prevented disease (Warrick et al., 1999). Contradictory results in the same study showed that the number or size of inclusions were not altered, suggesting that the inclusions did not contain misfolded protein. However, when another group looked specifically at the dynamics of mutant ataxin-3 inclusions they found that the NIIs were immobile indicating the existence of aggregated protein (Chai et al., 2002). As with most of the polyglutamine diseases, this evidence demonstrates that there does not exist a clear correlation between the existence of inclusions or aggregates with neurodegeneration. It can be concluded that NIIs and aggregates are important to MJD/SCA3, either as a sign of progression or potentially as a pathogenic mechanism.

Proteolytic processing of mutant ataxin-3 may be a key step in MJD/SCA3 pathogenesis. In *Drosophila*, the carboxyl-terminal fragment appears to be more toxic than the full length version because it lacks the UIMs and DUB activity of the JD (Warrick et al., 2005). However, there have been inconsistencies in the detection of mutant ataxin-3 fragments in animal models and in patient brains. Some investigators were able to identify carboxyl-terminal fragments of expanded but not normal ataxin-3 (Yamamoto et al., 2001; Goti et al., 2004) while others found no evidence of carboxyl-terminal fragments in either mouse models (Cemal et al., 2002) or in patient brains (Paulson et al., 1997a). In addition, the cause of proteolysis is not clear with one study suggesting that caspase-1 is the protease involved in cleavage (Berke et al., 2004). The only consistency is in the observation that carboxyl-terminal fragments aggregate more easily than their counterparts (Chai et al., 1999; Yoshizawa et al., 2001; Berke et al.,

2004). This is presumably due the lack of structural stability that is normally provided by the JD.

Lastly, the subcellular localization of mutant ataxin-3 is altered as seen in animal models and in patients. The distribution of normal ataxin-3 has been observed to be both nuclear and cytoplasmic depending on the cell type. Studies looking at normal brain tissue have shown that ataxin-3 resides primarily in the cytoplasm (Paulson et al., 1997a; Goti et al., 2004; Figure 2). Whereas accumulation of expanded ataxin-3 in the nucleus, often as NIIs, is selectively seen in the neurons of affected brain tissue (Fujigasaki et al., 2000; Goti et al., 2004; Figure 2). In immortalized cell lines the distribution of ataxin-3 is highly variable. For example, normal ataxin-3 was detected predominantly, but not exclusively, in the nucleus of COS-7 and neuroblastoma cells (Tait et al., 1998). This same study showed that an expanded polyglutamine tract is not required to translocate ataxin-3 into the nucleus. In HeLa cells the majority of ataxin-3 is cytosolic, but immunofluorescence and subcellular fractionation studies indicated the presence of ataxin-3, particularly certain minor isoforms, in the nucleus (Trottier et al., 1998). In our lab, it has been observed that both normal and expanded ataxin-3 over-expressed as fluorescent fusion proteins, have similar pancellular distributions in mouse epithelial (NIH3T3), mouse striatal (*STHdh^{Q7/Q7}*), human breast cancer (MCF7) and human embryonic kidney (HEK 293) cells. The exact mode of nucleocytoplasmic transport of ataxin-3 in either direction has not been thoroughly investigated. Understanding transport may be important in understanding the variable cellular distribution of the normal and mutant protein.

1.7 The Nuclear Pore Complex and Nucleocytoplasmic Transport

In order for ataxin-3 to translocate into and out of the nucleus it must cross the nuclear envelope (NE), which separates the nucleus from the rest of the cytoplasm in eukaryotes. The NE is composed of a double, lipid bilayer membrane, the lamina and the nuclear pore complex (NPC). It is the NPC that functions as the mediator of transport of molecules between the two compartments. It is a large complex of dynamically assembled protein that spans the NE at sites where the outer and inner nuclear membranes are fused.

The mass of the NPC has been estimated at ~125 MDa in vertebrates and ~60 MDa in yeast (Reichelt et al., 1990; Rout and Blobel, 1993). It is shaped like an hour-glass and has a length of ~ 90 nm and a diameter of ~ 40 nm at its narrowest point across the pore (Lim and Fahrenkrog, 2006). The NPC is composed of ~ 30 proteins, known as nucleoporins many of which are present in eight copies to reflect the eight-fold symmetry of the complex (Rout, 2000; Cronshaw, 2002). There are two classes of nucleoporins that are differentiated by function and protein fold. One class represents the structural components of the NPC and has two specific fold types, β propeller and α solenoid (Wente, 2000). The other class is comprised of nucleoporins that contain phenylalanine-glycine (FG) repeats. These repeats are involved in nucleocytoplasmic transport through

facilitated diffusion by associating and dissociating with soluble transport receptors (Rout and Aitchison, 2001).

It is not precisely known how molecules traverse through the NPC but it is known that molecules can diffuse through the pore or can be actively translocated with the assistance of transport receptors known as karyopherins. The diffusion limit of the NPC is ~ 40 to 60 kDa and is also dependent on the fold of the macromolecule and its ability to interact with the nucleoporin FG repeats (Fried and Kutay, 2003). Diffusion mediated transport is bi-directional, whereas receptor mediated transport is unidirectional. Karyopherins are the mobile proteins involved with translocation into and out of the nucleus. They facilitate transport via transient interactions with nucleoporins containing FG repeats (Stewart et al., 2001). The interaction of karyopherins with their cargo is energy dependent and is regulated by the Ran-GDP/GTP gradient. The gradient is maintained by the physical separation of the GTPase, RanGAP in the cytoplasm and the GTP exchange factor, RanGEF in the nucleus. The overall result is a high concentration of Ran-GDP in the cytoplasm and a high concentration of Ran-GTP in the nucleus (Gorlich et al., 1996).

Macromolecules that require active transport into the nucleus generally require a nuclear localization signal (NLS) in order to be recognized by importins. Certain NLS containing cargos interact with importin- β 1 via an adaptor protein known as importin- α thus forming a complex (Goldfarb et al., 2004; Pemberton and Paschal, 2005). There are at least eleven known importins in eukaryotes with different levels of expression in different cell types (Fried and Kutay, 2003). The best known NLS is the basic or classical NLS and can consist of either one cluster of four or five basic residues or two clusters that are separated by a short linker (Gorlich and Kutay, 1999). However, there are many NLSs that do not follow this consensus, including the importin- β 2 dependent, glycine rich M9 NLS, which contains a newly described consensus sequence with a conserved proline and tyrosine at the carboxyl-terminus of the sequence (Lee et al., 2006).

There are seven known exportins, which recognize specific cargo for the purpose of nuclear export (Fried and Kutay, 2003). Some cargo proteins contain a nuclear export signal (NES) such as the one first identified in the HIV-1 Rev protein (Fischer et al., 1995). This NES is well characterized and contains a loosely conserved, hydrophobic consensus sequence of Φ _x₂₋₃ Φ _x₂₋₃ Φ _x₁₋₂ Φ , where Φ represents hydrophobic residues and x is any residue. At least 75 proteins contain this type of NES and all are recognized by CRM1/exportin-1, an exportin ubiquitously expressed in eukaryotes (Fornerod et al., 1997; Kudo et al., 1997). Other types of cargo recognized by export receptors include RNA, importin- α and other proteins that do not contain a leucine-rich NES (Kutay et al., 1997; Lei and Silver, 2002).

There are many proteins that shuttle in and out of the nucleus. Such bi-directional transport is an important regulatory mechanism for a variety of cellular processes including, but not exclusive to transcription, cell cycle regulation, mRNA transport and signal transduction (Gama-Carvalho and Carmo-Fonseca, 2001). Shuttling proteins are not always directly involved in a cellular process but instead act to translocate and alter the localization of their binding partners. This is demonstrated by the nucleocytoplasmic shuttling protein, APC in its ability to control the levels of beta-catenin, an oncogenic

transcription activator, through nuclear export (Henerson, 2000). The import and export of shuttling proteins can also be tightly regulated by post-translational modifications such as phosphorylation and ubiquitination. For example, phosphorylation of the shuttling protein histone deacetylase 4, causes its dissociation from MEF2 thus exposing its NES and allowing nuclear export (McKinsey et al., 2000).

Of the nine polyglutamine disease proteins six have the ability to shuttle in and out of the nucleus. As previously stressed, understanding the mechanism and regulation of shuttling of some of the polyglutamine proteins has led to a better understanding of the associated disease. Nuclear import and export have been well characterized for ataxin-7, atrophin-1 and the androgen receptor, while the mechanisms of nuclear localization for huntingtin and nuclear export for ataxin-1 are still unknown (Klemment et al, 1998; Nucifora et al., 2003; Saporita et al., 2003; Taylor et al., 2006; Xia et al., 2002).

I have shown that ataxin-3 is also able to shuttle in and out of the nucleus. However, the precise mechanisms of nuclear import and export have not been characterized. Through sequence analysis two putative leucine-rich NES motifs have been located at amino acids 77-86 (IQVISNALKV) and 349-357 (FIMFATFTL). In addition a putative classical NLS, at amino acids 291-297 (LRKRREA) has been previously described (Albrecht et al., 2004). The characterization of these putative transport signals could lead to an understanding of how ataxin-3 translocates across the nuclear pore. Moreover, it could lead to insights on how and why the subcellular localization of mutant ataxin-3 differs from that of the normal protein. Fluorescent protein technology and microscopic imaging are commonly used to investigate such questions.

1.8 Fluorescent Protein Technology

In 1994, the green fluorescent protein (GFP) gene from *Aequorea victoria*, a bioluminescent jellyfish, was cloned and expressed in *E. coli* (Chalfie et al., 1994). GFP is an extremely useful tool in cellular biology. It is suitable to use as a reporter and a fusion protein because of its small size of 26 kDa, its low toxicity in mammalian cell lines and its intrinsic ability to fluoresce without the need for cofactors. Fluorescent proteins from other organisms have since been cloned and studied, such as the sea pansy, which also expresses GFP (Matz et al., 1999) and coral, which produces a red fluorescent protein, DsRed (Ward and Cormier, 1978). Despite differences at the primary sequence level, all fluorescent proteins form a β -barrel 'can' with an α -helix situated in the center (Ormo et al., 1996). It is in the α -helix where the chromophore is located and in GFP it is formed by a cyclic tripeptide of residues 65Ser-Tyr-Gly67 (Cody et al., 1993).

The protein environment surrounding the chromophore controls certain properties such as excitation and emission spectrum, quantum yield, fluorescence lifetime, brightness and photobleaching. By mutating different residues within the original GFP a now commonly used enhanced version (eGFP) was produced, which fluoresces 35 times more brightly and has a red-shifted excitation and emission spectrum (Cormack et al., 1996). Several groups exploring further mutations have collectively produced a variety of

different colours such as yellow (eYFP; Ormo et al., 1996), cyan (eCFP; Heim and Tsien, 1996) and blue (eBFP; Heim et al., 1994). A newer version of eYFP, monomeric citrine, was produced in order to maintain the brightness of eYFP but reduce its environmental sensitivities to pH and photobleaching (Griesbeck et al., 2001). Monomeric cerulean (mCer) is an improvement of eCFP as it is 2.5 times brighter and has an improved quantum yield and a higher extinction coefficient (Rizzo et al., 2004).

Fluorescent proteins closer to the red end of the visible spectrum are mainly derivatives of DsRed. One of the problems found in using DsRed as a fusion protein was that in order to fluoresce it must form a tetramer, which could affect the function and localization of the fused protein of interest. A mutation of 33 residues produced a red-shifted and monomeric form known as mRFP1 (Campbell et al., 2002). A separate mutational analysis produced a series of DsRed variants that ranged from yellow to purple, all of which were named after fruit, (Shaner et al., 2004). One of the proteins produced, known as mCherry has now replaced mRFP1 in our lab because it is less sensitive to amino-terminal fusions and is slightly brighter (Shaner et al., 2004). Due the non-overlapping spectrum of the developed fluorescent proteins we are now able to perform triple co-expression studies with the use of either eYFP, mCer and mCherry or photoswitching-CFP, eGFP and mCherry (Xia et al., 2006).

A common technique used to study the dynamics of proteins is fluorescent recovery after photobleaching (FRAP), which was first developed 30 years ago to study proteins tagged to fluorescent dyes (Axelrod et al., 1976). This technique takes advantage of the fact that when a fluorophore is exposed to an intense light source its fluorescence ability is permanently destroyed. The use of fluorescent proteins has made FRAP a commonly used technique (Lippincott-Schwartz et al., 2003). Frequent uses for FRAP include the study of membrane protein dynamics (Chen et al., 2006), nucleocytoplasmic shuttling (Howell and Truant, 2002) and distinguishing soluble from insoluble fractions of a protein (Carrero et al., 2003).

The majority of experiments in this thesis involved expressing fluorescent proteins fused to ataxin-3 or other proteins of interest in mammalian cells lines for visualization using fluorescence microscopy. This allows the use of live-cell imaging to monitor the cellular distribution and the dynamics of ataxin-3 in real-time. The use of eYFP and mCer allowed for the co-expression and simultaneous visualization of two different proteins, which proved to be extremely useful for co-localization and cellular distribution studies. The ability of eGFP to photobleach under an intense laser source has been valuable for the study of nucleocytoplasmic dynamics of ataxin-3.

1.9 Project Overview

The subcellular localization of both normal and mutant ataxin-3 is varied in the affected neurons of humans and mice. In immortalized cells lines the distribution varies between different cell types. The mechanisms that govern these differences are currently unknown. Furthermore, the exact pathway of ataxin-3 translocation between the nucleus and the cytoplasm has not been explored. This project sets out to investigate both the

shuttling capabilities of normal and expanded ataxin-3 and the mechanisms of nuclear entry and nuclear export of normal ataxin-3.

We hypothesized that ataxin-3 is able to shuttle in and out of the nucleus. In addition we also wanted to test whether the length of the polyglutamine tract affected the kinetics of shuttling. We used eGFP tagged ataxin-3 with three different polyglutamine lengths of Q0, Q28 and Q84. We expressed these ataxin-3 moieties in HEK 293 cells, photobleached the nucleus or the cytoplasm and monitored the recovery of fluorescence after photobleaching of either compartment.

Next, we hypothesized that ataxin-3 contained a classic NLS within its amino acid sequence and that this sequence is mediating the import of ataxin-3. To test this hypothesis, an NLS deletion mutant was constructed by removing the four basic residues of the putative NLS. We also hypothesized that ataxin-3 contained either one or potentially two leucine-rich NES, which would mediate its export out of the nucleus. Initially, this was tested by performing point mutations on the last two hydrophobic residues of the putative NES. The NLS deletion mutant and the NES mutants were expressed in NIH3T3 cells and then imaged to analyze their subcellular localization, which was compared to wild-type ataxin-3. The results obtained from the NES point mutations prompted further testing, which was done by deleting the entire putative NES sequence followed by imaging to assess the localization. Overall, these results indicated that the putative signals identified in the sequence did not mediate the transport of ataxin-3 across the nuclear envelope. Ataxin-3 may contain other transport signals that are currently uncharacterized or it may translocate by an entirely different mechanism.

To ensure that ataxin-3 did not contain any NESs, cells expressing ataxin-3 were treated with leptomycin B (LMB). This drug inhibits nuclear export that is mediated by the export receptor, CRM1, which recognizes substrates that contain the leucine-rich NES. We tested whether LMB treatment would change the subcellular localization of ataxin-3 and confirm the presence of a CRM1 dependent NES in ataxin-3. Four different cell lines were used including, HEK 293, mouse striatal (*STHdh^{Q7/Q7}*), NIH3T3 and MCF7 cells. Results from this analysis showed that ataxin-3 was more LMB sensitive in HEK 293 and *STHdh^{Q7/Q7}* and only marginally sensitive in the other cell lines. This suggested that there was not an endogenous CRM1 dependent NES in ataxin-3, as all cell lines did not show a similar result. This result also suggested that there is an unknown factor specific to HEK 293 and *STHdh^{Q7/Q7}* cells that may contain an NES that is used to export ataxin-3.

We hypothesized that this unknown factor could potentially be one of the known binding partners of ataxin-3. During preliminary testing we found that the tubulin deacetylating protein, HDAC6 was the most promising candidate. It had been postulated that this protein contained an NES and an NLS (Bertos et al., 2004) and we hypothesized that our deletion mutations would confirm this. As well, we hypothesized that HDAC6 had the ability to alter the subcellular localization. This was examined by co-expressing ataxin-3 and different variations of HDAC6 (wild-type, NES mutant and NLS mutant) in NIH3T3 cells and analyzing the subcellular localization of ataxin-3. Our results show that HDAC6 does contain an NES and an NLS and that although it does slightly affect the cellular distribution of ataxin-3, we believe it does not act as a shuttling component of

ataxin-3. Further investigations to identify a shuttling factor could potentially be an interesting extension of this project. This factor could be isolated and identified by performing a co-immunoprecipitation using eGFP-ataxin-3 as bait and HEK 293 and NIH3T3 cell lysate. It would be expected that the ataxin-3 shuttling factor would only be present in HEK 293 cells.

Materials and Methods:

2.1 Plasmids

All fluorescent fusion protein constructs were cloned into the same plasmid background and multiple cloning site as peGFP-C1 (BD Clontech). peGFP-C1, peYFP-C1 and pIkB-eGFP were all purchased from BD Clontech. pmRFP-C1 was made by Joanna Graczyk by PCR amplifying mRFP DNA (Campbell et al. 2002), (kind gift of R.Y. Tsien, University of California, San Diego), using the primers RT0335 and RT0337 to introduce *NheI* and *BspEI* restriction sites. The PCR product and peGFP-C1, were digested by the mentioned restriction endonucleases and ligated with T4 DNA ligase (Fermentas) with the result being an mRFP gene against the peGFP-C1 background. pmCher-C1 was made by Jianrun Xia by PCR amplifying mCher DNA (Shaner et al. 2004), (kind gift of R.Y. Tsien, University of California, San Diego), using the primers RT0797 and RT0798 to introduce *AgeI* and *BspEI* restriction sites. The insert and peGFP-C1 vector were digested by the mentioned restriction endonucleases and ligated with T4 DNA ligase. PmCer-C1 was a kind gift from D. W. Piston (Vanderbilt University).

peGFP-ataxin-3 [Q28], peGFP-ataxin-3 [84] and pataxin-3-eGFP [Q166] were kind gifts from R. N. Pittman (University of Pennsylvania, Philadelphia). The NLS deletion mutant was made by deleting the residues, ²⁹²RKRR₂₉₅ in ataxin-3 using peGFP-ataxin-3 [Q28] as a template. This was accomplished by site-directed mutagenesis using the QuikChange kit (Stratagene) and the mutagenesis primers RT0805 and RT0806, which flanked the putative NLS. The first NES mutant was made by introducing point mutations encoding for the I77A, L84S and V86A amino acid changes in the first putative NES of ataxin-3 using peGFP-ataxin-3 [Q28] as a template. This was accomplished by performing two site-directed mutagenesis reactions using the QuikChange kit. In the first reaction mutagenesis primers RT0766 and RT0767 were used to make changes to L84 and V86. In the second reaction the above mutant was used as a template and mutagenesis primers RT0846 and RT0847 were used to make the change to I77. Another ataxin-3 mutant was made, which destroyed the second putative NES by introducing point mutations encoding for the F355A and L357S amino acid changes using peGFP-ataxin-3 [Q28] as a template. This was again accomplished by site-directed mutagenesis using the QuikChange kit and the mutagenesis primers RT0823 and RT0824. The NES double deletion mutant involved deleting both putative NES mutants, ⁷⁷IQVISNALKV₈₆ and ³⁴⁹FIMFATFTL₃₅₇ in ataxin-3 using peGFP-ataxin-3 [Q28] as a template. This was accomplished by site-directed mutagenesis using the QuikChange kit. However, both mutations were introduced simultaneously by using four mutagenesis primers in the PCR reaction. These primers were RT0938, RT0939, RT0940 and RT0941. The ataxin-3 [Q0] construct was made by deleting the polyglutamine tract of ataxin-3 using peGFP-ataxin-3 [Q28] as a template. Inverse PCR was performed using Pfu Ultra DNA polymerase (Stratagene) and PCR primers RT0836 and RT0837. PeYFP-ataxin-3 [Q28] was made by the following method. Ataxin-3 was PCR amplified from peGFP-ataxin-3 [Q28] using PCR primers RT0813 and RT0814 in order to introduce two *BamHI*

restriction sites. Both PCR product and peGFP-ataxin-3 [Q28] were digested with *Bam*HI and the resultant insert and vector products were ligated with T4 DNA ligase.

pmRFP-I κ B was made by Meghan Holmes in the following manner. I κ B was PCR amplified using primers RT0794 and RT0795 in order to introduce *Eco*RI and *Xba*I restriction sites. The pmRFP-C1 vector and the PCR product were digested with the named restriction endonucleases and the resulting products were ligated with T4 DNA ligase.

pmyc-hHDAC1 and pflag-hHDAC2 were kind gifts from R. N. Pittman (University of Pennsylvania, Philadelphia). peGFP-hHDAC6 and peGFP-hHDAC6 Δ SE14 were kind gifts from X. Yang (McGill University). The hHDAC6 Δ SE14 has residues ₈₈₄SASFGGEESTPGQTN₈₉₇ deleted. mCer-hHDAC6 and mCer-hHDAC6 Δ SE14 were both constructed by the following method. hHDAC6 and hHDAC6 Δ SE14 were PCR amplified using primers RT0891 and RT0892 and restriction sites *Bgl*II and *Hind*III. The vector, pmCer-C1 and the PCR product were both digested with the name restriction endonucleases and the resulting products were ligated with T4 DNA ligase. The NES double deletion mutant was made using both the mCER-hHDAC6 and the mCER-hHDAC6 Δ SE14 background. The mutation involved deleting both putative NES mutants, ₆₇LIVGLQGMDLNL₇₈ and ₁₀₄₉LIGSLRTLLEL₁₀₅₈. This was accomplished in a similar manner as the double deletion, using site-directed mutagenesis and the QuikChange kit. The four primers used in the PCR reaction were RT0907, RT0908, RT0909 and RT0910. The NLS deletion mutant, where residues 14-44 were deleted, was made in a similar method as the other deletion mutants using the Quikchange kit and primers, RT0952 and RT0953. Both mCer-hHDAC6 and mCER-hHDAC6 Δ SE14 were used as templates.

All cloning involving PCR amplification used Deep Vent (New England Bioscience) unless otherwise stated. All restriction endonucleases were also from New England Biosciences. Newly made plasmid constructs were verified by PCR sequencing by the McMaster Mobix facility (McMaster University).

2.2 Tissue Culture

The cells lines used in this study were NIH3T3 (ATCC, CCL-2), MCF7 (kind gift from D. W. Andrews, McMaster University), HEK 293 (kind gift from D. W. Andrews, McMaster University) and *STHdh*^{Q7/Q7} (kind gift from M. E. McDonald, Harvard University). NIH3T3, MCF7 and *STHdh*^{Q7/Q7} cells were cultured in Dulbecco's Modified Eagle Medium (Invitrogen) and were supplemented with 10% Fetal Bovine Serum (Invitrogen) and incubated at 37°C with 10% CO₂. *STHdh*^{Q7/Q7} cells were further supplemented with 200 μ g/mL of Geneticin (Invitrogen) and incubated at 33°C in order to maintain clonality. HEK 293 cells were grown in Alpha Minimal Essential Medium (Invitrogen) and incubated at 37°C with 10% CO₂.

Cells were passaged when grown to 80 % confluency with 10 % trypsin-EDTA (Invitrogen). HEK 293 cells were passaged in the absence of trypsin-EDTA. Frozen cells were stored in 10 % DMSO in a liquid nitrogen tank. For live-cell imaging 70,000 to 150,000 cells were seeded onto 35 mm, glass bottomed dishes 16 to 24 hours before

transfection with the exception of HEK 293 cells, which were transfected immediately following seeding. Glass bottomed dishes were prepared as previously described (Howell and Truant, 2002) and stored in 70 % ethanol and washed twice with phosphate buffered saline before use. For fixed-cell imaging 70,000 to 100,000 cells were seeded onto a 35 mm dish with a cover slip resting on the bottom. Similar waiting times prior to transfection were followed as described for live-cell imaging.

2.3 Transfections

All cells were transfected using polyethylenimine (ExGEN 500, Fermentas) using a slightly modified protocol from the manufacturers instructions. A total of 3 μ g or less of DNA was added to 75 μ L of PBS. When transfecting with 4 μ g or more of DNA, an additional 25 μ L of PBS was used for each μ g of DNA. All plasmids used for transfections were purified using the GenElute™ Plasmid Miniprep Kit (Sigma Aldridge) or the PEG/lithium chloride method.

2.4 Leptomycin B Assay

Cells expressing eGFP, eGFP-ataxin-3 [Q28] or eGFP-I κ B were treated with 10 ng/mL of leptomycin B (LMB, Sigma) for 8, 16 and 24 hours in serum free media. Co-expression studies with eGFP-ataxin-3 [Q28] and other constructs of interest were treated with the drug for 24 hours in serum free media. All cells, including untreated controls were incubated in serum free media for 24 hours to maintain consistent growth conditions. Following the LMB treatment cells were washed 2 x in PBS and were fixed in 4 % paraformaldehyde for 30 min. Fixed cells were then washed 2 x in PBS and mounted onto glass slides in 90 % glycerol and sealed with clear nail polish.

2.5 Epifluorescence Microscopy

Live-cell and fixed-cell microscopy was performed on a Nikon TE200 inverted fluorescence microscope with a 175 W xenon arc lamp light source (Sutter Instruments LB-LS/17). Nikon 63X plan apochromat (numerical aperture of 1.3) oil immersion objective was used. The following filter sets denoting bandpass excitation and emission filters for each fluorophore were used: Hoechst dye: 387 nm and 447 nm, Cerulean: 438 nm and 483 nm, eGFP: 472 nm and 520 nm, eYFP: 500 nm and 542 nm, mRFP and mCherry: 562 nm and 624 nm (Semrock). Images were captured in each channel separately using a monochrome camera (Hamamatsu model C4743-95 and controller). The software used to control the microscope and to capture and pseudo-colour merged images was Simple PCI version 5.3.1.081004 (Compix, Inc.). Exposure time for each image ranged from 0.1 to 1.5 seconds at a resolution of 1024 x 768 pixels or 1024 x 1024 pixels. Images were saved as 24 bit RGB, tagged image file format (TIFF)

uncompressed files. TIFF files were then subject to pseudo-colouring as well as brightness and contrast adjustments using Laser Scanning Microscope (LSM) Image Browser version 4.0.0.157 (Carl Zeiss). Digital deconvolution was performed on some of the images using Autodeblur version 9.3 (Autoquant Imaging, Inc.) Gold Edition. Corel Photopaint and Corel Draw version 12 (Corel Corporation) was used to further brighten, contrast and prepare images for publication.

2.6 Laser Confocal Microscopy

All iFRAP experiments were performed on the MP Leica SP5 Laser Scanning Microscope (Leica Microsystems) with a 63X glycerol immersion objective (numerical aperture of 1.3). An Argon ion laser at 95 % intensity was used for excitation and photobleaching of eGFP at 488 nm. For the time-lapsed recovery images the laser was used at a 5 to 6 % intensity. The software used to control the instrument, photobleach and capture images was LAS AF confocal (Leica Microsystems). Images were captured at 400 Hz. Corel Photopaint and Corel Draw version 12 (Corel Corporation) was used to further brighten, contrast and prepare images for publication.

2.7 Inverse Fluorescence Recovery After Photobleaching

HEK 293 cells were used for all iFRAP experiments. 35 mm dishes were treated with poly-L-lysine prior to being seeded with cells. Cells were transfected 24 hours prior to imaging with 1 µg of peGFP-C1, peGFP-ataxin-3 [Q0], peGFP-ataxin-3 [Q28] or peGFP-ataxin-3 [Q84] expression plasmids. Prior to bleaching two images were taken of the cell and were designated as pre-bleach images. For each iFRAP experiment either the entire nucleus or the entire cytoplasm was bleached. A nuclear bleach involved four passes of the laser at full power every 1.301 s, while a cytoplasm bleach involved six or seven passes of the laser. Fluorescence recovery was monitored and imaged over time until the amount of fluorescence intensity in the bleached and non-bleached regions equilibrated. Four to six cells were used for each iFRAP trial.

2.8 Image Analysis

All images were analyzed using ImageJ version 1.34s (National Institute of Health, USA). In order to measure the percent nuclear fluorescence intensity three region of interests (ROI) were manually defined for each image. These included the nucleus, the total cell and the background. An output of area in number of pixels and mean fluorescence intensity was provided for each ROI defined. Background fluorescence intensity was calculated by obtaining the mean fluorescence intensity of the area outside of the cell and multiplying it by either the area of the nucleus or the area of the total cell. These values were then subtracted from the nuclear mean fluorescence intensity and the

total cell mean fluorescence intensity respectively. The corrected nuclear fluorescence intensity was then divided by the corrected total cell fluorescence intensity and multiplied by 100 % to yield the percent nuclear fluorescence intensity (%NFI; Figure 3A).

All iFRAP experiments were analyzed in the following manner. Firstly, the raw data was quantified, which involved calculating the %NFI for every cell imaged at each selected time point. In the case of cytoplasmic recovery this value was subtracted from 100 % in order to obtain percent cytoplasmic fluorescence intensity (%CFI). Secondly, the quantified data was normalized to allow direct comparison of iFRAP events in different cells. This involved the use of a slightly modified version of equation (1) from Goodwin and Kenwothy (Goodwin and Kenwothy, 2005). The average of the two pre-bleach images ($\%NFI_{\text{pre-bleach}}$) was set to 100 % fluorescence recovery and the post-bleach image at $t = 0$ seconds ($\%NFI_{\text{post-bleach}(t=0)}$) was set to 0 % fluorescence recovery (Figure 3B). The remaining time-lapse images were normalized against the pre-bleach and post-bleach($t=0$) images and by subtracting the background fluorescence as per equation (2; Figure 3B). Lastly, the % nuclear and cytoplasmic recovery for each protein was plotted against time to obtain the recovery curves. The half-times and the recovery endpoint (curve amplitude) was determined by tracing the time to 50 % recovery of fluorescence intensity from the recovery curves.

2.9 Statistical Analysis

All data was analyzed in Microsoft Excel 2003 (Microsoft Corporation). All mean error bars shown were calculated using the standard error of the mean (σ_M) equation. Where the standard deviation was divided by the square root of the number of samples N . Significance testing involved using the two-tailed Students T-test, with a confidence level (α) of 0.001. P-values were obtained from either charts found in a text book (Moore and McCabe, 2003) or calculated using software (retrieved from <http://www.physics.csbsju.edu/stats/t-test.html>, 2006).

Results and Discussion:

3.1 *Ataxin-3 is able to shuttle in and out of the nucleus*

The subcellular localization of ataxin-3 is highly variable depending on the type of cell expressing ataxin-3 (Paulson et al., 1997; Tait et al., 1998; Trottier et al., 1998; Cemal et al., 2002). This variable localization suggests that ataxin-3 is able to translocate across the nuclear envelope and shuttle in and out of the nucleus. Inverse fluorescence recovery after photobleaching (iFRAP) was used to test the shuttling capabilities of ataxin-3. Cells expressing fluorescently tagged ataxin-3 were photobleached at a high laser intensity, in either the cytoplasm or the nucleus. This was followed by time lapsed imaging at a lower laser intensity to monitor fluorescent recovery into the bleached compartment from the unbleached compartment. In addition, the influence of the polyglutamine tract on shuttling dynamics was examined. As a control, the shuttling ability of eGFP was tested to compare the recovery of ataxin-3 to a small protein without transport signals that is able to diffuse across the NPC.

Expression plasmids for eGFP or eGFP-ataxin-3 [Q0], [Q28] or [Q84] were transiently transfected in HEK 293 cells and following 24 - 28 hours of expression, either the nucleus or the cytoplasm of a single cell was photobleached and monitored for fluorescent recovery. The duration of the post-bleach analysis was optimized based on the time required for fluorescence to reach an equilibrium between the nucleus and the cytoplasm post photobleaching. This is known as the recovery endvalue. The pre-bleach and post-bleach images of four to six cells per iFRAP experiment were analyzed by measuring the percent nuclear fluorescence intensity (%NFI) at different time points during recovery (Figure 3A). These values were then corrected for cell to cell variations in protein expression levels, background fluorescence and loss of total fluorescence after bleaching (Figure 3B). The recovery half-time for each iFRAP condition was determined by tracing the time to 50 % recovery of fluorescence intensity from the recovery curves. The endvalue was obtained from the maximum amplitude from the recovery curves.

Figure 4A illustrates the pre-bleach localization of eGFP-ataxin-3 [Q28] (Figure 4A,a-b), the cytoplasmic photobleaching event (Figure 4A,c-d), the time-lapsed fluorescence recovery (Figure 4A,e-r) and the corresponding brightfield images. Similarly, Figure 4B shows an iFRAP experiment where the nucleus is bleached followed by time-lapsed fluorescence recovery (Figure 4B,a-r). This demonstrates the ability of eGFP-ataxin-3 to translocate into and out of the nucleus.

From the recovery curves of eGFP it was found that both cytoplasmic and nuclear fluorescence recovery occurred at about 150 seconds to an endvalue of approximately 75 % and 88 %, respectively and had half-times of approximately 39 and 42 seconds respectively (Figure 4A,t; 4B,x). Next, the cytoplasmic recovery of ataxin-3 was examined with different polyglutamine lengths (Figure 4A,s). The curve appears to contain two phases, however only a single half-time was determined since the number of data points within the first phase of recovery is too small. eGFP-ataxin-3 [Q0] and [Q84] reached a recovery endvalue of about 37 % at approximately 75 seconds and 30 % at 35 seconds respectively, whereas it took the [Q28] protein about 170 seconds to recover to

approximately 41 %. The half-times for [Q0], [Q28] and [Q84] were approximately 12, 30 and 11 seconds respectively.

The ataxin-3 cytoplasmic recovery curves were interesting when compared to the eGFP curves. eGFP-ataxin-3 [Q28] had a similar endvalue recovery time and half-time to that of eGFP even though this fusion protein has an increased mass of 43 kDa. As well, it appears that eGFP-ataxin-3 recovery is biphasic. This initial stage of recovery is very fast with the latter stage of recovery occurring at a much slower rate. Moreover, removing the polyglutamine tract or increasing the number of repeats to 84 causes eGFP-ataxin-3 to initially exit the nucleus at a faster rate than normal eGFP-ataxin-3. Also observed, was the low endvalues for eGFP-ataxin-3 compared to eGFP, implying that an immobile fraction of ataxin-3 was retained in the nucleus.

Finally, the nuclear recovery of eGFP-ataxin-3 was studied (Figure 4B,s). The most drastic difference between cytoplasmic and nuclear recovery was the amount of time it took to reach the recovery endvalue. [Q0], [Q28] and [Q84] plateaued in about 15 minutes to approximately 70 %, 17 minutes to 57 % and 7 minutes to 34 % respectively. The half-times also increased to approximately 4.1, 3.8 and 1.1 minutes respectively. It appeared as though protein entering the nucleus from the cytoplasm was quickly exiting the nucleus thus increasing the amount of time it took to reach the recovery equilibrium between the two compartments. It was also observed that as the polyglutamine length in ataxin-3 increased, the nuclear recovery endvalue decreased. Lastly, eGFP-ataxin-3 [Q84] reached maximum recovery about 3.5 times faster than [Q0] and [Q28]. It is apparent that the polyglutamine tract is altering the recovery and the mobility of cytoplasmic ataxin-3.

The results shown in Figure 4 clearly demonstrate that ataxin-3 is able to shuttle in and out of the nucleus. This is in agreement with its variable subcellular localization patterns in different cell types. Further insight on the dynamics of nuclear import and export of ataxin-3 were also revealed. We have shown that the recovery of ataxin-3 has at least two stages compared to eGFP alone, that cytoplasmic recovery is faster than nuclear recovery and that the polyglutamine tract in ataxin-3 affects its nuclear recovery.

In the cytoplasmic photobleaching experiment the first recovery phase lasted about 15 seconds and consisted of soluble protein quickly entering the cytoplasm followed by a slower and incomplete recovery of the remaining ataxin-3. We believe that the initial recovery is that of a pool of over-expressed ataxin-3 that is in excess of any cellular factors or targets. HEK 293 cells are known for their high expression levels of transfected protein. Thus, it is possible that this excess protein is non-functional and is in a mobile form that is readily able to recover quickly into the nucleus.

The second phase of cytoplasmic recovery is slower with endvalues that range from about 30 % to 41 %. These values are lower than the endvalue of eGFP cytoplasmic recovery. This suggests that there is an immobile fraction of ataxin-3. A study by Chai et al., looked at the ability of ataxin-3 [Q84] to recover into small areas bleached within the nucleus and found that while soluble protein recovered very quickly, the inclusions did not recover at all (Chai et al., 2002). It is possible that within the nucleus inclusions are forming that are beyond the visible limit of the microscope. These inclusions would have mobilities that are dependent on polyglutamine length, which would explain why the

recovery endvalue is smaller for ataxin-3 than eGFP, which is inert in the cell. These inclusions could also contain interaction partners that may sequester ataxin-3, therefore retaining it in the nucleus.

The nuclear fluorescence recovery in Figure 4B shows that ataxin-3 is able to enter the nucleus. The dynamics of this recovery differ from that observed in eGFP nuclear recovery and ataxin-3 cytoplasmic recovery, in that it takes about six times as long (Figure 4A,s; 4B,s). As seen with the cytoplasmic recovery curves, there is an initial recovery phase that is very rapid, which is then followed by a second, slower recovery phase (Figure 4B,s). However, unlike the second phase of cytoplasmic recovery, which was about 3 minutes long, the second phase of nuclear recovery was 19 minutes long. We believe that this slower phase of recovery is due to the rapid export of ataxin-3 from the nucleus, such that as soon as protein is entering the nucleus it is quickly exiting followed by another round of re-entry causing a long delay in reaching maximum recovery. Faster nuclear export is in agreement with the cytoplasmic localization that is observed in the brain tissue of humans with normal ataxin-3 (Paulson et al., 1997). As well, HEK 293s also exhibit expression patterns where ataxin-3 appears to be more concentrated in the cytoplasm as oppose to being evenly distributed (Figure 4A,a; 4B,a; quantification not shown). Thus, the faster nuclear export seen in this iFRAP study illustrates that the dynamic equilibrium of protein localization is towards the cytoplasm. It would be beneficial to observe whether performing similar experiments on other cell lines such NIH3T3 cells, which have a more nuclear ataxin-3 distribution, would alter the recovery kinetics seen in HEK 293 cells.

The most interesting observation in the iFRAP nuclear recovery experiment is the effect that the polyglutamine length had on the recovery trends. As the number of glutamines in the tract increased the recovery endvalue decreased. We believe that this is due to the polyglutamine tract either mediating the formation of insoluble cytoplasmic inclusions or influencing protein-protein interactions. In terms of nuclear recovery the effect would be similar to what was observed in cytoplasmic recovery where we believe that the formation of inclusions in the cytoplasm influences the rate of nuclear recovery. Evidence accumulated by *in vitro* and cellular studies have shown that an abnormal polyglutamine tract causes the formation of insoluble aggregates while normal length ataxin-3 forms SDS soluble inclusions (Paulson et al., 1997; Bevivino and Loll, 2001; Chai et al., 2002). However, there are no studies on cytoplasmic inclusions. In the Truant lab cytoplasmic inclusions are commonly seen in NIH3T3, *STHdh*^{Q7/Q7} and MCF7 cell lines and are formed by both normal and polyglutamine expanded ataxin-3 but not the [Q0] version. In fact, a 6.5 hour movie illustrates that ataxin-3 [Q166]-eGFP expressed in a *STHdh*^{Q7/Q7} cell forms both nuclear and cytoplasmic inclusions (Supplemental Video 1). The cytoplasmic inclusions were small, highly mobile and did not appear to behave like aggregates. Whereas the nuclear inclusions were larger in size and were less mobile. It is possible that the inclusions eventually aggregate after a greater concentration has accumulated within the cell. Moreover, a longer polyglutamine tract could increase the likelihood for protein to become sequestered into the inclusions. This model could fit with the nuclear recovery data observed here.

The polyglutamine tract may also influence the affinity of different protein interactions. This would be in accordance with the data obtained by nuclear iFRAP. Of the known ataxin-3 binding partners, only the interaction with VCP/p97 has been found to be affected by the polyglutamine tract such that pathogenic ataxin-3 has a greater affinity for VCP/p97 (Hirabayashi et al., 2001; Zhong and Pittman, 2006). Interactions with ubiquitin (Berke et al., 2005) and hHRad23a and b (Wang et al., 2000) have also been tested but do not appear to be affected by the polyglutamine region. As described in the introduction, VCP/p97 is a AAA-ATPases chaperone that is abundantly expressed and essential to cells. Recently, it has been implicated, along with ataxin-3, in ER associated protein degradation (ERAD). It is thought that both proteins work together to extract misfolded protein from the ER and transport it to the proteasome for degradation with ataxin-3 specifically working to regulate this process through its deubiquitinating activity (Zhong and Pittman, 2006). It is plausible that during the iFRAP process ER stress occurs due to the high intensity laser that bleaches the nucleus. This could cause an increase in the activity of VCP/p97 and ataxin-3. As well, with a polyglutamine length of [Q0] the expressed ataxin-3 would not be able to associate with VCP/p97 and would be more available to translocate into the nucleus. In the other extreme, ataxin-3 [Q84] would form stronger interactions with VCP/p97 and would not be as available to recover into the nucleus.

3.2 The two putative NES motifs and the NLS found in ataxin-3 do not function as nucleocytoplasmic transport signals.

Visual inspection of the amino acid sequence of ataxin-3 has revealed two putative leucine-rich nuclear export signals (NES) and a nuclear localization signal (NLS). The location of the first NES (NESI) is within the Josephin domain (JD), the second NES (NESII) is located at the carboxyl-terminus and the NLS is located just upstream of the polyglutamine tract (Figure 5A,a). The sequence of NESI (₇₆SIQVISNALKVW₈₇) and NESII (₃₄₉PFIMFATFTLY₃₅₇) follow the loose consensus sequence of NES motifs that are HIV-1 Rev-like, leucine-rich and are dependent on the CRM1 receptor for export. The leucine can be replaced by hydrophobic residues such as isoleucine, valine, phenylalanine and methionine. The sequence of the NLS (₃₅₆LKRRE₃₆₁) follows the consensus of the classical, monopartite NLSs, which contain a series of four to six basic residues, as seen in the SV40 large T antigen NLS (Kalderon et al., 1984). Both NESI and NLS are highly conserved among ataxin-3 orthologs (Figure 5A,b,d). NESII is only found in the MJD1a isoform (Figure 5A,c). We hypothesized that these putative export and import signals may contribute to the nucleocytoplasmic translocation of ataxin-3. We also hypothesized that by mutating the signals in ataxin-3 and expressing the mutants in cells there would be a change in the subcellular localization of ataxin-3.

It has been demonstrated that mutating the last two hydrophobic residues of an NES effectively abolishes export activity (Xia et al., 2003). Thus, in both NESI and NESII such mutations were made (Figure 5A,e). In addition, I77 in NESI was also

mutated because according to the NMR structure of the JD it is one of two residues (the other is V86) that are exposed (Figure 5A,f). The putative NLS contains four consecutive basic residues and thus deleting those residues should abolish any potential import activity that may be due to that signal (Figure 5A,f).

eGFP-ataxin-3 [Q28] was used in order to measure the subcellular localization of the wild type and mutant protein. Wild type, NESmI, NESmII and Δ NLSm eGFP-ataxin-3 [Q28] expression plasmids were transiently transfected into *STHdh^{Q7/Q7}* cells, which were then imaged 24-28 hours post-transfection. 80-100 images were captured for each construct tested. Each image was analyzed for percent nuclear fluorescence intensity (%NFI) using the software ImageJ version 1.33 (National Institute of Health, USA) and the equations found in Figure 3A.

The %NFI of eGFP-ataxin-3 [Q28] was 36.6 % in *STHdh^{Q7/Q7}* cells. The %NFI for NESmI, NESmII and Δ NLSm were 38.1, 37.4 and 36.3 % respectively (Figure 5B). The small changes in subcellular localization of the mutants were not statistically significant. The lack of change in %NFI suggests that the subcellular localization of ataxin-3 was not altered. It was expected that mutating the putative NES motifs would cause an increase in %NFI and that deleting the NLS would cause a decrease in %NFI. These results suggest that the putative export and import signals that were tested are not functional and do not participate in the nucleocytoplasmic transport of ataxin-3.

The amino acid sequence of both the putative NES motifs and the NLS appear to indicate that they are export and import recognition signals. These results have indicated otherwise. With regards to the putative NES motifs this is not entirely surprising. The APC tumor suppressor protein, p53 and STAT-1 have solved protein structures and have known leucine-rich, CRM1 dependent NES motifs (Neufeld et al., 2000; Stommel et al., 1999; Begitt et al., 2000). These NES motifs are located on an alpha-helix with the first three hydrophobic residues showing similar unidirectional orientation and the last hydrophobic residue in slightly varied positions (Figure 6A,a-b; Tickenbrock et al., 2002). When examining the solved structures of the above NES containing proteins, it was found that either the hydrophobic residues were exposed to the surface of the protein or were masked by another alpha-helix. In ataxin-3 the solution structure of the JD had been solved and this portion of the protein contains NESI (Mao et al., 2005; Nicastro et al., 2005). According to the structure the putative NES is also located within an alpha-helix. However, only the first (I77) and last (V86) hydrophobic residues are exposed at the surface, the second (I80) and third (L84) residues are buried within the protein and the orientation of the first three hydrophobic residues are not unidirectional (Figure 6B,a-c). This is different than the structure of the NES motifs found in the APC tumor suppressor protein, p53 and STAT-1. The second putative NES of ataxin-3 is located in the unstructured region of the carboxyl-terminus and the orientation of its hydrophobic residues is not known. It has been proposed that this region is unstructured and may not contain alpha-helices (Masino et al., 2003). This data reinforces the importance of functional testing of NES sequences, despite the fit to the known NES consensus. Software alignment is not sufficient to describe an NES in a protein.

At 43 kDa it is possible that the mode of nuclear export for ataxin-3 is through passive diffusion. When fused to eGFP the size is increased to 69 kDa, which may

arguably be beyond the diffusion limit. Even if ataxin-3 was able to diffuse it may still have active transport signals. For example, HIV-1 Rev is only 13 kDa and contains the most studied leucine-rich NES (Fischer et al., 1999). Mutating this NES causes a significant change in subcellular localization regardless of the ability of HIV-1 Rev to diffuse. There are also eight other karyopherins that are involved in nuclear export with signals that are not well characterized and may be found in ataxin-3 (Table 1). Nonetheless, in order to be sure that there are no leucine-rich, CRM1 dependent NESs in ataxin-3 leptomycin B export assays were performed in several different cell lines (next section).

The lack of change in subcellular localization following the deletion of the putative NLS in ataxin-3 demonstrates that this stretch of sequence is not a functional import signal. Recently, this region has been found to contain another function. It has the ability, along with the polyglutamine tract, to mediate binding of VCP/p97 (Goodrich et al., 2006). This same study also showed that the RRKR motif is found in the ubiquitin chain assembly factor E4B. E4B has the ability to interact with VCP through this motif and to date does not appear to localize to the nucleus. This data presented here and the study by Goodrich et al., suggests that this basic stretch of residues act as a VCP/p97 binding motif and not as an NLS.

Recent communication with our collaborator, Dr. Randall Pittman at the University of Pennsylvania, has shed some light on the mechanism of ataxin-3 nuclear transport. Using a nuclear import assay with permeabilized HeLa cells they found that ataxin-3 import is temperature, ATP and reticulocyte lysate dependent. However, they also found that ataxin-3 does not bind to importin- α or β 1. These findings imply two potential import scenarios. Firstly, the mode of nuclear entry may be mediated by one of the other eleven nuclear import receptors that have not been well characterized and as such do not have an NLS within ataxin-3 that could be easily identified (Table 1). Secondly, a “piggy-back” mechanism could be occurring where a binding partner imports ataxin-3 into the nucleus. Such “piggy-back” mechanisms have been seen in import and export (Shiota et al., 1999; Llorian et al., 2005).

3.3 Ataxin-3 is more leptomycin B sensitive in HEK 293 and STHdh^{Q7/Q7} cells than in NIH3T3 and MCF7 cells.

Proteins that contain leucine-rich NES motifs are exported from the nucleus via the export receptor, CRM1 when it is complexed to RAN-GTP. The compound Leptomycin B (LMB) can specifically and potently inhibit this process by covalently binding to Cys529 of the CRM1 protein (Kudo et al., 1999; Wolff et al., 1997). The structure and function of CRM1 are conserved throughout eukaryotes in all tissues (Kudo et al., 1997). Accordingly, any protein containing a CRM1 dependent NES should show nuclear retention in all eukaryotic cells when treated with LMB (Neville et al., 1999).

The mutational studies performed to test the putative NESs in ataxin-3 revealed that they were non-functional. However, to further validate this result a LMB assay was performed on ataxin-3. Dr. Randall Pittman at the University of Pennsylvania, had

informed us that ataxin-3 is LMB sensitive in HEK 293 cells (unpublished data). Thus, we also wanted to confirm their result. The LMB sensitivity assay was repeated in four different immortalized cell lines, transiently over-expressing eGFP-ataxin-3[Q28] including HEK 293, *STHdh*^{Q7/Q7}, NIH3T3 and MCF7 cells. As a negative control eGFP was used to account for the toxic effects that LMB confers on cells. The positive control used was eGFP-IκB, a protein that normally localizes almost exclusively to the cytoplasm and upon LMB treatment becomes retained in the nucleus (Huang et al., 2000).

The expression plasmids with the gene for the eGFP fusion proteins were transiently transfected and following 24 hours of expression the media was changed to a serum-free version and the cells were subject to treatment with 10 ng/mL of LMB, while control cells were left untreated. For HEK 293 cells the duration of the treatment was 8 hours and for the other cell lines it was 8, 16 and 24 hours. It was found that if HEK 293 cells were treated for longer than 10 hours the cells tended to round up and die. After the LMB treatment, cells were fixed using 4% paraformaldehyde and mounted on slides. Alternatively, HEK 293s were not fixed because the process caused the majority of the cells to lift up off the cover slip and did not provide useful images. These cells were instead imaged in our homemade live-cell dishes. For each experimental condition 80-100 cells were imaged and analyzed for percent nuclear fluorescence intensity.

In HEK 293 cells it was observed that the untreated group contained a mixed population of cells that expressed eGFP-ataxin-3 mainly in the cytoplasm and cells that expressed ataxin-3 in both the nucleus and the cytoplasm (Figure 7C,a). Conversely, cells treated with LMB contained eGFP-ataxin-3 that was localized in both the nucleus and the cytoplasm (Figure 7C,b). The mean %NFI of the group of treated and untreated cells was plotted and the difference in mean %NFI was slightly greater than 12 % (Figure 7C,d). The eGFP-IκB expressing cells demonstrated that the LMB was effective (Figure 7B,a-c). The mean %NFI of the eGFP expressing cells were slightly increased upon LMB treatment, which was expected and is most likely due to cellular toxicity (Figure 7A,a-c). From these results it was concluded that ataxin-3 is LMB sensitive in HEK 293 cells after an eight hour treatment.

Next, the LMB assay was tested in the *STHdh*^{Q7/Q7} cell line with similar methods of analysis. When comparing the values obtained from untreated cells expressing eGFP-ataxin-3 to cells treated for 8 hours with LMB, it was found that there was no significant change in %NFI (Figure 8C,a-b). However, for a 24 hour LMB treatment hours there was a significant increase of 9.3 % in the %NFI of ataxin-3 (Figure 8B,a,d,e). Therefore, in mouse striatal cells ataxin-3 is LMB sensitive. Cells expressing eGFP alone showed expected results (Figure 8A,a-c). Cells expressing eGFP-IκB were almost at the upper limit of the mean %NFI at the 8 hour LMB treatment (Figure 8B,a-e).

Lastly, the assay was tested on NIH3T3 and MCF7 cells. Comparable test conditions to the striatal cell line were used. In NIH3T3 cells the mean %NFI eGFP-ataxin-3 increased by 5 % between the untreated and 24 hour LMB treated cells (Figure 9C,a-e). This change is considered statistically significant and is greater than the observed change when looking at eGFP alone (Figure 9A,a-c). Similar results were seen when the LMB assay was performed in the MCF7 cell line (Figure 10). Cells expressing eGFP and eGFP-IκB showed results that were comparable to all of the cell lines (Figure

9A,a-c,B,a-e and 10A,a-c,B,a-e). From this data it is reasonable to conclude that ataxin-3 is only marginally LMB sensitive in NIH3T3 and MCF7 cells even though there is a statistically significant increase in mean %NFI after 24 hours of LMB treatment.

In the previous section, two putative NES motifs were shown to be non-functional as CRM1 dependent export signals. This set of data suggests that ataxin-3 is moderately sensitive to LMB in *STHdh*^{Q7/Q7} cells, the most sensitive in HEK 293 cells and only slightly sensitive in NIH3T3 and MCF7 cells. The difference in degrees of sensitivity indicate that ataxin-3 does not contain an NES that functions through the CRM1 dependent pathway. It could be debated that the difference in sensitivity between NIH3T3, MCF7 and *STHdh*^{Q7/Q7} cells were not very large. However, HEK 293 cells were only treated with LMB for 8 hours and the change in mean %NFI of eGFP-ataxin-3 was the greatest amongst the four cell lines. If there was an endogenous CRM1 dependent NES it would cause ataxin-3 to be sensitive to LMB to a similar extent in all cell types tested. This was observed for the positive control, IκB.

The characteristics of the two cell lines where ataxin-3 was more LMB sensitive is very intriguing. *STHdh*^{Q7/Q7} cells were derived from primary medium spiny striatal neurons in *Hdh*^{Q7/Q7} knock-in mice (Trettel et al., 2000). The striatum does not normally experience severe neurodegeneration in MJD/SCA3 but some neuronal dysfunction has been observed (Taniwaki et al., 1997). Although HEK 293 cells were derived from primary human kidney embryonic cells, they exhibit expression profiles that are very similar to that of neuronal stem cells and are very different from kidney cells (Shaw et al., 2002). Results that were re-examined from past studies using HEK 293 cells by other groups have also shown that this cell type demonstrates similar phenotypes to neuronal cells (Dautzenberg et al., 2002). Thus, the two cell lines that displayed greater LMB sensitivity to ataxin-3 have characteristics of neuronal cells. This could be relevant to the mechanism of pathogenesis since only a subset of neurons are affected by polyglutamine expanded ataxin-3.

An explanation for why ataxin-3 is only sensitive in certain cell types is that there could be an exogenous, CRM1 dependent NES that is located on a binding partner of ataxin-3. This factor may be expressed in higher levels in *STHdh*^{Q7/Q7} and HEK 293 cells when compared to NIH3T3 and MCF7 cells. The link to neurons is also very intriguing and an important discovery would be made if a factor that is specific to neurons was found to control the subcellular localization of ataxin-3. It is possible that a single protein could “piggy-back” ataxin-3 into and out of the nucleus or perhaps each direction would have its own transport factor. The “piggy-back” mechanism has been demonstrated for both nuclear import (Shiota et al., 1999; Llorian et al., 2005) and export (Huang et al., 2000). The following section describes a set of experiments that test four ataxin-3 binding partners for their ability to export ataxin-3.

3.4 HDAC6 does not shuttle ataxin-3 but it does alter the subcellular localization.

Continuing our studies from the previous results, we examined whether some of the known binding partners of ataxin-3 may have contributed to its selective sensitivity to

LMB. Additionally, if the binding partner tested assisted ataxin-3 in nuclear import, this could be observed in the same set of experiments. The experiments were performed by carrying out the LMB assay on NIH3T3 cells that co-expressed ataxin-3 and the selected binding partner. This cell line was chosen because ataxin-3, when expressed on its own, was only marginally LMB sensitive after 24 hours, therefore any additional increases in nuclear localization would be attributed to the co-expression of the binding partner.

In preliminary studies the following ataxin-3 binding partners were tested, human homolog Rad23b (hHRad23b), human histone deacetylase 6 (hHDAC6), human histone deacetylase 1 (hHDAC1) and human histone deacetylase 2 (hHDAC2). mRFP-ataxin-3 was co-expressed with eGFP-hHRad23b (Supplemental Figure 1A) or eGFP-hHDAC6 (data not shown) for 24 hours followed by a change to serum-free media, a 24 hour treatment of 10 ng/mL of LMB and imaging by widefield fluorescent microscopy. Through personal communication with Dr. Randall Pittman, we were informed that hHDAC1 and hHDAC2 were also potential binding partners of ataxin-3 and the expression plasmids were kindly provided for this project. hHDAC1 and hHDAC2 belong to the same class of histone deacetylases and both play a role in transcriptional repression by regulating chromatin architecture (Hassig and Schreiber, 1997). eGFP-ataxin-3 was co-expressed with myc-hHDAC1 and flag-hHDAC2 in a similar manner as described in the above (Supplemental Figure 1B, 1C).

Following a 24 hour LMB treatment in NIH3T3 cells, hHRad23b, hHDAC1 and hHDAC2 did not show a large effect on the subcellular localization of ataxin-3 when compared to ataxin-3 being expressed alone (Supplemental Figure 1)¹. However, there was a substantial increase in nuclear localization of ataxin-3 when hHDAC6 was tested and it was decided that further analysis of this protein with ataxin-3 would be pursued. Moreover, hHDAC6 contains putative import and CRM1 dependent export signals and have been partially tested by comparing the localization of full length hHDAC6 to deletion mutants where one or more of the signals were missing (Verdel et al., 2000; Kawaguchi et al., 2003).

HDAC6 is a part of a family of histone deacetylases that work to regulate transcription by deacetylating lysine groups on histones. Although hHDAC6 is implicated as a histone deacetylase it is better characterized as a cytoplasmic microtubule-associated deacetylase that can regulate microtubule acetylation and chemotactic cell motility (Hubbert et al., 2002). As described in the introduction, both ataxin-3 and HDAC6 are thought to be necessary for the formation of aggresomes and have been shown to directly interact (Burnett and Pittman, 2005). HDAC6 binds polyubiquitinated proteins and interacts with the dynein motor complex, facilitating

¹ This preliminary data was incorporated as a Supplemental Figure for a number of reasons. Firstly, mRFP-ataxin-3 was used for co-expression studies with hHRAD23a and hHDAC6. mRFP fusion proteins being expressed for longer than two days have altered expression patterns such that inclusions appear in the cytoplasm that are solely due to mRFP (Appendix I, Supplemental Figure 2). Secondly, hHDAC1 and hHDAC2 were not fused to a fluorescent protein and only hHDAC1 was visualized by immunofluorescence. The antibody used for hHDAC2 did not work, making it difficult to conclude if hHDAC2 was actually co-expressed with ataxin-3.

transport of misfolded proteins to the microtubule organizing center (MTOC) (Kawaguchi et al., 2003). In addition it has been shown to interact with another ataxin-3 binding partner, VCP/p97 and is able to associate with ubiquitin through its zinc-finger ubiquitin interaction (ZnF-UBP) domain (Seigneurin-Berny et al., 2001).

In 2000, an NES was identified in HDAC6 in a study that looked at the murine version of the protein (Verdel et al., 2000). Another study showed that murine HDAC6 is LMB sensitive and that the human version was LMB insensitive unless it lacked the amino acid sequence, ⁸⁸⁴SASFGGEESTPGQTN₁₀₂₂ (SE14; Bertos et al., 2004). This same study partially confirmed the presence of two NES motifs and an NLS (Figure 11A,a). The SE14 region is speculated to have a role in retaining hHDAC6 in the cytoplasm as it is only present in the human version of the protein.

With what is known about the NES and the SE14 region of hHDAC6 it was decided that the LMB assay would be performed by co-expressing ataxin-3 with different versions of hHDAC6. These included wild type hHDAC6, an SE14 deletion mutant, an NES deletion mutant, a mutant where both SE14 and the NESs were deleted and lastly, a mutant where both SE14 and the putative NLS were deleted. To ensure that the NESm caused a change in hHDAC6 localization, both of the NES motifs in hHDAC6 were deleted (Figure 11A,b) and the mean %NFI of mCER-hHDAC6 Δ SE14 and mCER-hHDAC6 Δ SE14 NESm were compared (Figure 11B,a-c). The mean %NFI of the NESm was significantly greater than the non-mutated version and it was concluded that hHDAC6 does contain at least one leucine-rich NES.

Since the use of mRFP or mCherry was not appropriate for this experiment (Supplemental Figure 2), ataxin-3 was fused to eYFP and hHDAC6 and its variants were fused to mCER, a derivative of eCFP (Rizzo et al., 2004). NIH3T3 cells were used as the model cell line. Cells co-transfected with expression plasmids containing eYFP-ataxin-3 and the mCER-hHDAC6 variants were expressed for 24 hours followed by a change to serum-free media and the addition of 10 ng/mL of LMB for 24 hours, while control cells were left untreated. Cells were then fixed and mounted onto slides to be imaged and observed for changes in subcellular localization in terms of %NFI. As a control, the effect of LMB on ataxin-3 when it was co-expressed with mCER alone was also tested (Table 2; Figure 12,a-f).

The mean %NFI of eYFP-ataxin-3 for each condition are displayed in Table 2. Images from the experiments illustrate that there was not a visible difference in ataxin-3 nuclear localization when co-expressed with wild type hHDAC6, the Δ SE14 + NESm nor the Δ SE14 + NLSm (Figure 12,g-x). In all five cases the %NFI of ataxin-3 slightly decreased when co-expressed with any of the hHDAC6 variants in untreated cells and increased in LMB treated cells (Table 1). Although the changes in ataxin-3 subcellular localization were all statistically significant the effects were not very severe. From these results it was concluded that hHDAC6 does not shuttle ataxin-3 in and out of the nucleus yet it does have an effect on its subcellular localization. It is also very interesting to note that when cells expressing mCER-hHDAC6 Δ SE14 NLSm were treated with LMB the mCER fusion protein entered the nucleus (Figure 12,s,v). This implies that hHDAC6 has another mechanism for nuclear entry and that the putative NLS that was deleted did not fully prevent hHDAC6 from entering the nucleus.

The changes in ataxin-3 subcellular localization due to hHDAC6 are not very drastic. Thus, these results demonstrate that hHDAC6 is probably not involved in the translocation of ataxin-3 into or out of the nucleus. The changes in localization seen might even be due to the over-expressed levels of both proteins. Therefore, it is not entirely clear whether changes in endogenous hHDAC6 localization could affect endogenous levels of ataxin-3. However, what these results do provide is further evidence that the two proteins may associate with one another.

The role of HDAC6 as a microtubule deacetylase, its association with dynein/dynactin and its role in transporting misfolded protein to the MTOC all imply that HDAC6 is involved in retrograde transport (Hubert et al., 2002; Burnett and Pittman et al., 2005). The ZnF-UBP domain, the ability for HDAC6 to interact with free ubiquitin and ubiquitinated proteins and its ability to interact with VCP/p97 (Seigneurin-Berny et al., 2001) greatly imply a role in the UPP and in ERAD. Ataxin-3 is also highly implicated as being involved in the UPP and in ERAD through its UIMs, its interaction with ubiquitin, VCP/p97 and hHRAD23. It is possible that a connection exists between ataxin-3, HDAC6 and VCP/p97 and this may be worth examining. This connection most likely does not affect nucleocytoplasmic transport of ataxin-3 but it may have a role in the pathogenesis of MJD/SCA3.

Future Directions:

There are several directions in which this research could proceed. Two avenues involve an expansion of the iFRAP data and the findings of the LMB assay. The iFRAP experiment, which examined nuclear recovery of ataxin-3, revealed that the longer the polyglutamine tract the lower the recovery endvalue. A smaller endvalue implies that there is a greater immobile fraction of ataxin-3. We believe that this immobility is due to either the formation of insoluble inclusions or specific interactions with another protein, both of which would be mediated by the length of the polyglutamine tract. Further experiments involving iFRAP and in particular fluorescence loss in photobleaching (FLIP) could be valuable in obtaining information regarding how the polyglutamine tract affects the mobility of ataxin-3 in the cytoplasm.

FLIP requires the continuous bleaching of a small region of interest within the cell. This causes an overall loss in fluorescence of the surrounding area (Koster et al, 2005). Monitoring and analyzing this loss provides information on the dynamics of the protein of interest. The observation that certain areas of the cell do not lose any fluorescence suggests that the protein is immobile in that region and is not able to translocate to the area that is being bleached.

In terms of understanding the cytoplasmic mobility of ataxin-3 one could perform a simple FLIP experiment. It would involve the continuous bleaching of a small area in the cytoplasm that is distant from the nucleus. This would be followed by monitoring the loss in fluorescence in another location of the cytoplasm, as well by monitoring the fluorescence of the bleached area itself. Since it is expected that both regions of interest would exhibit very rapid recovery it would be important to capture as many post-bleach images as possible within the first minute of the experiment. If the recovery curves differ between the various polyglutamine lengths then there is strong evidence that it does have an effect on cytoplasmic mobility. It is important to note that this does not verify whether the immobility is due to the formation of inclusions or due to protein interactions.

It would also be worthwhile to perform iFRAP experiments on HEK 293 cells expressing ataxin-3 that have been treated with LMB. This would determine whether a shift in localization alters the dynamic of nucleocytoplasmic transport. As well, the use of NIH3T3 or MCF7 cells to observe if ataxin-3 displays different recovery rates in different cell lines. Lastly, one could perform FRAP and FLIP experiments on cells that contain cytoplasmic and/or nuclear inclusions of ataxin-3 with various polyglutamine lengths. A similar study was conducted by Chai et al., except that they focused on larger, immobile, nuclear inclusions of ataxin-3 [Q84] (Chai et al., 2002). This study would look at mobile cytoplasmic inclusions to obtain valuable information regarding whether the lower recovery endvalues are due to the increase in immobile ataxin-3 [Q84] protein trapped in inclusions as is the case with nuclear inclusions.

Another future experiment would be a continuation of the LMB assay performed on ataxin-3 in the four different cell lines. Our results had implied that ataxin-3 was being exported from the nucleus via the “piggy-back” mechanism by a protein that is able to export in a CRM1 dependent manner. As of yet we have not been able to identify this protein. If this factor was only found in neuronal cell lines, such as HEK 293 and

STHdh^{Q7/Q7} cells, but not in other cell types it could potentially be a very important clue in deciphering the pathogenesis of disease.

A future experiment that could obtain and identify this factor would be to perform a comparative co-immunoprecipitations (Co-IP) using eGFP-ataxin-3 as bait to pull out potential factors from the two different cell lines, HEK 293 and NIH3T3. In HEK 293 cells we would hope to obtain the factor that mediates ataxin-3 localization. Whereas in NIH3T3 cells, we would expect to either not to find this protein or to detect it at very low levels. For this experiment one would first express eGFP-ataxin-3 [Q28] in the different cell lines. One would then couple an eGFP antibody to immobilized Protein A or Protein G beads in a column. This would be followed by incubating the beads with the appropriate cell lysate. The beads would then be adequately washed and the bound protein would be eluted from the column and analyzed by SDS-PAGE. One lane would contain protein purified from the HEK 293 cell lysate and another would contain protein purified from the NIH3T3 cell lysate. Both lanes should contain a band that matches eGFP-ataxin-3 [Q28] as well as other bands that correspond to binding partners of ataxin-3. Additional lanes would contain the appropriate controls. It is hoped that there would be bands visualized in the HEK 293 lane that are not present in the NIH3T3 lane, which would specifically correspond to the ataxin-3 exporting factor(s). Identification of the gel-bands would be done by mass spectrometry. Candidate proteins that contain CRM1 dependent NESs would be tested in a similar manner as hHDAC6 was herein or by the use of RNA interference to reduce levels of the candidate protein followed by monitoring the affects on ataxin-3.

We feel that the direction of this project lies in performing more FRAP and FLIP experiments to investigate ataxin-3 cellular mobility and to identify the binding partner that acts to mediate ataxin-3 subcellular localization. It is anticipated that the experiments suggested in this section will resolve some of the questions posed throughout this thesis based on the results of the work completed.

Concluding Remarks:

The nine known polyglutamine diseases all involved proteins of different function that only have the polyglutamine tract in common and it is the genetic mutation in this region that is the cause of disease. Several aspects of the pathogenesis of disease have been examined over the years. These include the formation of nuclear inclusions, protein misfolding and aggregation, altered protein quality control, proteolytic processing, subcellular localization and transcriptional dysfunction. The work presented in this thesis specifically examined the subcellular localization of ataxin-3, the protein of interest in Machado-Joseph Disease/Spinocerebellar ataxia type 3 (MJD/SCA3). Studying the subcellular localization and the mode of nucleocytoplasmic translocation of both normal and aberrant polyglutamine proteins has been important to the understanding of many polyglutamine diseases. This has been the most apparent in spinal and bulbar muscular atrophy (SBMA), where a potential drug that inhibits nuclear localization of the affected polyglutamine protein is now in clinical trials. This thesis set out to answer the following: 1. Does ataxin-3 shuttle in and out of the nucleus? and 2. What mediates this nucleocytoplasmic shuttling?

The iFRAP results demonstrated that ataxin-3 is a nucleocytoplasmic shuttling protein. As well, it was found that its nuclear recovery is at least six times slower than its cytoplasmic recovery. Most interestingly, it was observed that there were differences between the nuclear recovery curves of ataxin-3 [Q0], [Q28] and [Q84], indicating that an increase in the number of glutamines results in a decrease of nuclear recovery endvalues. The last point implies that a certain amount of ataxin-3 is immobile in the cytoplasm due to its involvement with cytoplasmic inclusions or protein-protein interactions and that having a pathogenic polyglutamine tract decreases its mobility. This result should be further investigated as it may have implications to the pathogenesis of disease.

Data presented here also shows that the two putative NESs and the putative NLS in ataxin-3 are not functional transport signals. With regards to nuclear import this confirms the results obtained by others that the basic region tested has a different function and that ataxin-3 does not bind importin- α/β 1, although its transport is energy dependent. We believe that it must be entering the nucleus via a “piggy-back” mechanism or by using another, uncharacterized import method. Regarding nuclear export, it was found that ataxin-3 is more LMB sensitive in *STHdh*^{Q7/Q7} and HEK 293 cell lines than in NIH3T3 and MCF7 cell lines. This last result reveals that ataxin-3 does not contain an NES that is dependent on the CRM1 export receptor. However, it does show that another LMB sensitive factor may have a role in exporting ataxin-3 or retaining it in the cytoplasm. The identity of this protein factor was sought after and it was decided that further studies involving hHDAC6 and its variants would be pursued. The results prompted us to believe that hHDAC6 does not shuttle ataxin-3 nor does it have a large role in its localization. With this factor still unknown it would be worthwhile to pursue this study using HEK 293 cells as a source for purification.

In conclusion, this thesis data has successfully shown that ataxin-3 does not translocate across the nuclear envelope using the well known classical pathways such as

CRM1 mediated export and importin- α/β 1 mediated import. However, this project has opened up several interesting questions that are worth exploring. The most important being: 1. to further expand on the iFRAP results by investigating how and why the different polyglutamine lengths are affecting nuclear recovery and 2. to identify the factor(s) that cause ataxin-3 to be more sensitive to LMB treatments in HEK 293 cells.

Figures and Tables

Figure 1: The amino acid sequence of wild-type ataxin-3, isoform MJD1a with highlighted regions of interest. The regions of interest are indicated in colour. Included is the Josephin domain (green), the putative NESs (brown), the ubiquitin interacting motif (pink), the putative NLS (dark blue) and the polyglutamine tract (light blue). Note: These colours identify the same regions of interest in the construct maps in subsequent figures.

Ataxin-3, MJD1a Isoform

1 MESIFHEKQE GSLCAQHCLN NLLQGEYFSP VELSSIAHQL DEEERMRMAE GGVTSEDYRT
61 FLQQPSGNMD DSGFFSIQVI **SNALKVWGLE** LILFNSPEYQ RLRIDPINER SFICNYKEHW
121 FTVRKLGKQW FNLNSLLTGP ELISDTYLAL FLAQLQEGY SIFVVKGDLP DCEADQLLQM
181 IRVQQMHRPK LIGEELAQLK EQRVHKTDLE RMLEANDGSG **MLDEEEDLQ** **RALALSRQEI**
241 **DMEDEEADLR** **RAIQLSMQGS** **SRNISQDMTQ** TSGTNLTSEE LRKREAYFE **KQQQKQQQQQ**
301 **QQQQQQQQQQ** **QQQQQQQRDL** SGQSSHPCER PATSSGALGS DLGKACSPFI **MFATFTLYLT**
361 YELHVIFALH YSSFPL

Features

Josephin Domain: 1 - 186

Putative NESI: 77 - 86

Ubiquitin Interacting Motif: 224 - 243, 244 - 263

Putative NLS: 282 - 285

Polyglutamine Tract: 292 - 317

Putative NESII: 349 - 357

Figure 1

Figure 2: The subcellular localization of ataxin-3 [Q20] and [Q71] in mouse midline deep cerebellar nuclei. Ataxin-3 immunostained neurons from [Q20] (a) and [Q71] (b) transgenic mice. Paraffin embedded midsagittal brain and spinal cord sections of the indicated animals were stained with ataxin-3 antibody as indicated in Goti et al. The intranuclear inclusions are highlighted with an arrow (b). (Adapted from Goti et al., 2004).

Murine Midline Deep Cerebellar Nuclei

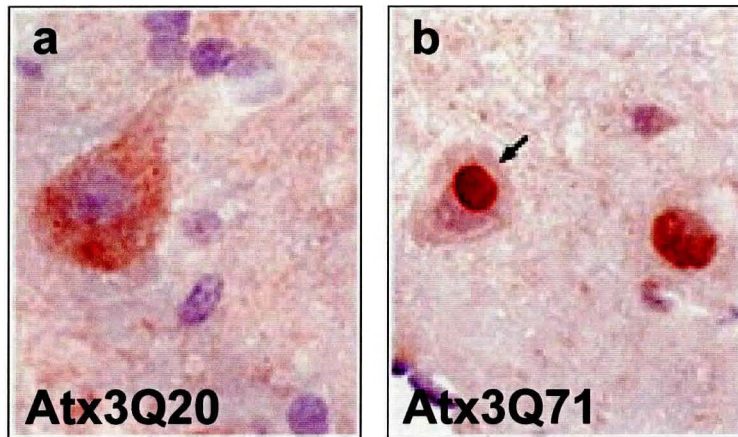


Figure 2

Figure 3: The equations used to quantify images for percent nuclear fluorescence intensity and for iFRAP analysis. Figure 3A. Equation (1) is used to calculate the percent nuclear fluorescence intensity (%NFI). The area is measured in pixels and FI is the mean fluorescence intensity of the region of interest. The background (bkgd) is the mean fluorescence intensity of a region outside of the cell within the field of view.

Figure 3B. The steps illustrated here allow for the normalization of each set of iFRAP data in order to correct for the variations between individual cells. Equation (2) is for the normalization of cells bleached in the nucleus and equation (3) is for the normalization of cells bleached in the cytoplasm.

A

$$\text{Percent Nuclear Fluorescence Intensity} = \frac{(FI_{\text{nucleus}} \times \text{Area}_{\text{nucleus}}) - (FI_{\text{bkgd}} \times \text{Area}_{\text{nucleus}})}{(FI_{\text{cell}} \times \text{Area}_{\text{cell}}) - (FI_{\text{bkgd}} \times \text{Area}_{\text{cell}})} \times 100\% \quad (1)$$

B

Nuclear Recovery

Step 1: Use equation (1) to obtain the %NFI of the pre-bleach image.

%NFI_{pre-bleach}

Step 2: Obtain the %NFI of the remaining time-lapse recovery images at the selected time-points, starting at t = 0.

%NFI_{post-bleach(t)}

Step 3: Correct the %NFI_{post-bleach(t)} using equation (2).

$$\text{Corrected \%NFI}_{\text{post-bleach}(t)} = \frac{\%NFI_{\text{post-bleach}(t)} - \%NFI_{\text{post-bleach}(t=0)}}{\%NFI_{\text{pre-bleach}} - \%NFI_{\text{post-bleach}(t=0)}} \times 100\% \quad (2)$$

Step 4: Set %NFI_{pre-bleach} to 100 % and %NFI_{post-bleach(t=0)} to 0 %.

Step 5: Plot the recovery curve using the corrected %NFI.

Cytoplasmic Recovery

Step 1: Follow the same steps used for nuclear recovery except use percent cytoplasmic fluorescence intensity (%CFI) in place of %NFI.

$$\%CFI = 100 - \%NFI \quad (3)$$

Figure 3

Figure 4: Ataxin-3 is able to translocate to and from the nucleus and recovery into the nucleus is dependent on the length of the polyglutamine tract. eGFP, eGFP-ataxin-3 [Q0], [Q28] and [Q84] were transiently expressed in HEK 293 cells for 24 - 28 hours before imaging. Each iFRAP experiment involved bleaching the nucleus or the cytoplasm of 4 to 6 cells. The pre-bleach cell was set at 100 % fluorescence recovery and the post-bleach_(t=0 s) image was set at 0 % fluorescence recovery for analysis. The subsequent recovery images fall into a scale between the pre-bleach cell and the post-bleach_(t=0 s) cell. **Figure 4A.** Representative confocal and corresponding brightfield images of an iFRAP event where the cytoplasm of a cell expressing eGFP-ataxin-3 [Q28] is bleached followed by time-lapsed recovery (a-r). The cytoplasmic recovery curves for eGFP-ataxin-3 [Q0], [Q28], [Q84] and eGFP (s, t). The recovery half-times were approximately 12, 30, 11 and 39 seconds respectively. **Figure 4B.** Representative confocal and corresponding brightfield images of an iFRAP event where the nucleus of a cell expressing eGFP-ataxin-3 [Q28] is bleached followed by time-lapsed recovery (a-r). The nuclear recovery curves for eGFP-ataxin-3 [Q0], [Q28], [Q84] and eGFP (s, t). The recovery half-times for [Q0], [Q28] and [Q84] were approximately 4.1, 3.8 and 1.1 minutes respectively and for eGFP the half-time was approximately 42 seconds. Error bars represent the standard error of the mean for each experiment. Scale bars are ~ 10 μm .

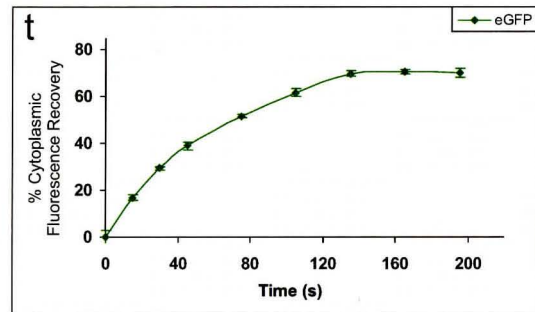
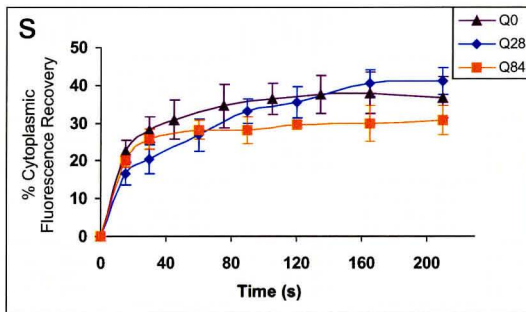
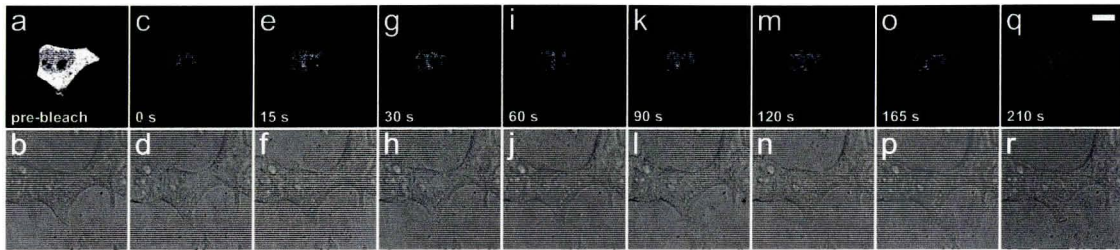
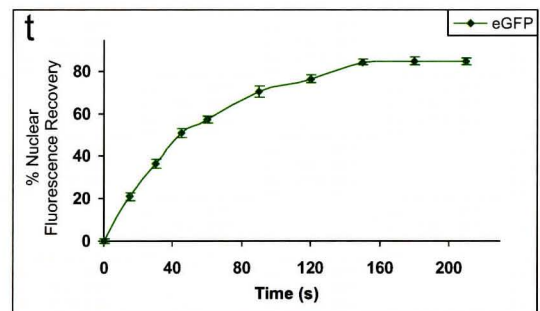
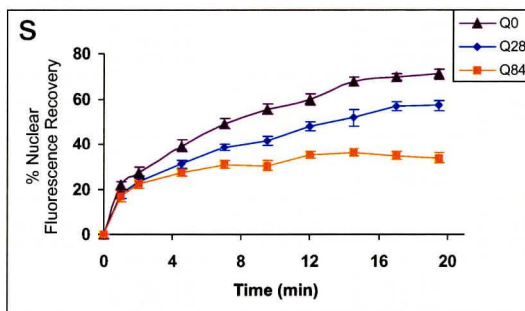
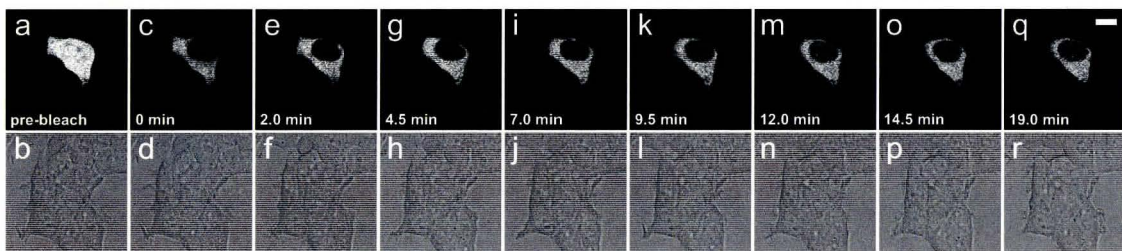
A**B****Figure 4**

Figure 5: The two putative NES motifs and the NLS found in ataxin-3 do not function as nucleocytoplasmic transport signals when analyzed by mutational studies. The three putative nucleocytoplasmic transport signals were identified in ataxin-3 by sequence analysis. Their functionality was tested by mutating the residues that were crucial to its function. The wild-type and mutant ataxin-3 variants, as eGFP fusion proteins, were transiently transfected in *STHdh^{Q7/Q7}* cells, expressed for 24 - 26 hours and imaged by widefield fluorescence microscopy. 80 - 100 cells were imaged in order to analyze and compare the changes in the percent nuclear fluorescence intensity (%NFI). **Figure 5A.** A cartoon representation of the 42 kDa protein, ataxin-3, illustrating the JD, UIMs, the polyglutamine tract and the putative NES and NLS motifs (a). The conservation of the putative NESs and NLS of ataxin-3 in different species are shown here (b-d). To abrogate the transport functions, residues I77, L84 and V86 in NESI were mutated to Ala, Ser and Ala respectively, F355 and L357 in NESII were mutated to Ala and Ser and the putative NLS, ₂₈₂RRKR₂₈₆, was deleted (e). A Pymol representation of the surface protein structure of the JD showing the residues within NESI in colour, with the hydrophobic residues in red (f). **Figure 5B.** Representative images of wild-type and the mutant versions of eGFP-ataxin-3[Q28], over-expressed in *STHdh^{Q7/Q7}* cells (a-d). A plot of the mean %NFI for each construct tested is shown here (e). P value of NESmI, NESmII and Δ NLSm compared to WT were 0.34, 0.01 and 0.40 respectively. Error bars represent standard error of the mean for each experiment. Scale bar is $\sim 10 \mu\text{m}$.

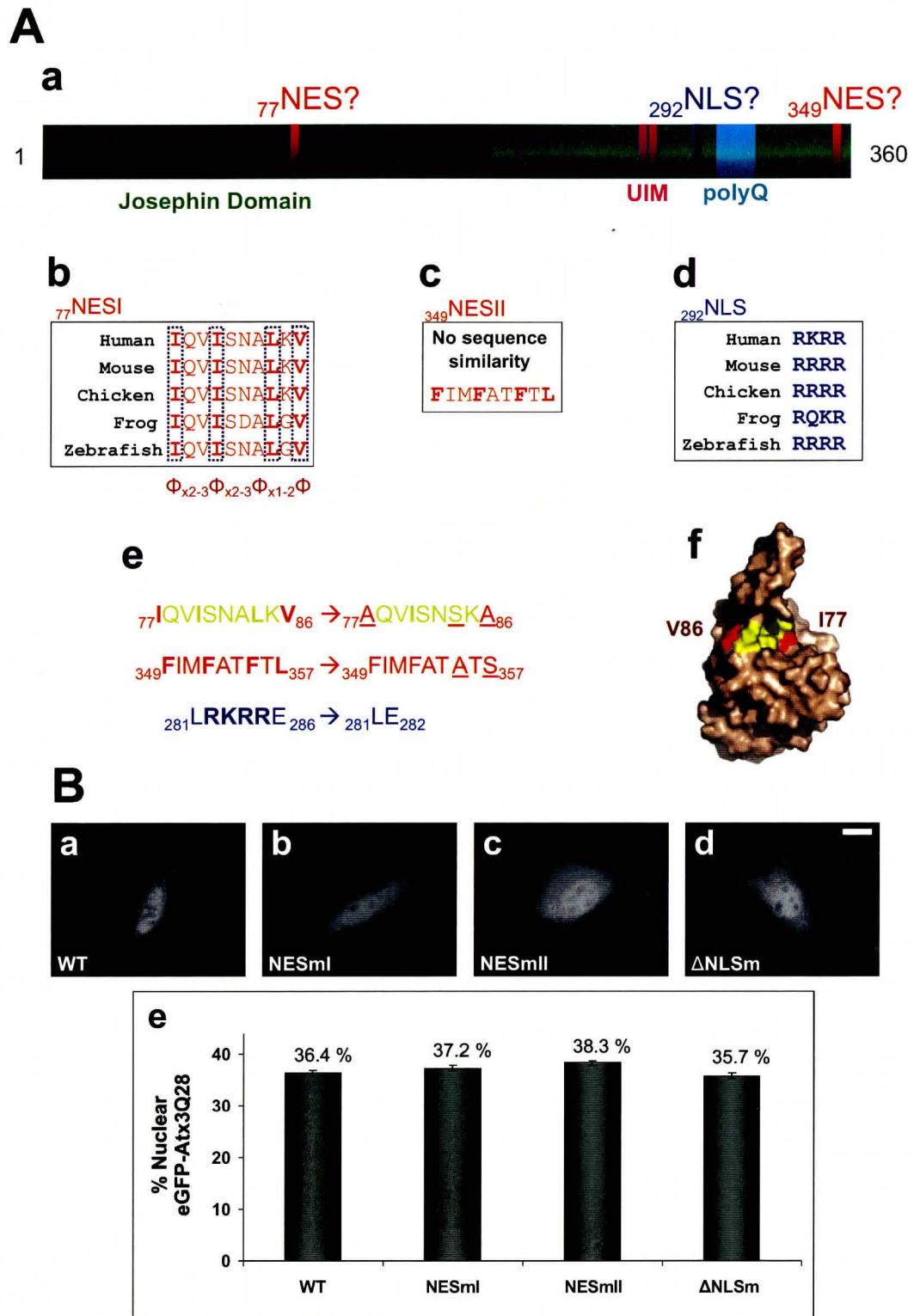


Figure 5

Figure 6: A structural comparison of the putative NESI in ataxin-3 to other known NES motifs in APC, p53 and STAT-1. The putative NESI of ataxin-3 is compared to the NES in the proteins APC, p53 and STAT-1. The structures of the three proteins are known and the activities of their NES within the context of the full-length protein have been proven. **Figure 6A.** The NES sequences from the three proteins highlighting the hydrophobic residues (a). A superimposition of the NES motifs with the hydrophobic residues in stick form and coloured for APC (gray), p53 (light blue), and STAT-1 (dark blue) (b). **Figure 6B.** The putative NESI sequence of ataxin-3 with the hydrophobic residues highlighted (a). The Pymol ribbon representation of the α -helix that contains the NES is shown with the hydrophobic residues coloured red (b). A Pymol representation of the protein structure of the JD showing the residues within NESI in colour, with the hydrophobic residues coloured red (c). (Adapted from Tickenbrock et al., 2002).

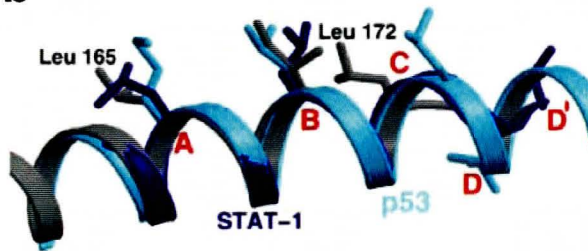
A

a

		A	B	C	D	
APC	163	QNLTKR	IDS	LPL		174
P53	339	EMFREL	NEALEL			350
STAT-1	306	FSLFQQL	IQSSFM	VE		320

D'

b

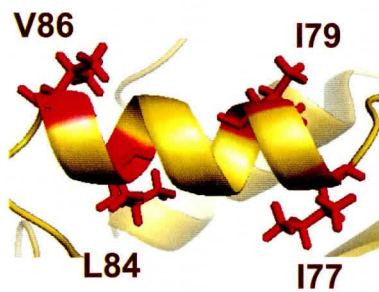


B

a

Ataxin-3 77 IQVINSNALKV 86

b



c

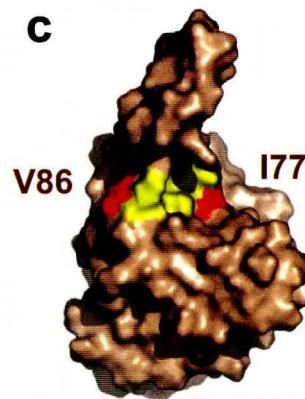


Figure 6

Table 1: Proteins in the karyopherin- β family. Members of the karyopherin- β family from humans are shown with their yeast homologs. As well an examples of their characterized cargoes with the molecular weight and a brief description of function for each kayropherin. (Adapted from Chook and Blobel, 2001; Pemberton and Paschal, 2005).

Table 1

Human Karyopherin	Yeast Homolog	Cargo Eg., MW	Function of Cargo
Importins			
importin- α/β 1 complex	Kap60p, Kap95p	SV40 large T antigen, 82 kDa	initiates DNA unwinding and replication
importin- β 1	Kap95p	Cyclin B1, 48 kDa	cell cycle protein
importin- β 2	Kap104p	hnRNP A1, 39 kDa	transports mRNA
importin- β 3	Kap121p	ribosomal proteins	ribosomal proteins
importin-4	NA	RPS3A, 30 kDa	ribosomal protein
importin-7	NA	Histone H1, 21 kDa	condensation of nucleosome chains
importin-8	NA	SRP19, 19 kDa	signal-recognition-particle assembly
importin-9	NA	Histone H2B, 14 kDa	condensation of nucleosome chains
importin-11	NA	UbcM2, 22 kDa	ubiquitin-conjugating enzyme
Transportin SR1	Kap111p	SR proteins	pre-mRNA splicing proteins
Transportin SR2	NA	HuR proteins	human rotavirus structural proteins
Exportins			
CRM1	Kap124p	HIV-1 Rev, 13 kDa	exports mRNA
CAS	Kap109p	importin- α , 60 kDa	importin adaptor protein
exportin-4	NA	Smad3, 48 kDa	transcriptional factor
exportin-5	NA	microRNA precursors	microRNA precursors
exportin-6	NA	profilin, 15 kDa	regulates cytoskeletal structure
exportin-7	NA	14-3-3B, 28 kDa	phosphoserine/threonine binding, signalling protein
exportin-T	Kap127p, Los1p	aminoacylated tRNA	aminoacylated tRNA
Bidirectional Transport			
exportin-5	Kap142p	microRNA precursors	microRNA precursors
importin-13	NA	imports UBC9, 18	SUMO-1 conjugating enzyme
Uncharacterized			
RanBP8	NA	NA	NA
RanBP16	NA	NA	NA
RanBP17	NA	NA	NA

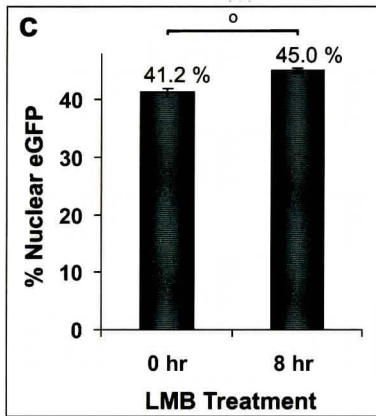
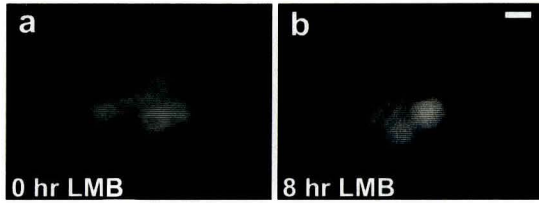
NA, not available.

MW, molecular weight.

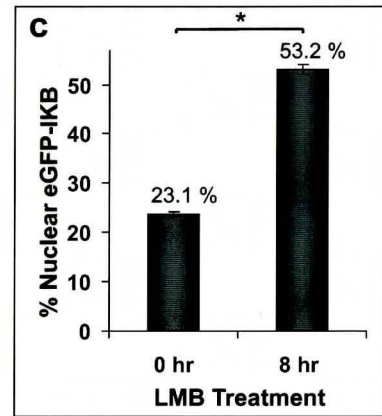
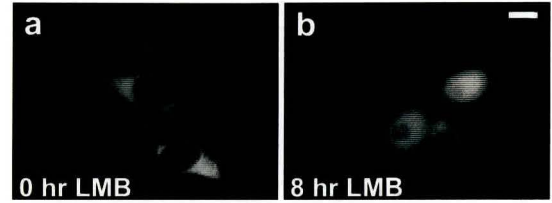
Figure 7: Ataxin-3 is leptomycin B sensitive in HEK 293 cells. The LMB export inhibition assay in HEK 293 cells. eGFP, eGFP-I κ B and eGFP-ataxin-3 [Q28] were transiently expressed in HEK 293 cells for 24 hours, followed by a change to serum-free media and treatment with 10 ng/mL of LMB for 8 hours. 80-100 live cells were imaged by widefield fluorescent microscopy and the mean %NFI was calculated for each set of data. **Figure 7A.** Representative images of untreated and LMB treated cells expressing eGFP (a-b). A plot of the mean %NFI for each of the conditions tested (c). **Figure 7B.** Representative images of untreated and LMB treated cells expressing eGFP-I κ B (a-b). A plot of the mean %NFI for each of the conditions tested (c). **Figure 7C.** Representative images of untreated and LMB treated cells expressing eGFP-ataxin-3 [Q28] (a-b). A plot of the mean %NFI for each of the conditions tested (c). Error bars represent the standard error of the mean for each experiment. * indicates $p < 0.001$ and ° indicates $p < 0.05$. Scale bars are $\sim 10 \mu\text{m}$.

HEK 293 cells

A



B



C

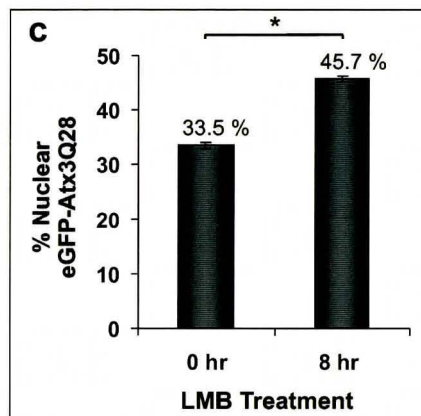
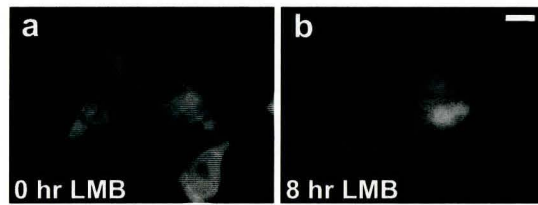


Figure 7

Figure 8: Ataxin-3 is slightly sensitive to leptomycin B in *SThdh*^{Q7/Q7} cells. The LMB export inhibition assay in *SThdh*^{Q7/Q7} cells. eGFP, eGFP-I κ B and eGFP-ataxin-3 [Q28] were transiently expressed in *SThdh*^{Q7/Q7} cells for 24 hours, followed by a change to serum-free media and treatment with 10 ng/mL of LMB for 8, 16 or 24 hours. 80-100 fixed cells were imaged by widefield fluorescent microscopy and the mean %NFI was calculated for each set of data. **Figure 8A.** Representative images of untreated and 8 to 24 hour LMB treated cells expressing eGFP (a-b). A plot of the mean %NFI for each of the conditions tested (c). **Figure 8B.** Representative images of untreated and 8 to 24 hour LMB treated cells expressing eGFP-I κ B (a-d). A plot of the mean %NFI for each of the conditions tested (e). **Figure 8C.** Representative images of untreated and 8 to 24 hour LMB treated cells expressing eGFP-ataxin-3 [Q28] (a-d). A graph of the mean %NFI for each of the conditions tested (e). Error bars represent the standard error of the mean for each experiment. * indicates $p < 0.001$ and ° indicates $p < 0.05$. Scale bars are $\sim 10 \mu\text{m}$.

STHdh^{Q7/Q7} cells

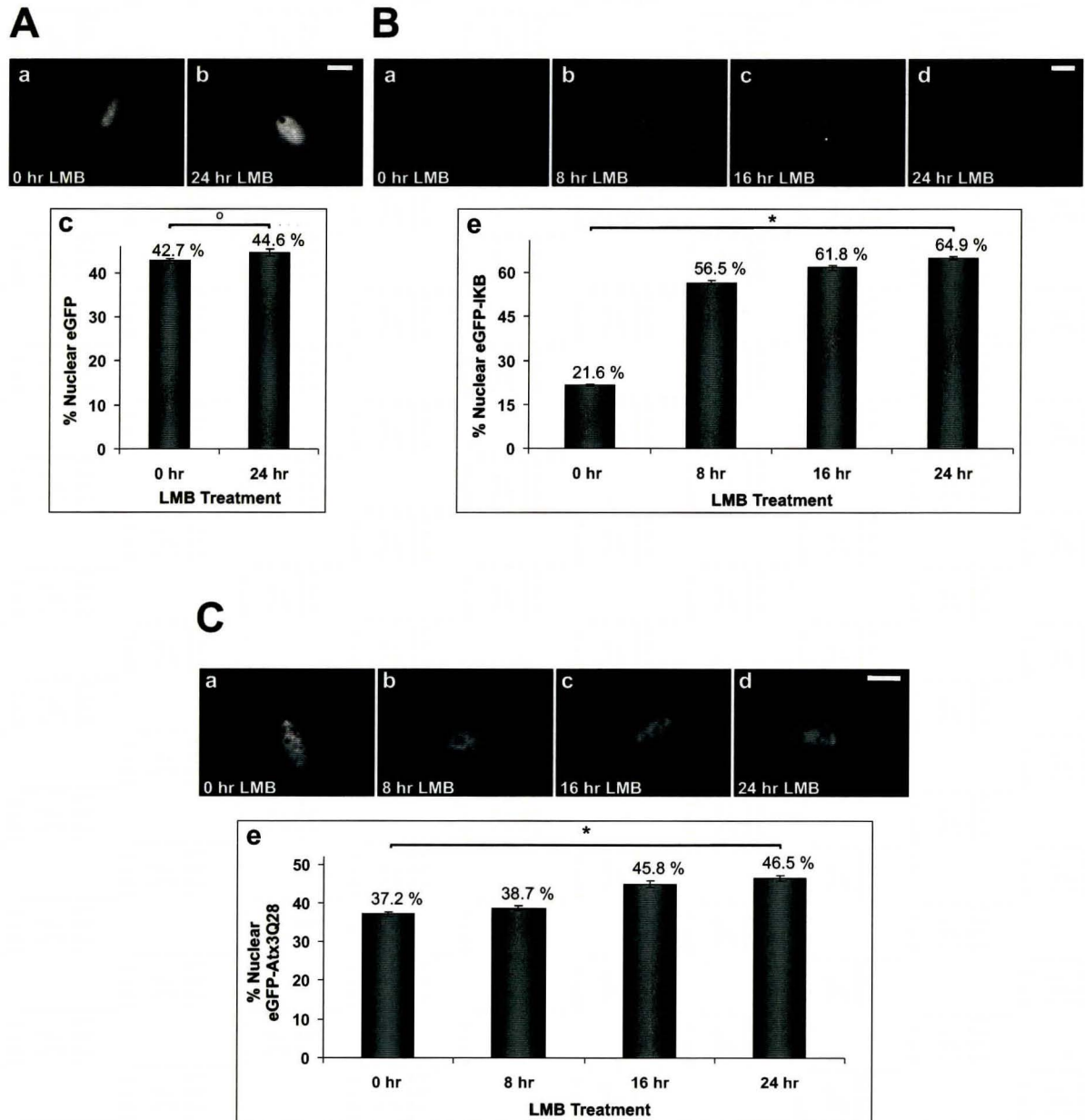
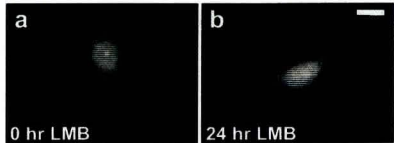


Figure 8

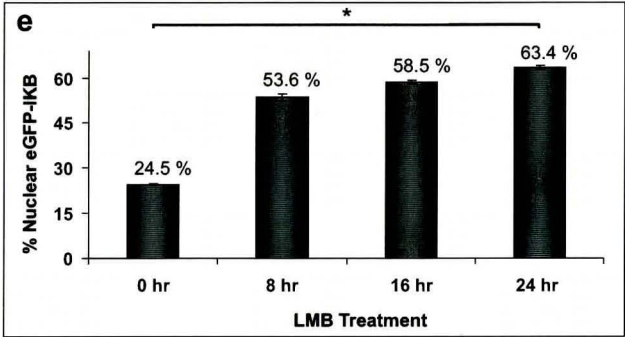
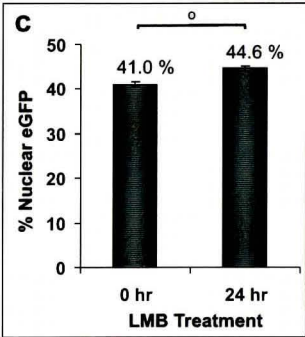
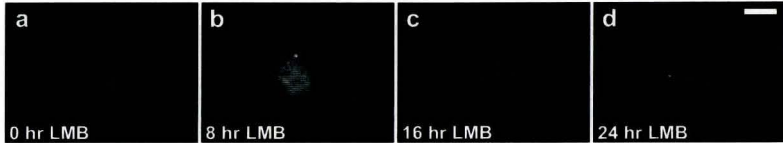
Figure 9: Ataxin-3 is marginally leptomycin B sensitive in NIH3T3 cells. The LMB export inhibition assay in NIH3T3 cells. eGFP, eGFP-I κ B and eGFP-ataxin-3 [Q28] were transiently expressed in NIH3T3 cells for 24 hours, followed by a change to serum-free media and treatment with 10 ng/mL of LMB for 8, 16 or 24 hours. 80-100 fixed cells were imaged by widefield fluorescent microscopy and the mean %NFI was calculated for each set of data. **Figure 9A.** Representative images of untreated and 8 to 24 hour LMB treated cells expressing eGFP (a-b). A plot of the mean %NFI for each of the conditions tested (c). **Figure 9B.** Representative images of untreated and 8 to 24 hour LMB treated cells expressing eGFP-I κ B (a-d). A plot of the mean %NFI for each of the conditions tested (e). **Figure 9C.** Representative images of untreated and 8 to 24 hour LMB treated cells expressing eGFP-ataxin-3 [Q28] (a-d). A plot of the mean %NFI for each of the conditions tested (e). Error bars represent the standard error of the mean for each experiment. * indicates $p < 0.001$ and ° indicates $p < 0.05$. Scale bars are $\sim 10 \mu\text{m}$.

NIH3T3 cells

A



B



C

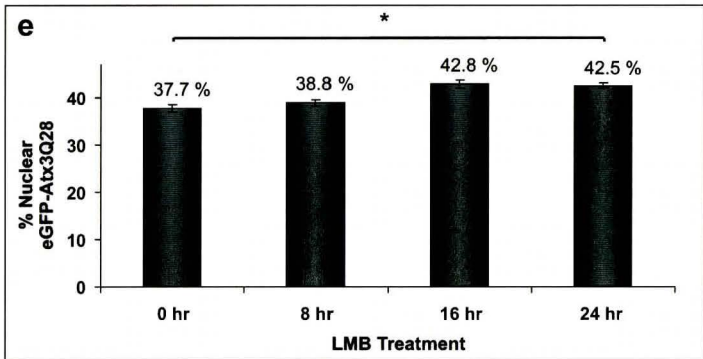
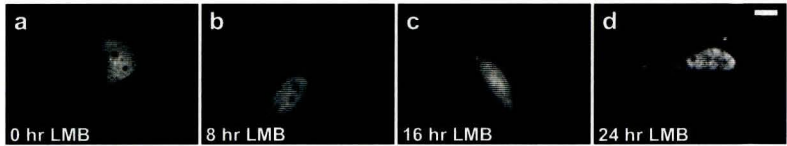
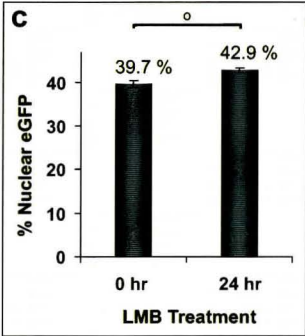
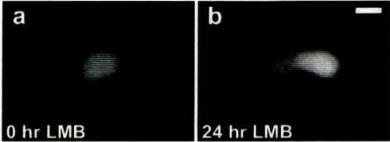


Figure 9

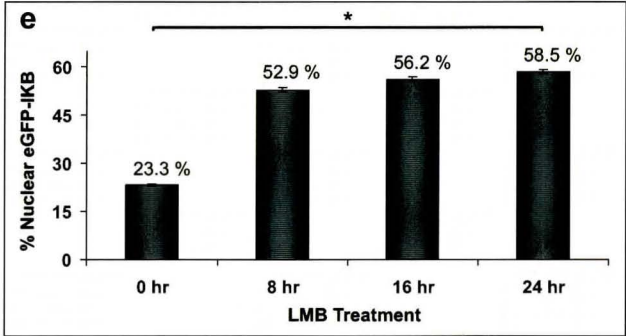
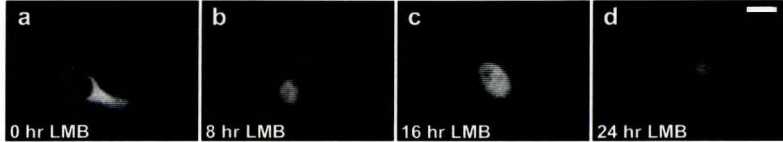
Figure 10: Ataxin-3 is marginally leptomycin B sensitive in MCF7 cells. The LMB export inhibition assay in MCF7 cells. eGFP-I κ B and eGFP-ataxin-3 [Q28] were transiently expressed in MCF7 cells for 24 hours, followed by a change to serum-free media and treatment with 10 ng/mL of LMB for 8, 16 or 24 hours. 80-100 fixed cells were imaged by widefield fluorescent microscopy and the mean %NFI was calculated for each set of data.. **Figure 10A.** Representative images of untreated and 8 to 24 hour LMB treated cells expressing eGFP (a-b). A plot of the mean %NFI for each of the conditions tested (c). **Figure 10B.** Representative images of untreated and 8 to 24 hour LMB treated cells expressing eGFP-I κ B (a-d). A plot of the mean %NFI for each of the conditions tested (e). **Figure 10C.** Representative images of untreated and 8 to 24 hour LMB treated cells expressing eGFP-ataxin-3 [Q28] (a-d). A plot of the mean %NFI for each of the conditions tested (e). Error bars represent the standard error of the mean for each experiment. * indicates $p < 0.001$ and ° indicates $p < 0.05$. Scale bars are $\sim 10 \mu\text{m}$.

MCF7 cells

A



B



C

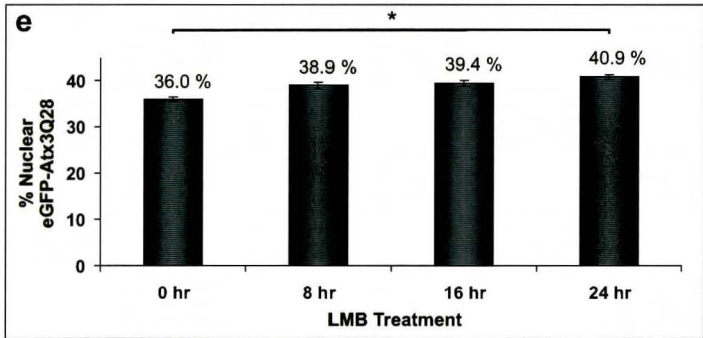
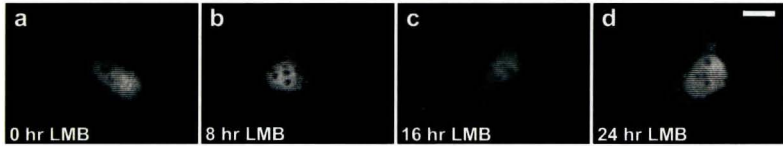


Figure 10

Figure 11: hHDAC6 contains a functional NES. Figure 11A. Cartoon representation of hHDAC6 illustrating the two deacetylase regions, the two putative NESs, the putative NLS and the serine and glutamic acid rich sequence (SE14) (a). The mutations in the NESm, which involves the deletion of both NES motifs (b). **Figure 11B.** mCer-hHDAC6 Δ SE14 and mCer-hHDAC6 Δ SE14 NESm were transiently expressed in NIH3T3 cells for 24 hours, imaged using widefield fluorescence microscopy and analyzed for the mean %NFI. Representative images of live NIH3T3 cells over-expressing mCer-hHDAC6 Δ SE14 and mCer-hHDAC6 Δ SE14 NESm (a-b). A plot of the mean %NFI for each construct tested (c). Error bars represent the standard error of the mean. * indicates $p < 0.001$. Scale bar is $\sim 10 \mu\text{m}$.

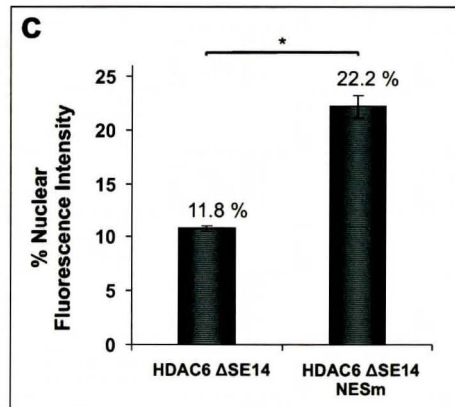
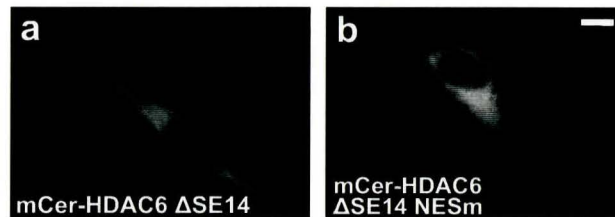
A**a****b****NES deletion mutations** ${}^{65}\text{EDLIVGLQGMDLNLEA}_{80} \rightarrow {}^{65}\text{EDEA}_{68}$ ${}^{1047}\text{STLIGSLRTLELGS}_{1060} \rightarrow {}^{1047}\text{STGS}_{1050}$ **B****Figure 11**

Table 2: hHDAC6 does not shuttle ataxin-3 but does alter its subcellular localization. eYFP-ataxin-3 [Q28] was transiently co-expressed with mCer, mCer-hHDAC6, mCer-hHDAC6 NESm, mCer-hHDAC6 Δ SE14, mCer-hHDAC6 Δ SE14 NESm and mCer-hHDAC6 Δ SE14 NLSm in NIH3T3 cells. Following 24 hours of expression, cells were treated with 10 ng/mL of LMB for 24 hours, fixed and imaged by widefield fluorescence microscopy. 80-100 cells were imaged and analyzed for the mean %NFI. This is shown for each co-expression study for treated and untreated cells. The mean %NFI is also shown for treated and untreated eGFP.

Table 2

	%NFI of eYFP-ataxin-3 [Q28] when co-expressed with HDAC6 variants			
	0 hr LMB	SEM	24 hr LMB	SEM
mCer^a	39.40	0.53	44.77	0.54
mCer-HDAC6^b	36.19	0.68	45.27	0.69
mCer-HDAC6 NESm^b	37.65	0.53	46.65	0.52
mCer-HDAC6 ΔSE14^b	39.19	0.43	49.58	0.51
mCer-HDAC6 ΔSE14 + NESm^b	35.40	0.40	48.61	0.68
mCer-HDAC6 ΔSE14 + NLSm^b	35.33	0.50	46.21	0.87
eGFP^{a,c}	41.03	0.51	44.46	0.44

a p<0.05

b p<0.001

c The % nuclear fluorescence of eGFP alone.

SEM - standard error of the mean

Figure 12: Representative images of co-expressed eYFP-ataxin-3 [Q28] and mCer-hHDAC6 variants and in NIH3T3 cells. Representative images of the co-expression, LMB studies shown in Table 2 (a-x). Merged images were pseudocoloured to represent the mCer and eYFP fusion proteins (c,f,i,l,o,r,u,x). Scale bar is ~ 10 μ m.

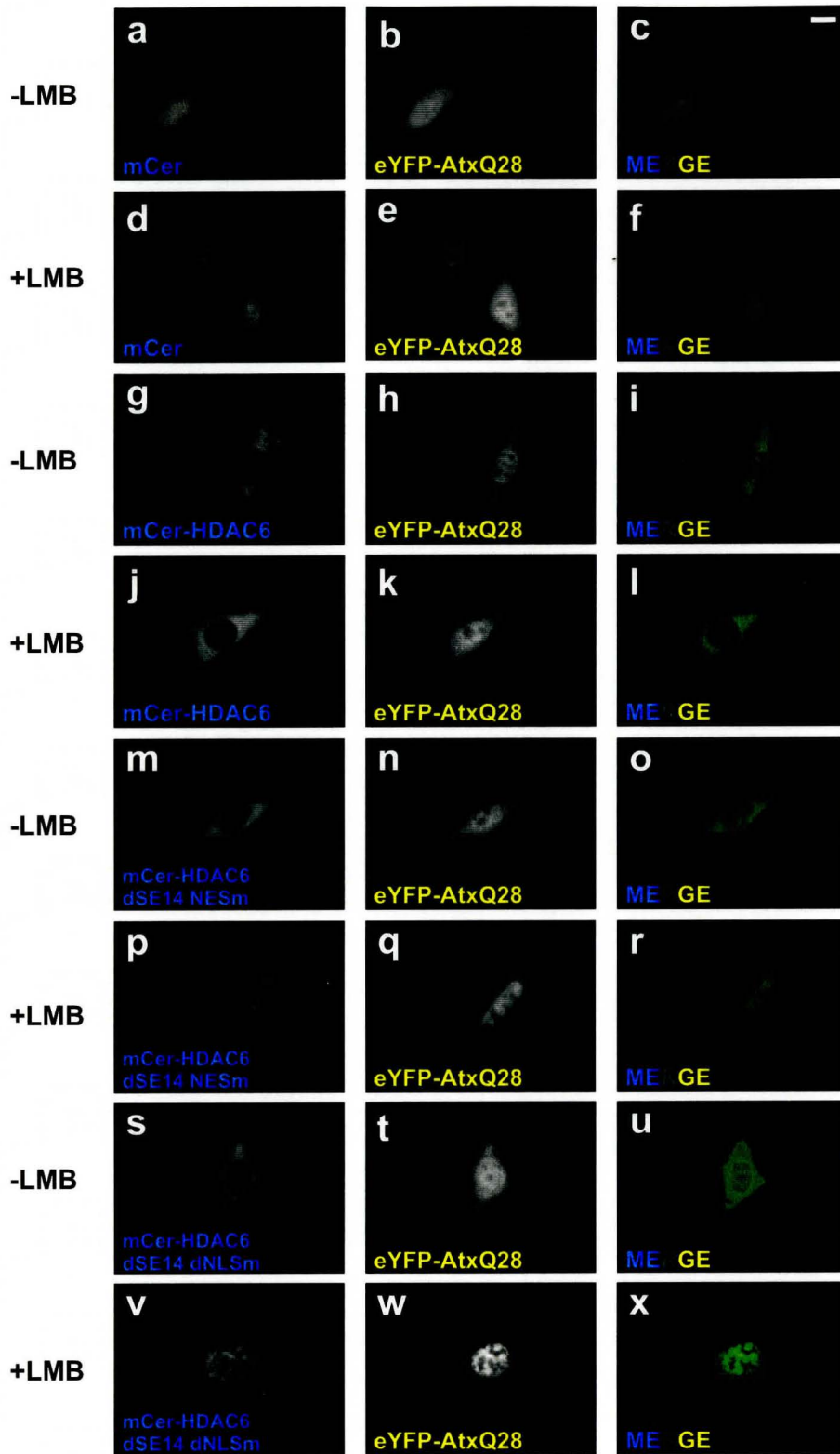
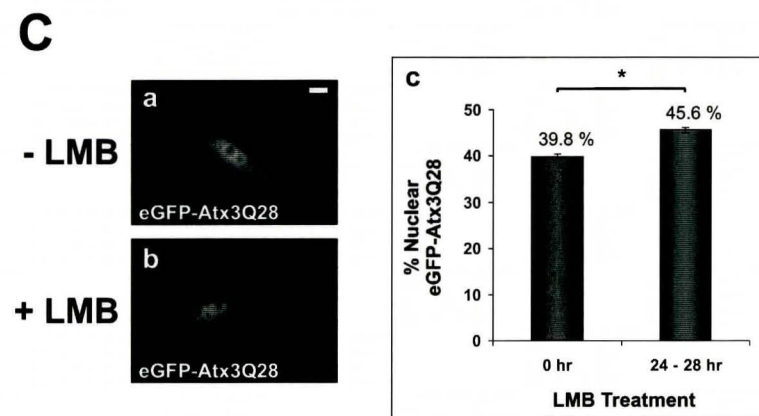
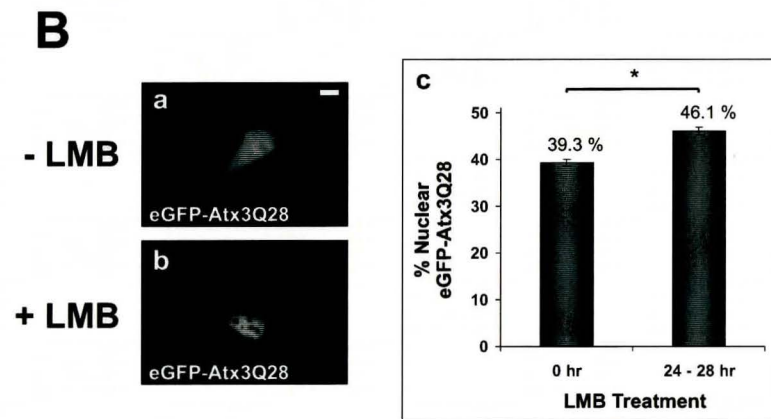
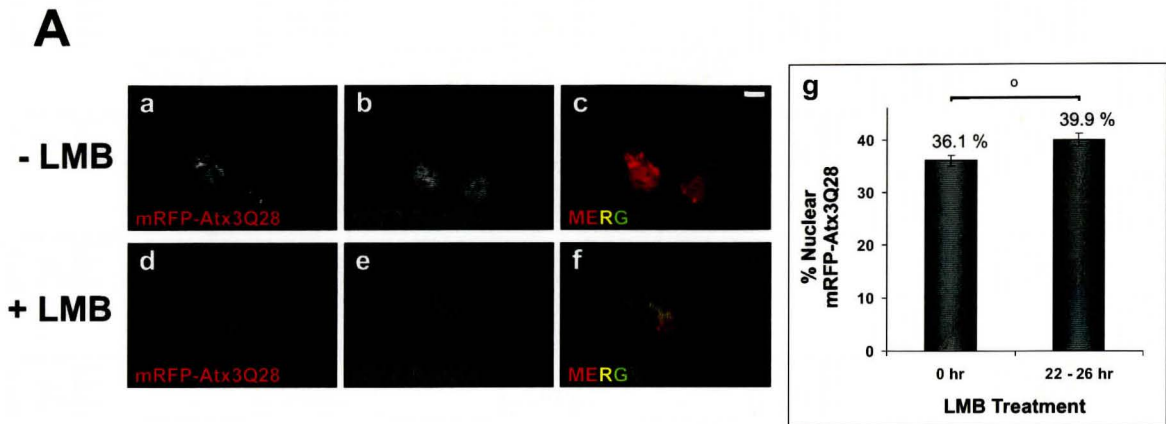


Figure 12

Supplemental Video and Figures

Supplemental Video 1: A time lapsed video showing the formation of nuclear and cytoplasmic inclusions in a *STHdh*^{Q7/Q7} cell, over-expressing ataxin-3 [Q166]-eGFP. Ataxin-3 [Q166]-eGFP was expressed in *STHdh*^{Q7/Q7} and was imaged for 6.5 hours. An image was captured every 5 minutes and the video speed was 1.1 frames per second.

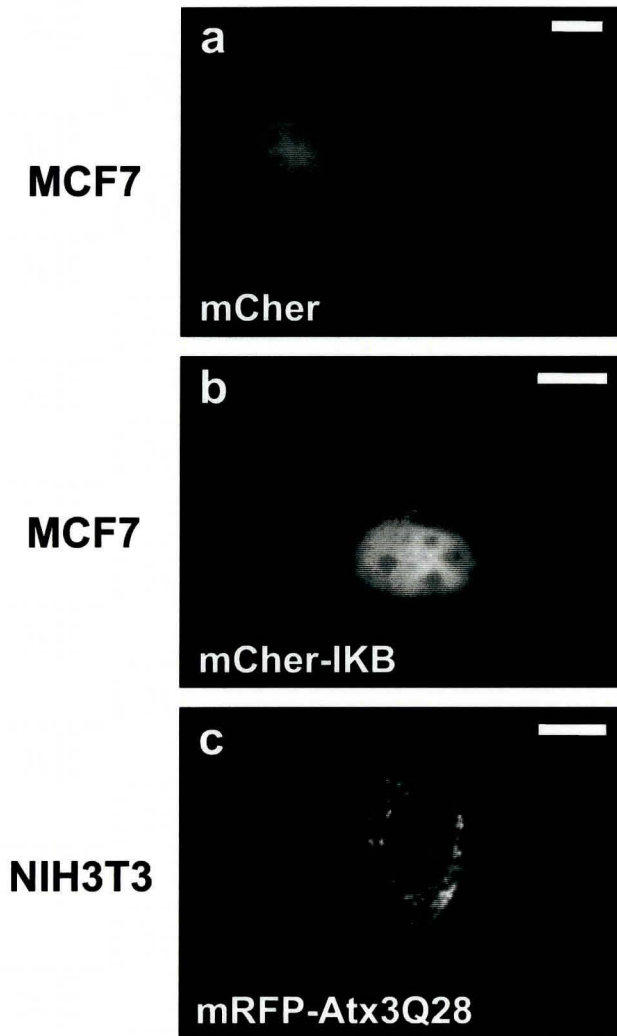
Supplemental Figure 1: LMB assay of ataxin-3 in NIH3T3 cells co-expressed with hHRad23b, hHDAC1 and hHDAC2. The LMB assay was performed on NIH3T3 cells co-expressed with mRFP-ataxin-3 [Q28] and eGFP-Rad23b, eGFP-ataxin-3 [Q28] and myc-HDAC1 and flag-HDAC2. The mean %NFI was calculated for ataxin-3 in each experiment. **Figure 1A.** Representative images of mRFP-ataxin-3 [Q28] and eGFP-Rad23b in untreated and LMB treated cells (a-f). A plot of the mean %NFI for each of the conditions tested (g). **Figure 1B.** Representative images of eGFP-ataxin-3 [Q28] and myc-HDAC1 in untreated and LMB treated cells (a-b). HDAC1 was not visualized for this experiment. A plot of the mean %NFI for each of the conditions tested (c). **Figure 1C.** Representative images of eGFP-ataxin-3 [Q28] and flag-HDAC2 in untreated and LMB treated cells (a-b). HDAC2 was not visualized for this experiment. A plot of the mean %NFI for each of the conditions tested (c). Error bars represent the standard error of the mean for each experiment. * indicates $p < 0.001$. Scale bars are $\sim 10 \mu\text{m}$.



Supplemental Figure 1

Supplemental Figure 2: The formation of cytoplasmic inclusions occurs after 48 hours of mRFP or mCherry over-expression alone or as a fusion protein. mCherry or mCher-IκB transiently over-expressed in MCF7 cells for 2 days show the appearance of cytoplasmic inclusions (a-b). mRFP-ataxin-3 [Q28] over-expressed in NIH3T3 cells for 2 days also show the appearance of cytoplasmic inclusions (c). Scale bars are ~ 10 μm.

36 to 48 hours post-transfection



Supplemental Figure 2

References:

- Albrecht, A. and Mundlos, S. (2005) The other trinucleotide repeat: polyalanine expansion disorders. *Curr Opin Genet Dev.* 15 (3):285-93.
- Albrecht, M., Hoffmann, D., Evert, B. O., Schmitt, I., Wullner, U. and Lengauer, T. (2003) Structural modeling of ataxin-3 reveals distant homology to adaptins. *Proteins.* 50 (2):355-70.
- Albrecht, M., Golatta, M., Wullner, U. and Lengauer, T. (2004) Structural and functional analysis of ataxin-2 and ataxin-3. *Eur J Biochem.* 271 (15):3155-70.
- Axelrod, D., Koppel, D. E., Schlessinger, J., Elson, E. and Webb, W. W. (1976) Mobility measurement by analysis of fluorescence photobleaching recovery kinetics. *Biophys J.* 16 (9):1055-69.
- Banno, H., Adachi, H., Katsuno, M., Suzuki, K., Atsuta, N., Watanabe, H., Tanaka, F., Doyu, M. and Sobue, G. (2006) Mutant androgen receptor accumulation in spinal and bulbar muscular atrophy scrotal skin: a pathogenic marker. *Ann Neurol.* 59 (3):520-6.
- Becher, M. W., Kotzuc, J. A., Sharp, A. H., Davies, S. W., Bates, G. P., Price, D. L. and Ross, C. A. (1998) Intranuclear neuronal inclusions in Huntington's disease and dentatorubral and pallidolusian atrophy: correlation between the density of inclusions and IT15 CAG triplet repeat length. *Neurobiol Dis* 4 (6):387-97.
- Begitt, A., Meyer, T., van Rossum, M. and Vinkemeier, U. (2000) Nucleocytoplasmic translocation of Stat1 is regulated by a leucine-rich export signal in the coiled-coil domain. *Proc Natl Acad Sci U S A.* 97 (19):10418-23.
- Berke, S. J., Schmied FA, Brunt ER, Ellerby LM, Paulson HL. (2004) Caspase-mediated proteolysis of the polyglutamine disease protein ataxin-3. *J Neurochem.* 89 (4):908-18.
- Berke, S. J., Chai, Y., Marrs, G. L., Wen, H. and Paulson, H. L. (2005) Defining the role of ubiquitin-interacting motifs in the polyglutamine disease protein, ataxin-3. *J Biol Chem.* 280 (36):32026-34.
- Bertos, N. R., Gilquin, B., Chan, G. K., Yen, T. J., Khochbin, S., Yang, X. J. (2004) Role of the tetradecapeptide repeat domain of human histone deacetylase 6 in cytoplasmic retention. *J Biol Chem.* 279 (46):48246-54.
- Bevivino, A. E., and Loll, P. J. (2001) An expanded glutamine repeat destabilizes native ataxin-3 structure and mediates formation of parallel β -fibrils. *Proc. Natl. Acad. Sci. U. S. A.* 98 (21):11955-11960.

Boeddrich, A., Gaumer, S., Haacke, A., Tzvetkov, N., Albrecht, M., Evert, B. O., Muller, E. C., Lurz, R., Breuer, P., Schugardt, N., Plassmann, S., Xu, K., Warrick, J. M., Suopanki, J., Wullner, U., Frank, R., Hartl, U. F., Bonini, N. M. and Wanker, E. E. (2006) An arginine/lysine-rich motif is crucial for VCP/p97-mediated modulation of ataxin-3 fibrillogenesis. *EMBO J.* 25 (7):1547-58.

Brown, L. Y. and Brown, S. A. (2004) Alanine tracts: the expanding story of human illness and trinucleotide repeats. *Trends Genet.* 20 (1):51-8.

Burnett, B., Li, F. and Pittman, R. N. (2003) The polyglutamine neurodegenerative protein ataxin-3 binds polyubiquitylated proteins and has ubiquitin protease activity. *Hum Mol Genet* 12 (23):3195-205.

Burnett, B. G. and Pittman, R. N. (2005) The polyglutamine neurodegenerative protein ataxin 3 regulates aggresome formation. *Proc Natl Acad Sci U S A.* 102 (12):4330-5.

Campbell, R.,E., Tour, O., Palmer, A., E., Steinbach, P., A., Baird, G., S., Zacharias, D., A. and Tsien, R., Y. (2002) A monomeric red fluorescent protein. *Proc Natl Acad Sci U S A.* 99 (12): 7877-82.

Carpenter, N. J. (1994) Genetic anticipation. Expanding tandem repeats. *Neurol Clin.* 12 (4):683-97.

Carrero, G., McDonald, D., Crawford, E., de Vries, G. and Hendzel, M. J. (2003) Using FRAP and mathematical modeling to determine the in vivo kinetics of nuclear proteins. *Methods.* 29 (1):14-28.

Cemal, C. K., Carroll, C. J., Lawrence, L., Lowrie, M. B., Ruddle, P., Al-Mahdawi, S., King, R. H., Pook, M. A., Huxley, C. and Chamberlain, S. (2002) YAC transgenic mice carrying pathological alleles of the MJD1 locus exhibit a mild and slowly progressive cerebellar deficit. *Hum Mol Genet* 11 (9):1075-94.

Chai, Y., Koppenhafer, S. L., Shoesmith, S. J., Perez, M. K. and Paulson, H. L. (1999) Evidence for proteasome involvement in polyglutamine disease: localization to nuclear inclusions in SCA3/MJD and suppression of polyglutamine aggregation in vitro. *Hum Mol Genet.* 8 (4):673-82.

Chai, Y., Wu, L., Griffin, J. D. and Paulson, H. L. (2001) The role of protein composition in specifying nuclear inclusion formation in polyglutamine disease. *J Biol Chem.* 276 (48):44889-97.

Chai, Y., Shao, J., Miller, V. M., Williams, A. and Paulson H.L. (2002) Live-cell imaging reveals divergent intracellular dynamics of polyglutamine disease proteins and supports a sequestration model of pathogenesis. *Proc Natl Acad Sci U S A.* 99 (14):9310-5.

Chai, Y., Berke, S. S., Cohen, R. E. and Paulson, H. L. (2004) Poly-ubiquitin binding by the polyglutamine disease protein ataxin-3 links its normal function to protein surveillance pathways. *J Biol Chem.* 279 (5):3605-11.

Chalfie, M., Tu, Y., Euskirchen, G., Ward, W. W. and Prasher, D. C. (1994) Green fluorescent protein as a marker for gene expression. *Science.* 263 (5148):802-5.

Chen, S., Berthelie, V., Yang, W., and Wetzel, R. (2001) Polyglutamine aggregation behavior in vitro supports a recruitment mechanism of cytotoxicity. *J. Mol. Biol.* 311 (1):173-182

Chen, Y., Lagerholm, B. C., Yang, B. and Jacobson, K. (2006) Methods to measure the lateral diffusion of membrane lipids and proteins. *Methods.* 39 (2):147-53.

Chevalier-Larsen, E. S., O'Brien, C. J., Wang, H., Jenkins, S. C., Holder, L., Lieberman, A. P. and Merry, D. E. (2004) Castration restores function and neurofilament alterations of aged symptomatic males in a transgenic mouse model of spinal and bulbar muscular atrophy. *J Neurosci.* 24 (20):4778-86.

Chook, Y. M. and Blobel, G. (2001) Karyopherins and nuclear import. *Curr Opin Struct Biol.* 11 (6):703-15.

Chow, M. K., Paulson, H. L. and Bottomley, S. P. (2004a) Destabilization of a non-pathological variant of ataxin-3 results in fibrillogenesis via a partially folded intermediate: a model for misfolding in polyglutamine disease. *J Mol Biol.* 335 (1):333-41.

Chow, M. K., Ellisdon, A. M., Cabrita, L. D., and Bottomley, S. P. (2004b) Polyglutamine Expansion in Ataxin-3 Does Not Affect Protein Stability. *J. Biol. Chem.* 279 (46) 47643-47651.

Cleary, J.D., Nichol, K., Wang, Y.-H. and Pearson, C. E. (2002) Evidence of *cis*-acting factors in replication-mediated trinucleotide repeat instability in primate cells. *Nature Genet.* . 31, 37-46.

Cody, C. W., Prasher, D. C., Westler, W. M., Prendergast, F. G. and Ward, W. W. (1993) Chemical structure of the hexapeptide chromophore of the *Aequorea* green-fluorescent protein. *Biochemistry.* 32 (5):1212-8.

Colomer Gould, V. F. (2005) Mouse models of Machado-Joseph disease and other polyglutamine spinocerebellar ataxias. *NeuroRx.* 2 (3):480-3.

Cormack, B. P., Valdivia, R. H. and Falkow, S. (1996) FACS-optimized mutants of the green fluorescent protein (GFP). *Gene*. 173 (1):33-8.

Cronshaw, J. M., Krutchinsky, A. N., Zhang, W., Chait, B. T. and Matunis, M. J. (2002) Proteomic analysis of the mammalian nuclear pore complex. *J Cell Biol*. 158 (5):915-27.

Cummings, C.J. and Zoghbi, H. Y. (2000) Fourteen and counting: unraveling trinucleotide repeat diseases. *Hum Mol Genet*. 9 (6):909-16.

Dautzenberg, F. M., Higelin, J. and Teichert, U. (2000) Functional characterization of corticotropin-releasing factor type 1 receptor endogenously expressed in human embryonic kidney 293 cells. *Eur J Pharmacol*. 390 (1-2): 51-9.

DiFiglia, M., Sapp, E., Chase, K. O., Davies, S. W., Bates, G. P., Vonsattel, J. P. and Aronin N. (1997) Aggregation of huntingtin in neuronal intranuclear inclusions and dystrophic neurites in brain. *Science*. 277 (5334):1990-3.

Donaldson, K. M., Li, W., Ching, K. A., Batalov, S., Tsai, C. C. and Joazeiro, C. A. (2003) Ubiquitin-mediated sequestration of normal cellular proteins into polyglutamine aggregates. *Proc Natl Acad Sci U S A*. 100 (15):8892-7.

Doss-Pepe, E. W., Stenroos, E. S., Johnson, W. G. and Madura, K. (2003) Ataxin-3 interactions with rad23 and valosin-containing protein and its associations with ubiquitin chains and the proteasome are consistent with a role in ubiquitin-mediated proteolysis. *Mol Cell Biol*. 23 (18):6469-83.

Durr, A., Stevanin, G., Cancel, G., Duyckaerts, C., Abbas, N., Didierjean, O., Chneiweiss, H., Benomar, A., Lyon-Caen, O., Julien, J., Serdaru, M., Penet, C., Agid, Y. and Brice, A. (1996) Spinocerebellar ataxia 3 and Machado-Joseph disease: clinical, molecular, and neuropathological features. *Ann Neurol* 39: 490-499.

Ellerby, L. M., Hackam, A. S., Propp, S. S., Ellerby, H. M., Rabizadeh, S., Cashman, N. R., Trifiro, M. A., Pinsky, L., Wellington, C. L., Salvesen, G. S., Hayden, M. R. and Bredesen, D. E. (1999) Kennedy's disease: caspase cleavage of the androgen receptor is a crucial event in cytotoxicity. *J Neurochem*. 72 (1):185-95.

Ellisdon, A. M., Thomas, B. and Bottomley, S. P. (2006) The two-stage pathway of ataxin-3 fibrillogenesis involves a polyglutamine-independent step. *J Biol Chem*. 281 (25):16888-96.

Evert, B.O., Wullner, U., Schulz, J. B., Weller, M., Groscurth, P., Trottier, Y., Brice, A. and Klockgether, T. (1999) High level expression of expanded full-length ataxin-3 in vitro causes cell death and formation of intranuclear inclusions in neuronal cells. *Hum Mol Genet*. 8 (7):1169-76.

- Fischer, U., Huber, J., Boelens, W. C., Mattaj, I. W. and Luhrmann, R. (1995) The HIV-1 Rev activation domain is a nuclear export signal that accesses an export pathway used by specific cellular RNAs. *Cell*. 82 (3):475-83.
- Fischer, U., Pollard, V. W., Luhrmann, R., Teufel, M., Michael, M. W., Dreyfuss, G. and Malim, M. H. (1999) Rev-mediated nuclear export of RNA is dominant over nuclear retention and is coupled to the Ran-GTPase cycle. *Nucleic Acids Res*. 27 (21):4128-34.
- Fornerod, M., Ohno, M., Yoshida, M. and Mattaj, I. W. (1997) CRM1 is an export receptor for leucine-rich nuclear export signals. *Cell*. 90 (6):1051-60.
- Fried, H. and Kutay, U. (2003) Nucleocytoplasmic transport: taking an inventory. *Cell Mol Life Sci*. 60 (8):1659–1688.
- Fujigasaki, H., Uchihara, T., Koyano, S., Iwabuchi, K., Yagishita, S., Makifuchi, T., Nakamura, A., Ishida, K., Toru, S., Hirai, S., Ishikawa, K., Tanabe, T. and Mizusawa, H. (2000) Ataxin-3 is translocated into the nucleus for the formation of intranuclear inclusions in normal and Machado-Joseph disease brains. *Exp Neurol*. 165 (2):248-56.
- Garcia-Mata, R., Bebok, Z., Sorscher, E. J. and Sztul, E. S. (1999) Characterization and dynamics of aggresome formation by a cytosolic GFP-chimera. *J Cell Biol*. 146 (6):1239-54.
- Gaspar, C., Lopes-Cendes, I., Hayes, S., Goto, J., Arvidsson, K., Dias, A., Silveira, I., Maciel, P., Coutinho, P., Lima, M., Zhou, Y. X., Soong, B. W., Watanabe, M., Giunti, P., Stevanin, G., Riess, O., Sasaki, H., Hsieh, M., Nicholson, G. A., Brunt, E., Higgins, J. J., Lauritzen, M., Tranebjaerg, L., Volpini, V., Wood, N., Ranum, L., Tsuji, S., Brice, A., Sequeiros, J. and Rouleau, G. A. (2001) Ancestral origins of the Machado-Joseph disease mutation: a worldwide haplotype study. *Am J Hum Genet*. 68 (2):523-8.
- Gatchel, J. R. and Zoghbi, H. Y. (2005) Diseases of unstable repeat expansion: mechanisms and common principles. *Nat Rev Genet*. 6 (10):743-55.
- Gilman, S. (2000) The spinocerebellar ataxias. *Clin Neuropharmacol*. 23 (6):296-303.
- Goldfarb, D. S., Corbett, A. H., Mason, D. A., Harreman, M. T. and Adam, S. A. (2004) Importin alpha: a multipurpose nuclear-transport receptor. *Trends Cell Biol*. 14 (9):505-14.
- Gomes-Pereira, M., Fortune, M.T., Monckton, D.G. (2001) Mouse tissue culture models of unstable triplet repeats: *in vitro* selection for larger alleles, mutational expansion bias and tissue specificity, but no association with cell division rates *Hum. Mol. Genet*, . 10, 845–854.

Goodwin, J., S. and Kenworthy, A., K. (2005) Photobleaching approaches to investigate diffusional mobility and trafficking of Ras in living cells. *Methods*. 37 (2):154-164.

Gorbunova, V., Seluanov, A., Mittelman, D. and Wilson, J. H. (2004) Genome-wide demethylation destabilizes CTG.CAG trinucleotide repeats in mammalian cells. *Hum Mol Genet*. 13 (23):2979-89.

Gorlich, D. and Kutay, U. (1999) Transport between the cell nucleus and the cytoplasm. *Annu Rev Cell Dev Biol*. 15:607-660.

Goti, D., Katzen, S. M., Mez, J., Kurtis, N., Kiluk, J., Ben-Haiem, L., Jenkins, N. A., Copeland, N. G., Kakizuka, A., Sharp, A. H., Ross, C. A., Mouton, P. R. and Colomer, V. (2004) A mutant ataxin-3 putative-cleavage fragment in brains of Machado-Joseph disease patients and transgenic mice is cytotoxic above a critical concentration. *J Neurosci*. 24 (45):10266-79.

Graham, R. K., Deng, Y., Slow, E. J., Haigh, B., Bissada, N., Lu, G., Pearson, J., Shehadeh, J., Bertram, L., Murphy, Z., Warby, S. C., Doty, C. N., Roy, S., Wellington, C. L., Leavitt, B. R., Raymond, L. A., Nicholson, D. W. and Hayden, M. R. (2006) Cleavage at the caspase-6 site is required for neuronal dysfunction and degeneration due to mutant huntingtin. *Cell*. 125 (6):1179-91.

Green, H. (1993) Human genetic diseases due to codon reiteration: relationship to an evolutionary mechanism. *Cell*. 74 (6):955-6.

Griesbeck, O., Baird, G. S., Campbell, R. E., Zacharias, D. A. and Tsien, R. Y. (2001) Reducing the environmental sensitivity of yellow fluorescent protein. Mechanism and applications. *J Biol Chem*. 276 (31):29188-94.

Hassig, C. A. and Schreiber, S. L. (1997) Nuclear histone acetylases and deacetylases and transcriptional regulation: HATs off to HDACs. *Curr. Opin. Chem. Biol*. 1(3):300-8.

Heim, R., Prasher, D. C. and Tsien, R. Y. (1994) Wavelength mutations and posttranslational autoxidation of green fluorescent protein. *Proc Natl Acad Sci U S A*. 91 (26):12501-4.

Helmlinger, D., Tora, L. and Devys, D. (2006) Transcriptional alterations and chromatin remodeling in polyglutamine diseases. *Trends Genet*. 2006 Aug 12

Hirabayashi, M., Inoue, K., Tanaka, K., Nakadate, K., Ohsawa, Y., Kamei, Y., Popiel, A. H., Sinohara, A., Iwamatsu, A., Kimura, Y., Uchiyama, Y., Hori, S. and Kakizuka, A. (2001) VCP/p97 in abnormal protein aggregates, cytoplasmic vacuoles, and cell death, phenotypes relevant to neurodegeneration. *Cell Death Differ*. 8 (10):977-84.

Howell, J. L. and Truant, R. (2002) Live-cell nucleocytoplasmic protein shuttle assay utilizing laser confocal microscopy and FRAP. *Biotechniques*. 32 (1): 80-2, 84, 86-7.

Housman, D. (1995) Gain of glutamines, gain of function? *Nat Genet*. 10 (1):3-4.

Huang, T. T., Kudo, N., Yoshida, M. and Miyamoto, S. (2000) A nuclear export signal in the N-terminal regulatory domain of IkappaBalpha controls cytoplasmic localization of inactive NF-kappaB/IkappaBalpha complexes. *Proc Natl Acad Sci U S A*. 97 (3):1014-9.

Hubbert, C., Guardiola, A., Shao, R., Kawaguchi, Y., Ito, A., Nixon, A., Yoshida, M., Wang, X. F. and Yao, T. P. (2002) HDAC6 is a microtubule-associated deacetylase. *Nature*. 417 (6887):455-8.

Ikeda, H., Yamaguchi, M., Sugai, S., Aze, Y., Narumiya, S. and Kakizuka, A. (1996) Expanded polyglutamine in the Machado-Joseph disease protein induces cell death in vitro and in vivo. *Nat Genet*. 13: 196-202.

Isashiki, Y., Kii, Y., Ohba, N. and Nakagawa, M.. (2000) Retinopathy associated with Machado-Joseph disease (spinocerebellar ataxia 3) with CAG trinucleotide repeat expansion. *Am J Ophthalmol*. 131 (6):808-10.

Jana, N. R., Dikshit, P., Goswami, A., Kotliarova, S., Murata, S., Tanaka, K. and Nukina N. (2005) Co-chaperone CHIP associates with expanded polyglutamine protein and promotes their degradation by proteasomes. *J Biol Chem*. 280 (12):11635-40.

Janknecht, R. (2002) The versatile functions of the transcriptional coactivators p300 and CBP and their roles in disease. *Histol Histopathol*. 17 (2):657-68.

Jarosch, E., Taxis, C., Volkwein, C., Bordallo, J., Finley, D., Wolf, D. H. and Sommer T. (2002) Protein dislocation from the ER requires polyubiquitination and the AAA-ATPase Cdc48. *Nat Cell Biol*. 4 (2):134-9.

Joel, D. (2001) Open interconnected model of basal ganglia-thalamocortical circuitry and its relevance to the clinical syndrome of Huntington's disease. *Mov Disord*. 16:407-23.

Johnston, J. A., Ward, C. L. and Kopito, R.R. (1998) Aggresomes: a cellular response to misfolded proteins. *J Cell Biol*. 143 (7):1883-98.

Kalderon, D., Roberts, B. L., Richardson, W. D. and Smith, A. E.(1984) A short amino acid sequence able to specify nuclear location. *Cell*. 39 (3 Pt 2):499-509.

Katsuno, M., Adachi, H., Kume, A., Li, M., Nakagomi, Y., Niwa, H., Sang, C., Kobayashi, Y., Doyu, M. and Sobue, G. (2002) Testosterone reduction prevents

phenotypic expression in a transgenic mouse model of spinal and bulbar muscular atrophy. *Neuron*. 35 (5):843-54.

Kawaguchi, Y., Okamoto, T., Taniwaki, M., Aizawa, M., Inoue, M., Katayama, H., Nakamura, S., Nishimura, M., Akiguchi, I., Kimura, J., Narumiya, S. and Kakizuka, A. (1994) CAG expansions in a novel gene for Machado-Joseph disease at chromosome 14q32.1. *Nature Genet.* 8: 221-228.

Kawaguchi, Y., Kovacs, J. J., McLaurin, A., Vance, J. M., Ito, A. and Yao, T. P. (2003) The deacetylase HDAC6 regulates aggresome formation and cell viability in response to misfolded protein stress. *Cell*. 115 (6):727-38.

Kawakami, H., Maruyama, H., Nakamura, S., Kawaguchi, Y., Kakizuka, A., Doyu, M. and Sobue, G. (1995) Unique features of the CAG repeats in Machado-Joseph disease. *Nat Genet.* 9 (4):344-5.

Kim, Y. T., Shin, S. M., Lee, W. Y., Kim, G. M. and Jin, D. K. (2004) Expression of expanded polyglutamine protein induces behavioral changes in *Drosophila* (polyglutamine-induced changes in *Drosophila*). *Cell Mol Neurobiol.* 24 (1):109-22.

Klement, I. A., Skinner, P. J., Kaytor, M. D., Yi, H., Hersch, S. M., Clark, H. B., Zoghbi, H. Y. and Orr, H. T. (1998) Ataxin-1 nuclear localization and aggregation: role in polyglutamine induced disease in SCA1 transgenic mice. *Cell* 95 (1):41-53.

Kobayashi, Y. and Sobue, G. (2001) Protective effect of chaperones on polyglutamine diseases. *Brain Res Bull.* 56 (3-4):165-8.

Kong, M., Barnes, E. A., Ollendorff, V. and Donoghue, D. J. (2000) Cyclin F regulates the nuclear localization of cyclin B1 through a cyclin-cyclin interaction. *EMBO J.* 19 (6): 1378-88.

Kopito, R. R. (2000) Aggresomes, inclusion bodies and protein aggregation. *Trends Cell Biol.* 10 (12):524-30.

Koster, M., Frahm, T. and Hauser, H. (2005) Nucleocytoplasmic shuttling revealed by FRAP and FLIP technologies. *Curr Opin Biotechnol.* 16 (1):28-34.

Kraft, S., Furtado, S., Ranaway, R., Parboosingh, J, Bleoo, S., McElligott, K., Bridge, P., Spacey, S., Das, S. and Suchowersky, O. (2005) Adult onset spinocerebellar ataxia in a Canadian movement disorders clinic. *Can J Neurol Sci.* 32 (4):450-8.

Kudo, N., Khochbin, S., Nishi, K., Kitano, K., Yanagida, M., Yoshida, M. and Horinouchi S. (1997) Molecular cloning and cell cycle-dependent expression of

mammalian CRM1, a protein involved in nuclear export of proteins. *J Biol Chem.* 272 (47): 29742-51.

Kudo, N., Matsumori, N., Taoka, H., Fujiwara, D., Schreiner, E. P., Wolff, B., Yoshida, M. and Horinouchi, S. (1999) Leptomycin B inactivates CRM1/exportin 1 by covalent modification at a cysteine residue in the central conserved region. *Proc Natl Acad Sci U S A.* 96 (16): 9112-7.

Kutay, U., Bischoff, F. R., Kostka, S., Kraft, R. and Gorlich, D. (1997) Export of importin alpha from the nucleus is mediated by a specific nuclear transport factor. *Cell.* 90 (6):1061-71.

Lawrence, A., Sahakian, B. and Robbins, T. (1998) Cognitive functions and corticostriatal circuits: insights from huntingtons disease. *Trends in Cognitive Sciences* 2 :379-88.

Lee, B. J., Cansizoglu, A. E., Suel, K. E., Louis, T. H., Zhang, Z. and Chook, Y. M. (2006) Rules for nuclear localization sequence recognition by karyopherin beta 2. *Cell.* 126 (3):543-58.

Lei, E. P. and Silver, P. A. (2002) Protein and RNA export from the nucleus. *Dev Cell.* 2 (3): 261–272.

Li, M., Nakagomi, Y., Kobayashi, Y., Merry, D. E., Tanaka, F., Doyu, M., Mitsuma, T., Hashizume, Y., Fischbeck, K. H. and Sobue, G. (1998b) Nonneural nuclear inclusions of androgen receptor protein in spinal and bulbar muscular atrophy. *Am J Pathol* 153:695–701.

Li, F., Macfarlan, T., Pittman, R. N. and Chakravarti, D. (2002) Ataxin-3 is a histone-binding protein with two independent transcriptional corepressor activities. *J Biol Chem.* 277 (47):45004-12.

Lim, R. Y. and Fahrenkrog, B. (2006) The nuclear pore complex up close. *Curr Opin Cell Biol.* 18 (3):342-7.

Lin, X., Cummings, C. J. and Zoghbi, H. Y. (1999) Expanding our understanding of polyglutamine diseases through mouse models. *Neuron.* 24 (3):499-502.

Lin, X., Antalffy, B., Kang, D., Orr, H. T. and Zoghbi, H. Y. (2000) Polyglutamine expansion down-regulates specific neuronal genes before pathologic changes in SCA1. *Nat Neurosci.* 3 (2):157-63.

- Lippincott-Schwartz, J., Altan-Bonnet, N. and Patterson, G. H. (2003) Photobleaching and photoactivation: following protein dynamics in living cells. *Nat Cell Biol. Suppl*:S7-14.
- Llorian, M., Beullens, M., Lesage, B., Nicolaescu, E., Beke, L., Landuyt, W., Ortiz, J. M. and Bollen, M. (2005) Nucleocytoplasmic shuttling of the splicing factor SIPP1. *J Biol Chem.* 280 (46):38862-9.
- Lunkes A, Trottier Y, Fagart J, Schultz P, Zeder-Lutz G, Moras D, Mandel JL. (1999) Properties of polyglutamine expansion in vitro and in a cellular model for Huntington's disease. *Philos Trans R Soc Lond B Biol Sci* 354 (1386):1013–9.
- Lunkes, A., Lindenberg, K. S., Ben-Haiem, L., Weber, C., Devys, D., Landwehrmeyer, G. B., Mandel, J. L. and Trottier, Y. (2002) Proteases acting on mutant huntingtin generate cleaved products that differentially build up cytoplasmic and nuclear inclusions. *Mol Cell* (10):259 –269.
- Maciel, P., Gaspar, C., Guimaraes, L., Goto, J., Lopes-Cendes, I., Hayes, S., Arvidsson, K., Dias, A., Sequeiros, J., Sousa, A. and Rouleau, G. A. (1995) Correlation between CAG repeat length and clinical features in Machado-Joseph disease. *Am J Hum Genet.* 57 (1):54-61.
- Maciel, P., Costa, M. C., Ferro, A., Rousseau, M., Santos, C. S., Gaspar, C., Barros, J., Rouleau, G. A., Coutinho, P. and Sequeiros, J. (2001) Improvement in the molecular diagnosis of Machado-Joseph disease. *Arch Neurol.* 58:1821-7.
- Mao, Y., Senic-Matuglia, F., Di, Fiore, P. P., Polo, S., Hodsdon, M. E. and De Camilli, P. (2005) Deubiquitinating function of ataxin-3: insights from the solution structure of the Josephin domain. *Proc Natl Acad Sci U S A.* 102 (36):12700-5.
- Masino, L., Musi, V., Menon, R. P., Fusi, P., Kelly, G., Frenkiel, T. A., Trottier, T. and Pastore, A. (2003) Domain architecture of the polyglutamine protein ataxin-3: a globular domain followed by a flexible tail. *FEBS Lett.* 549 (1-3):21-5.
- Matilla, T., McCall, A., Subramony, S. H. and Zoghbi, H. Y. (1995) Molecular and clinical correlations in spinocerebellar ataxia type 3 and Machado-Joseph disease. *Ann Neurol.* 38 (1):68-72.
- Matz, M. V., Fradkov, A. F., Labas, Y. A., Savitsky, A. P., Zaraisky, A. G., Markelov, M. L. and Lukyanov, S. A. (1999) Fluorescent proteins from nonbioluminescent Anthozoa species. *Nat Biotechnol.* 17 (10):969-73.

- McKinsey, T. A., Zhang, C. L., Lu, J. and Olson, E. N. (2000) Signal-dependent nuclear export of a histone deacetylase regulates muscle differentiation. *Nature*. 408 (6808):106-11.
- Moore, D., S. and McCabe, G., P. (2003) Introduction to the Practise of Statistics 4th Ed. W. H. Freeman and Company.
- Moore, J. D., Yang, J., Truant, R. and Kornbluth, S. (1999) Nuclear import of Cdk/cyclin complexes: identification of distinct mechanisms for import of Cdk2/cyclin E and Cdc2/cyclin B1. *J Cell Biol*. 144 (2):213-24
- Munchau, A., Dressler, D., Bhatia, K. P., Vogel, P. and Zuhlke, C. (1999) Machado-Joseph disease presenting as severe generalised dystonia in a German patient. *J Neurol*. 246 (9):840-2.
- Nakamura, K., Jeong, S., Uchihara, T., Anno, M., Nagashima, K., Nagashima, T., Ikeda, S., Tsuji, S. and Kanazawa I. (2001) SCA17, a novel autosomal dominant cerebellar ataxia caused by an expanded polyglutamine in TATA-binding protein. *Hum Mol Genet* 10 (14):1441-8.
- Nandi, D., Tahiliani, P., Kumar, A. and Chandu D. (2006) The ubiquitin-proteasome system. *J Biosci*. 31 (1):137-55.
- Neufeld, K. L., Nix, D. A., Bogerd, H., Kang, Y., Beckerle, M. C., Cullen, B. R. and White, R. L. (2000) Adenomatous polyposis coli protein contains two nuclear export signals and shuttles between the nucleus and cytoplasm. *Proc Natl Acad Sci U S A*. 97 (22):12085-90.
- Neville, M. and Rosbash, M. (1999) The NES-Crm1p export pathway is not a major mRNA export route in *Saccharomyces cerevisiae*. *EMBO J*. 18 (13): 3746-56.
- Nicastro G, Menon RP, Masino L, Knowles PP, McDonald NQ, Pastore A. (2005) The solution structure of the Josephin domain of ataxin-3: structural determinants for molecular recognition. *Proc Natl Acad Sci U S A*. 102 (30):10493-8.
- Nishiyama K, Murayama S, Goto J, Watanabe M, Hashida H, Katayama S, Nomura Y, Nakamura S, Kanazawa I. (1996) Regional and cellular expression of the Machado-Joseph disease gene in brains of normal and affected individuals. *Ann Neurol*. 40 (5):776-81.
- Nucifora, F. C. Jr, Ellerby, L. M., Wellington, C. L., Wood, J. D., Herring, W. J., Sawa, A., Hayden, M. R., Dawson, V. L., Dawson, T. M. and F Ross, C. A. (2003) Nuclear localization of a non-caspase truncation product of atrophin-1, with an expanded polyglutamine repeat, increases cellular toxicity. *J Biol Chem*. 278 (15):13047-55.

- Ormo, M., Cubitt, A. B., Kallio, K., Gross, L. A., Tsien, R. Y. and Remington, S. J. (1996) Crystal structure of the *Aequorea victoria* green fluorescent protein. *Science*. 273 (5280):1392-5.
- Paulson, H. L., Perez, M. K., Trotter, Y., Trojanowski, J. Q., Subramony, S. H., Das, S. S., Vig, P., Mandel, J. L., Fischbeck, K. H. and Pittman, R. N. (1997a) Intranuclear inclusions of expanded polyglutamine protein in spinocerebellar ataxia type 3. *Neuron* 19 (2):333-44.
- Paulson, H. L., Das, S. S., Crino, P. B., Perez, M. K., Patel, S. C., Gotsdiner, D., Fischbeck, K. H. and Pittman, R. N. (1997b) Machado-Joseph disease gene product is a cytoplasmic protein widely expressed in brain. *Ann Neurol*. 41 (4):453-62.
- Pearson, C. E., Tam, M., Wang, Y. H., Montgomery, S. E., Dar, A. C., Cleary, J. D. and Nichol, K. (2002) Slipped-strand DNAs formed by long (CAG)ⁿ(CTG) repeats: slipped-out repeats and slip-out junctions. *Nucleic Acids Res*. 30 (20):4534-47.
- Pearson, C. E. (2003) Slipping while sleeping? Trinucleotide repeat expansions in germ cells. *Trends Mol Med*. 9 (11):490-5.
- Pemberton, L. F. and Paschal, B. M. (2005) Mechanisms of receptor-mediated nuclear import and nuclear export. *Traffic*. 6 (3):187-98.
- Perez, M. K., Paulson, H. L., Pendse, S. J., Saionz, S. J., Bonini, N. M. and Pittman, R. N. (1998) Recruitment and the role of nuclear localization in polyglutamine-mediated aggregation. *J Cell Biol*. 143 (6):1457-70.
- Perutz, M. F., Johnson, T., Suzuki, M. and Finch J. T. (1994) Glutamine repeats as polar zippers: their possible role in inherited neurodegenerative diseases. *Proc Natl Acad Sci U S A*. 91 (12):5355-8.
- Piccioni, F., Simeoni, S., Andriola, I., Armatura, E., Bassanini, S., Pozzi, P. and Poletti, A. (2001) Polyglutamine tract expansion of the androgen receptor in a motoneuronal model of spinal and bulbar muscular atrophy. *Brain Res Bull*. 56 (3-4):215-20. Review.
- Reichelt, R., Holzenburg, A., Buhle, E. L., Jarnik Jr., M., Engel, A. and Aebi, U. (1990) Correlation between structure and mass distribution of the nuclear pore complex and of distinct pore complex components. *J. Cell Biol*. 110 (4):883-94
- Richards, R. I. and Sutherland, G. R. (1992) Dynamic mutations: a new class of mutations causing human disease. *Cell*. 70, 709-712.

- Richards, R. I. and Sutherland, G. R. (1994) Simple repeat DNA is not replicated simply. *Nat Genet.* 6 (2):114-6.
- Rizzo, M. A., Springer, G. H., Granada, B. and Piston, D. W. (2004) An improved cyan fluorescent protein variant useful for FRET. *Nat Biotechnol.* 22 (4):445-9.
- Rout, M. P. and Blobel, G. (1993) Isolation of the yeast nuclear pore complex. *J. Cell Biol.* 123 (4):771-83.
- Rout, M. P., Aitchison, J. D., Suprpto, A., Hjertaas, K., Zhao, Y. and Chait, B. T. (2000) The yeast nuclear pore complex: composition, architecture, and transport mechanism. *J Cell Biol.* 148 (4):635-51.
- Rubinsztein, D. C., Leggo, J., Coetzee, G. A., Irvine, R. A., Buckley, M. and Ferguson-Smith, M. A. (1995) Sequence variation and size ranges of CAG repeats in the Machado-Joseph disease, spinocerebellar ataxia type 1 and androgen receptor genes. *Hum Mol Genet.* 4 (9):1585-90.
- Sakahira, H., Breuer, P., Hayer-Hartl, M. K. and Hartl, F. U. (2002) Molecular chaperones as modulators of polyglutamine protein aggregation and toxicity. *Proc Natl Acad Sci U S A.* 99 Suppl 4:16412-8.
- Saporita, A. J., Zhang, Q., Navai, N., Dincer, Z., Hahn, J., Cai, X. and Wang, Z. (2003) Identification and characterization of a ligand-regulated nuclear export signal in androgen receptor. *J Biol Chem.* 278 (43):41998-2005.
- Saudou, F., Finkbeiner, S., Devys, D. and Greenberg, M. E. (1998) Huntingtin acts in the nucleus to induce apoptosis but death does not correlate with the formation of intranuclear inclusions. *Cell* 95 (1):55-66.
- Schauber, C., Chen, L., Tongaonkar, P., Vega, I., Lambertson, D., Potts, W. and Madura, K. (1998) Rad23 links DNA repair to the ubiquitin/proteasome pathway. *Nature.* 391 (6668):715-8.
- Scheel, H., Tomiuk, S. and Hofmann, K. (2003) Elucidation of ataxin-3 and ataxin-7 function by integrative bioinformatics. *Hum Mol Genet.* 12 (21):2845-52.
- Scherzinger, E., Lurz, R., Turmaine, M., Mangiarini, L., Hollenbach, B., Hasenbank, R., Bates, G. P., Davies, S. W., Lehrach, H., and Wanker, E. E. (1997) Huntingtin-encoded polyglutamine expansions form amyloid-like protein aggregates in vitro and in vivo. *Cell* 90 (3):549-558.
- Schilling, G., Jinnah, H. A., Gonzales, V., Coonfield, M. L., Kim, Y., Wood, J. D., Price, D. L., Li, X. J., Jenkins, N., Copeland, N., Moran, T., Ross, C. A., and Borchelt, D. R.

(2001) Distinct behavioral and neuropathological abnormalities in transgenic mouse models of HD and DRPLA. *Neurobiol Dis.* 8 (3):405-18.

Shiota, C., Coffey, J., Grimsby, J., Grippo, J. F. and Magnuson, M. A. (1999) Nuclear import of hepatic glucokinase depends upon glucokinase regulatory protein, whereas export is due to a nuclear export signal sequence in glucokinase. *J Biol Chem.* 274 (52):37125-30.

Schlotterer, C. and Tautz, D. (1992) Slippage synthesis of simple sequence DNA. *Nucleic Acids Res.* 20 (2):211–215.

Schmidt M, Hanna J, Elsasser S, Finley D. (2005) Proteasome-associated proteins: regulation of a proteolytic machine. *Biol Chem.* 386 (8):725-37.

Schmidt, T., Landwehrmeyer, G. B., Schmitt, I., Trottier, Y., Auburger, G., Laccone, F., Klockgether, T., Volpel, M., Epplen, J. T., Schols, L. and Riess, O. (1998) An isoform of ataxin-3 accumulates in the nucleus of neuronal cells in affected brain regions of SCA3 patients. *Brain Pathol.* 8 (4): 669-79.

Schols L, Vieira-Saecker AM, Schols S, Przuntek H, Epplen JT, Riess O. (1995) Trinucleotide expansion within the MJD1 gene presents clinically as spinocerebellar ataxia and occurs most frequently in German SCA patients. *Hum Mol Genet.* 4 (6):1001-5.

Schols L, Haan J, Riess O, Amoiridis G, Przuntek H. (1998) Sleep disturbance in spinocerebellar ataxias: is the SCA3 mutation a cause of restless legs syndrome? *Neurology.* 51 (6):1603-7.

Seigneurin-Berny, D., Verdel, A., Curtet, S., Lemerrier, C., Garin, J., Rousseaux, S. and Khochbin, S. (2001) Identification of components of the murine histone deacetylase 6 complex: link between acetylation and ubiquitination signaling pathways. *Mol Cell Biol.* 21 (23):8035-44.

Shaner, N., C., Campbell, R., E., Steinbach, P., A., Giepmans, B., N., Palmer, A., E. and Tsien, R., Y. (2004) Improved monomeric red, orange and yellow fluorescent proteins derived from *Discosoma* sp. red fluorescent protein. *Nat Biotechnol.* 22 (12):1567-72.

Shaw, G., Morse, S., Ararat, M. and Graham, F. L. (2002) Preferential transformation of human neuronal cells by human adenoviruses and the origin of HEK 293 cells. *FASEB J.* 16 (8): 869-71.

Silveira, I., Lopes-Cendes, I., Kish, S., Maciel, P., Gaspar, C., Coutinho, P., Botez, M. I., Teive, H., Arruda, W., Steiner, C. E., Pinto-Junior, W., Maciel, J. A., Jerin, S., Sack, G., Andermann, E.,

Sudarsky, L., Rosenberg, R., MacLeod, P., Chitayat, D., Babul, R., Sequeiros, J. and Rouleau, G. A. (1996) Frequency of spinocerebellar ataxia type 1, dentatorubropallidoluysian atrophy, and Machado-Joseph disease mutations in a large group of spinocerebellar ataxia patients. *Neurology*. 46 (1):214-8.

Skinner, P. J., Koshy, B. T., Cummings, C. J., Klement, I. A., Helin, K., Servadio, A., Zoghbi, H. Y. and Orr, H. T. (1997) Ataxin-1 with an expanded glutamine tract alters nuclear matrix-associated structures. *Nature* 389 (6654): 971-4.

Sobue, G., Doyu, M., Nakao, N., Shimada, N., Mitsuma, T., Maruyama, H., Kawakami, S. and Nakamura, S. (1996) Homozygosity for Machado-Joseph disease gene enhances phenotypic severity. *J Neurol Neurosurg Psychiatry*. 60 (3):354-6.

Stewart, M., Baker, R. P., Bayliss, R., Clayton, L., Grant, R. P., Littlewood, T. and Matsuura, Y. (2001) Molecular mechanism of translocation through nuclear pore complexes during nuclear protein import. *FEBS Lett*. 498 (2-3):145-9.

Stommel, J. M., Marchenko, N. D., Jimenez, G. S., Moll, U. M., Hope, T. J. and Wahl, G. M. (1999) A leucine-rich nuclear export signal in the p53 tetramerization domain: regulation of subcellular localization and p53 activity by NES masking. *EMBO J*. 18 (6):1660-72.

Sudarsky, L. and Coutinho, P. (1995) Machado-Joseph disease. *Clin Neurosci* 3: 17-22.

Tait, D., Riccio, M., Sittler, A., Scherzinger, E., Santi, S., Ognibene, A., Maraldi, N. M., Lehrach, H. and Wanker, E. E. (1998) Ataxin-3 is transported into the nucleus and associates with the nuclear matrix. *Hum Mol Genet*. 7 (6):991-7.

Tanaka, Y., Igarashi, S., Nakamura, M., Gafni, J., Torcassi, C., Schilling, G., Crippen, D., Wood, J. D., Sawa, A., Jenkins, N. A., Copeland, N. G., Borchelt, D. R., Ross, C. A. and Ellerby L. M. (2006) Progressive phenotype and nuclear accumulation of an amino-terminal cleavage fragment in a transgenic mouse model with inducible expression of full-length mutant huntingtin. *Neurobiol Dis*. 21 (2):381-91.

Taniwaki, T., Sakai, T., Kobayashi, T., Kuwabara, Y., Otsuka, M., Ichiya, Y., Masuda, K. and Goto, I. (1997) Positron emission tomography (PET) in Machado-Joseph disease. *J Neurol Sci*. 145 (1):63-7.

Taylor, J., Grote, S. K., Xia, J., Vandelft, M., Graczyk, J., Ellerby, L. M., La Spada, A. R. and Truant R. (2006) Ataxin-7 can export from the nucleus via a conserved exportin-dependent signal. *J Biol Chem*. 281 (5):2730-9.

Trettel, F., Rigamonti, D., Hilditch-Maguire, P., Wheeler, V. C., Sharp, A. H., Persichetti, F., Cattaneo, E., MacDonald, M. E. (2000) Dominant phenotypes produced by the HD mutation in STHdh(Q111) striatal cells. *Hum Mol Genet.* 9 (19):2799-809.

Tickenbrock, L., Cramer, J., Vetter, I. R. and Muller, O. (2002) The coiled coil region (amino acids 129-250) of the tumor suppressor protein adenomatous polyposis coli (APC). Its structure and its interaction with chromosome maintenance region 1 (Crm-1). *J Biol Chem.* 277 (35):32332-8.

Tran, E. J. and Wentz, S. R. (2006) Dynamic nuclear pore complexes: life on the edge. *Cell.* 125 (6):1041-53.

Trottier, Y., Cancel, G., An-Gourfinkel, I., Lutz, Y., Weber, C., Brice, A., Hirsch, E. and Mandel, J. L. (1998) Heterogeneous intracellular localization and expression of ataxin-3. *Neurobiol Dis.* 5 (5):335-47.

Tuite, P. J., Rogaeva, E. A., St George-Hyslop, P. H. and Lang, A. E. (1995) Dopa-responsive parkinsonism phenotype of Machado-Joseph disease: confirmation of 14q CAG expansion. *Ann Neurol.* 38 (4):684-7.

Vacher, C., Garcia-Oroz, L. and Rubinsztein, D. C. (2005) Overexpression of yeast hsp104 reduces polyglutamine aggregation and prolongs survival of a transgenic mouse model of Huntington's disease. *Hum Mol Genet.* 14 (22):3425-33.

Verdel, A., Curtet, S., Brocard, M. P., Rousseaux, S., Lemerrier, C., Yoshida, M. and Khochbin, S. (2000) Active maintenance of mHDAC2/mHDAC6 histone-deacetylase in the cytoplasm. *Curr Biol.* 10 (12): 747-9.

Walcott, J. L. and Merry, D. E. (2002) Ligand promotes intranuclear inclusions in a novel cell model of spinal and bulbar muscular atrophy. *J Biol Chem.* 277 (52):50855-9.

Wang, G., Sawai, N., Kotliarova, S., Kanazawa, I. and Nukina, N.. (2000) Ataxin-3, the MJD1 gene product, interacts with the two human homologs of yeast DNA repair protein RAD23, HHR23A and HHR23B. *Hum Mol Genet.* 9 (12):1795-803.

Ward, W. W. and Cormier, M. J. (1979) An energy transfer protein in coelenterate bioluminescence. Characterization of the Renilla green-fluorescent protein. *J Biol Chem.* 254 (3):781-8.

Warrick, J. M., Paulson, H. L., Gray-Board, G. L., Bui, Q. T., Fischbeck, K. H., Pittman, R. N. and Bonini, N. M. (1998) Expanded polyglutamine protein forms nuclear inclusions and causes neural degeneration in *Drosophila*. *Cell.* 93 (6):939-49.

Warrick, J. M., Chan, H. Y., Gray-Board, G. L., Chai, Y., Paulson, H. L. and Bonini, N. M. (1999) Suppression of polyglutamine-mediated neurodegeneration in *Drosophila* by the molecular chaperone HSP70. *Nat Genet.* 23 (4):425-8.

Warrick, J. M., Morabito, L. M., Bilen, J., Gordesky-Gold, B., Faust, L. Z., Paulson, H. L. and Bonini, N. M. (2005) Ataxin-3 suppresses polyglutamine neurodegeneration in *Drosophila* by a ubiquitin-associated mechanism. *Mol Cell.* 18 (1):37-48.

Wolff, B., Sanglier, J. J. and Wang, Y. (1997) Leptomycin B is an inhibitor of nuclear export: inhibition of nucleo-cytoplasmic translocation of the human immunodeficiency virus type 1 (HIV-1) Rev protein and Rev-dependent mRNA. *Chem Biol.* 4 (2): 139-47.

Xia, J., Lee, D. H., Taylor, J., Vandelft, M. and Truant, R. (2003). Huntingtin contains a highly conserved nuclear export signal. *Hum. Mol. Genet.* 12 (12):1393-1403.

Yamada, M., Hayashi, S., Tsuji, S. and Takahashi, H. (2001) Involvement of the cerebral cortex and autonomic ganglia in Machado-Joseph disease. *Acta Neuropathol (Berl).* 101 (2):140-4.

Yoo, S. Y., Pennesi, M. E., Weeber, E. J., Xu, B., Atkinson, R., Chen, S., Armstrong, D. L., Wu, S. M., Sweatt, J. D. and Zoghbi, H. Y. (2003) SCA7 knockin mice model human SCA7 and reveal gradual accumulation of mutant ataxin-7 in neurons and abnormalities in short-term plasticity. *Neuron.* 37 (3):383-401.

Yoshizawa, T., Yoshida, H. and Shoji, S. (2001) Differential susceptibility of cultured cell lines to aggregate formation and cell death produced by the truncated Machado-Joseph disease gene product with an expanded polyglutamine stretch. *Brain Res Bull.* 56 (3-4):349-52.

Yvert, G., Lindenberg, K. S., Devys, D., Helmlinger, D., Landwehrmeyer, G. B. and Mandel, J. L. (2001) SCA7 mouse models show selective stabilization of mutant ataxin-7 and similar cellular responses in different neuronal cell types. *Hum Mol Genet* 10 (16):1679-92.

Zoghbi, H. Y. and Orr, H. T. (1999) Polyglutamine diseases: protein cleavage and aggregation. *Curr Opin Neurobiol.* 9 (5):566-70.

Zhong, X. and Pittman, R. N. (2006) Ataxin-3 binds VCP/p97 and regulates retrotranslocation of ERAD substrates. *Hum Mol Genet.* 15 (16):2409-20.